Dissertation

Hemifusion and lateral lipid domain partition in lipid membranes of different complexity

zur Erlangung des akademischen Grades
doctor rerum naturalium (Dr. rer. nat.)
im Fach Biophysik

eingereicht an der
Mathematisch-Naturwissenschaftlichen Fakultät I
der Humboldt-Universität zu Berlin

von
Diplom Biophysiker Jörg Nikolaus

Präsident der Humboldt-Universität zu Berlin
Prof. Dr. Jan-Hendrik Olbertz

Dekan der Mathematisch-Naturwissenschaftlichen Fakultät I
Prof. Dr. Andreas Herrmann

Gutachter: 1. Prof. Dr. Andreas Herrmann

2. Prof. Dr. Sandro Keller

3. Prof. Dr. Daniel Huster

eingereicht: 16.12.2010

Datum der Promotion: 21.04.2011

„It’s unoptimized - by evolution”

Jacob Piehler (* 10.04.1968)

Zusammenfassung

Die Fusion von Membranen erfordert die Verschmelzung von zwei Phospholipiddoppelschichten, wobei dies immer über dieselben Zwischenschritte abzulaufen scheint. Eine lokale Störung (‚Stalk') stellt eine erste Verbindung der äußeren Membranhälften dar, die anschließend lateral expandiert und ein Hemifusionsdiaphragma (HD) bildet. Das Öffnen einer Fusionspore im HD führt zur vollständigen Fusion. Mittels konfokaler Mikroskopie wurde die Fusion von *Giant unilamellar vesicles* (GUVs) mit negativ geladenen Lipiden und transmembranen (TM) Peptiden in Anwesenheit von zweiwertigen Kationen beobachtet, wobei die Peptide bei der HD Entstehung völlig verdrängt wurden. Eine detaillierte Analyse zeigte, dass es sich bei diesem Mikrometer-großen Bereich um ein HD handelt, dessen Größe von der Lipidzusammensetzung und Peptidkonzentration in den GUVs abhängt.

Laterale Lipiddomänen gelten als entscheidend für Signal- und Sortierungsprozesse in der Zelle. *Liquid ordered* (Lo) Domänen in Modellsystemen wie GUVs ähneln den mit Sphingolipiden und Cholesterol angereicherten biologischen Raft-Domänen, allerdings scheinen Membraneigenschaften wie die Lipidpackung sich von biologischen Membranen zu unterscheiden. In diesem Zusammenhang wird die Sortierung des TM-verankerten Hemagglutinin (HA) des Influenzavirus und von lipidverankerten Ras-Proteinen in GUVs wie auch in abgelösten Plasmamembran-Ausstülpungen (GPMVs) untersucht. HA Protein und TM-Pepitde von HA wurden ausschließlich (GUVs) bzw. vorwiegend (GPMVs) in der *liquid disordered* (Ld) Domäne gefunden. K-Ras wurde inmitten der Ld detektiert, während N-Ras zur Lo/Ld Grenzlinie diffundierte. Diese Ergebnisse werden im Zusammenhang mit den Unterschieden der Lipidpackung innerhalb der verschiedenen membranverankerten Systeme diskutiert. Es ist wahrscheinlich, dass die Bildung, Größe und Stabilität sowie die physikalischen Eigenschaften der Lipiddomänen in biologischen Membranen stark von Protein-Lipid-Wechsel-wirkungen beeinflusst werden.

Schlagwörter:

Hemifusionsintermediat

Transmembrane Domäne

GUV

Lipiddomänen

Influenza Hemagglutinin

Ras Proteine

Abstract

Membrane fusion is ubiquitous in life and requires remodelling of two phospholipid bilayers. Fusion likely proceeds through similar sequential intermediates. A stalk between the contacting leaflets forms and radially expands into a hemifusion diaphragm (HD) wherein finally a fusion pore opens up. Direct experimental verification of this key structure is difficult due to its transient nature. Confocal microscopy was used to visualize the fusion of giant unilamellar vesicles (GUVs) comprising negatively charged phosphatidylserine and fluorescent transmembrane (TM) entities in the presence of divalent cations. A complete displacement of TM peptides preceded full fusion. This is consistent with HD formation. Detailed analysis provided proof that the micrometer sized structures are in fact HDs. HD size is dependent on lipid composition and peptide concentration.

Lateral lipid domain formation is believed to be essential for sorting and signalling processes in the cell. Liquid ordered (Lo) domains in model systems like GUVs resemble biological rafts enriched in sphingolipids and cholesterol, but their physical properties seem distinct from biological membranes as judged by e.g. lipid order and packing. In this context the sorting of TM anchored influenza virus hemagglutinin (HA) and different lipid anchored Ras proteins is studied in GUVs and giant plasma membrane derived vesicles (GPMVs). Authentic HA or the TM domain peptides were sorted exclusively (GUVs) or predominantly (GPMVs) to the liquid disordered (Ld) domains. Whereas K-Ras was found in the bulk Ld domains, N-Ras diffuses to the Lo/Ld interface. These results are discussed with respect to differences in lipid packing in the different membrane systems and regarding the membrane anchors and their hydrophobic matching. The results suggest that the formation, size and stability as well as the physical properties of lipid domains in biological membranes are tightly regulated by protein-lipid interactions.

Keywords:

membrane fusion

hemifusion intermediate

transmembrane domain

giant unilamellar vesicle

lipid domains

Influenza hemagglutinin

Ras proteins

Abbreviations

Å	Ångstrom
aa	Amino acid
AFM	Atomic force microscopy
C-	Carboxy-
C6-NBD-	1-Palmitoyl-2-[6-[(7-nitro-2-1,3-benzoxadiazol-4-yl)amino]hexanoyl]-sn-Glycero-3-
CFP, mCFP	Cyan fluorescent protein, monomeric cyan fluorescent protein
Chol	Cholesterol
DMSO	Dimethylsulfoxide
DNA	Deoxyribonucleic acid
DRM	Detergent resistant membrane
DSM	Detergent soluble membrane
EPR	Electron paramagnetic resonance
ER	Endoplasmic reticulum
F/-PALM	Fluorescence photoactivation localization microscopy
FLIM	Fluorescence lifetime imaging microscopy
FRET	Förster resonance energy transfer
GP	Generalized polarization
GPI	Glycosylphosphatidylinositol
GPMV	Giant plasma membrane vesicle
GUV	Giant unilamellar vesicle
HA	Hemagglutinin
HD	Hemifusion diaphragm
Hepes	4-(2-hydroxyethyl)-1-piperazineethanesulfonic acid
HOBt	1-Hydroxybenzotriazole
ITO	Indium tin oxide
K	Lysine
KALP/WALP	model peptides comprising an AL stretch flanked by K or W residues, respectively
Ld	Liquid disordered
Lo	Liquid ordered
LPC	Lysophosphatidylcholine
LUV	Large unilamellar vesicle
MD	Molecular dynamic
MLV	Mulitlamellar vesicle
MβCD	Methyl-β-Cylodextrin
N-	Amino-

NA	Neuraminidase
NBD	6-(7-nitro-2-1,3-benzoxadiazol-4-yl)amino
NMR	Nuclear magnetic resonance
P/L	Protein/Lipid
PAGE	Polyacrylamide gelelectrophoresis
Pal	Palmitoylation
PBS	Phosphate buffered saline
PC	Phosphatidylcholine
PE	Phosphatidylethanolamine
PI	Phosphatidylinositole
PMS	Plasma membrane spheres
PNA	Peptide nucleic acid
PS	Phosphatidylserine
PSM	N-palmitoyl-D-sphingomyelin
R18	Octadecyl rhodamine B chloride
RBC	Red blood cell
RT	Room temperature
SD	Standard deviation
SDS	Sodium dodecylsulfate
SEM	Standard error of the mean
SNARE	Soluble N-ethylmaleimide-sensitive-factor attachment receptor
SPT	Single particle tracking
SSM	N-stearoyl-D-sphingomyelin
SUV	Small unilamellar vesicle
TCSPC	Time correlated single photon counting
TEM	Transmission electron microscopy
TFA	trifluoroacetic acid
TFE	Trifluoroethoanol
TMD	Transmembrane domain
TMR	Tetramethylrhodamine
Trp	Tryptophan
WT	Wild type
YFP, mYFP	Yellow fluorescent protein, monomeric yellow fluorescent protein

Table of content

"Knowledge is a process of piling up facts;
wisdom lies in their simplification."

Martin Henry Fischer (* 10.11.1879; † 19.01.1962)

1 Introduction

1.1 Motivation

The roman encyclopedist Aulus Cornelius Celsus (ca 25 BC – ca 50 AD) was the first to use the term 'virus' (from Latin poison, sap of plants, slimy liquid) as early as in the first century BC describing that an illness like rabies was transmitted by a poison. But it was not until the end of the 19th century that the Dutch researcher Martinus W. Beijerinck (March 16, 1851 – January 1, 1931) found a pathogenic agent causing the tobacco mosaic disease that was smaller than a bacterium and could therefore not be separated by means of filtration. Also in 1898, the German bacteriologists Friedrich Loeffler (June 24, 1852 – April 9, 1915) and Paul Frosch (August 15, 1860 – June 2, 1928) were able to transfer the pathogenic agent of the foot-and-mouth disease thus identifying the first animal virus. Both experiments clearly showed that viruses are not just mere toxins but infectious agents that could replicate in living host organisms. While in 1898 Beijerinck thought that the tobacco mosaic viruses had a liquid nature, it wasn't until 1935 that Wendell M. Stanley (August 16, 1904 – June 15, 1971) demonstrated through crystallization that viruses are in fact particles.

In the years since the discovery of virus particles, about 5000 different viruses have been described so far that can be divided into seven different groups depending, amongst other factors, on their type of envelope and nucleic acid. One of those is the influenza virus killing

millions of people in several pandemics in the last centuries and still causing the death of 250,000 to 500,000 people worldwide in seasonal epidemics every year.

Influenza and other viruses have ever since been studied intensively by many scientists using various methods and many, but by far not all of its mechanisms are finally understood. The work presented below was started to unravel yet another detail leading to a better understanding of the viral machinery of influenza virus. In the future an even better understanding of the molecular mechanisms will hopefully help to circumvent viral infection and diseases.

The influenza virus is the starting point of this work while the lipid membrane will be the element linking the questions asked. Therefore not only membrane fusion and lateral sorting of viral but also of cancer related proteins at the membrane will be investigated. Besides these biological proteins also a new class of synthetic molecular rods functioning as an alternative transmembrane anchor for dyes or proteins will be studied.

Since all the above mentioned processes of fusion and sorting take place at a molecular level in cellular systems and are therefore only indirectly accessible for observation, membrane model systems especially designed to visualize these processes will be employed here to accomplish this task.

1.2 Membrane fusion

An early step in evolution was the self-assembly of simple amphiphilic molecules to supramolecular structures yielding a bilayer-like structure, which serves as a semipermeable barrier for soluble molecules. These early bilayers assembled from amphiphilic lipid-like molecules like fatty alcohols and fatty acids were much more permeable than phospholipid bilayers (Apel *et al.*, 2002; Deamer, 2008; Mansy *et al.*, 2008). Recent experiments showed that simple systems capable of enclosing nutrient molecules from the surrounding environment were not only able to grow by the uptake and incorporation of further lipid-like material but could also be divided into smaller vesicles by modest shear forces without loss of the captured contents (Zhu and Szostak, 2009; Markvoort *et al.*, 2010).

Over the last 3 to 4 billion years these first basic cell-like units have much evolved. Lipid bilayers of prokaryotic and eukaryotic cells are a billion times less permeable for electrically charged molecules than for small uncharged ones. Thus, nature created a huge variety of

specialized transporters to shuttle cargos across the lipid palisade and invented complex ways to convert incoming signals from the environment into a cellular response. As will be outlined in the second part of this work the function of a membrane is much more than just separating two compartments. The membrane has evolved into a complex and heterogeneous functional unit.

Ever since nature came up with lipid membranes separating cellular processes, it became also necessary to forge a rapid and regulated membrane fusion mechanism required to maintain cellular functions. Membrane fusion occurs in cell-cell fusion during fertilisation and also in cell growth and tissue genesis, intracellular vesicular trafficking in exocytosis and protein trafficking, neurotransmitter release and hormone secretion and also in tumorigenesis and infection by enveloped viruses (Shemer and Podbilewicz, 2003; Mohler *et al.*, 2002; Jahn *et al.*, 2003; Sudhof and Rothman, 2009; Ungermann and Langosch, 2005; Kielian and Rey, 2006; Earp *et al.*, 2005; Marsh and Helenius, 2006). All these membrane fusion events are mediated by a specialized set of proteins overcoming the repulsive force of the hydration energy between the polar heads of two approaching lipid bilayers (Rand and Parsegian, 1984). These proteins supply the energy for the lipid rearrangement necessary to merge the two apposing membranes. They are anchored in the membrane via a transmembrane anchor and establish a connection to the opposing bilayer either by insertion of a hydrophobic anchor peptide as in viral fusion or by zippering up with yet another protein anchored already in the opposed membrane by a transmembrane domain (TMD) as in intracellular fusion events mediated by SNARE (soluble N-ethylmaleimide-sensitive factor attachment protein receptor) proteins (for details see below).

1.2.1 Hemifusion

Although the protein machinery accomplishing membrane fusion in the different systems is quite distinct, the underlying pathway concerning lipid rearrangements within the bilayers seems to be similar within the three classes of developmental, intracellular and viral fusogen systems (Sapir *et al.*, 2008). Membrane fusion of biological membranes as well as of artificial protein-free bilayers is primarily of lipidic character – as described in the lipidic pore model, which will be reviewed below. Many experimental insights about the lipid remodelling in the fusion process came from early studies of protein-free liposome and flat bilayer fusion in the presence of e.g. calcium ions and poly(ethylene glycol) (PEG) or from vesicle systems with

high membrane curvature (L. V. Chernomordik *et al.*, 1987; J. Lee and Lentz, 1997) since protein-free bilayers do not fuse when just brought in very close contact (L. V. Chernomordik and Kozlov, 2003). The equilibrium distance of about 2-3 nm between two artificial bilayers of biologically relevant lipids like phosphatidylcholine (PC) is governed by water which fills that gap (Luzzati planes – interface dividing water and lipid phase) (Rand and Parsegian, 1989) with the hydration of the lipid head groups being the molecular basis of the hydration force. Osmotic removal of this water by addition of high molecular weight PEG is now able to reduce the distance between the apposing lipid headgroups to about 1 nm. Divalent ions like Ca^{2+} have similar effects on bilayers containing charged lipids. Decreasing distance increases the intermembrane hydration repulsion which drives the two apposing membranes into the remodelling of the bilayer structure which in turn reduces the induced stress as predicted in theory (Kozlovsky *et al.*, 2004) and as could be shown experimentally (Yang and Huang, 2003).

Lipid bilayers very likely fuse via the fusion through hemifusion pathway (Fig. 1). Based on the work of Helfrich (Helfrich, 1973), Kozlov and Markin (Kozlov and Markin, 1983) were the first to propose this mechanism. After close approach and the probable formation of a point-like protrusion (Fig. 1 Cb) (Efrat *et al.*, 2007) a subsequent deformation of two bilayers establishes a first connection between the two proximal lipid bilayer leaflets after dehydration of the initial site of contact (Kozlov and Markin, 1983; L. V. Chernomordik and Kozlov, 2003). This so called fusion stalk (Fig. 1 Ba) would comprise two highly curved proximal monolayers which subsequently expands radially into a hemifusion diaphragm (HD) with the distal membrane leaflets and the aqueous luminal contents remaining separated (Fig. 1 Ab, Bb and Cd) (L. V. Chernomordik *et al.*, 1987; Melikyan *et al.*, 1995; L. V. Chernomordik and Kozlov, 2003). Opening of an aqueous fusion pore within the HD would then allow for a connection between the opposing formerly separated compartments (Fig. 1 Ac and Cc). Besides a further irreversible enlargement of small fusion pores, closing of early fusion pores and even reversibility of hemifusion intermediates was found resulting again in the initial state of two separate bilayers (L. V. Chernomordik and Kozlov, 2008; Lentz *et al.*, 2000; Chanturiya *et al.*, 1997; Melikyan *et al.*, 1993; Giraudo *et al.*, 2005). For intracellular fusion events also a transient opening of a small pore releasing the vesicle content was observed by capacitance measurements (Klyachko and Jackson, 2002; Alvarez de Toledo *et al.*, 1993; Neher and Marty, 1982) and amperometry (Alvarez de Toledo *et al.*, 1993; C. T. Wang *et al.*,

2003). This was termed ‘kiss-and-run mechanism’, in which the vesicle would pull back and seal itself again instead of merging completely with the plasma membrane.

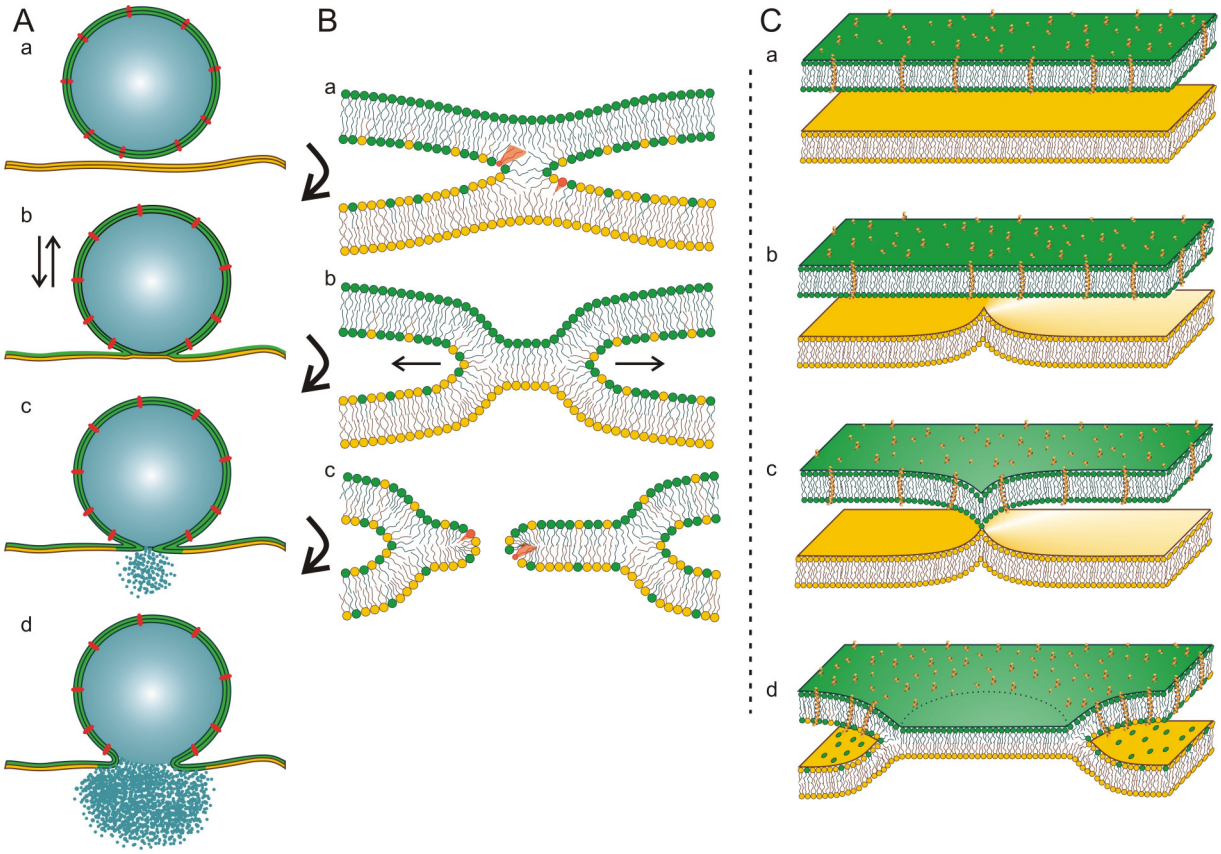

Fig. 1: Hemifusion. (**A**) Sequence of fusion with reversible attachment of both bilayers (**a**), formation of a hemifusion intermediate, where the outer contacting membrane leaflet is continuous allowing for lipid redistribution (**b**), opening of a first small fusion pore (**c**) that irreversibly expands and allows for content mixing (**d**). (**B**) Detailed view of fusion intermediates: stalk with a negative curvature (**a**), expanding diaphragm (**b**) and fusion pore with a positive curvature (**c**). Note that the cone-shaped lipid like PE and the inverted-cone-shape of e.g. LPC either enhance or inhibit the formation of the respective intermediate due to the required curvature. Also, tilting of the hydrocarbon chains allows filling the hydrophobic interstices that would otherwise have a huge energy deficit. (**C**) Illustrates the sequestering of transmembrane peptides (gold) from the forming HD. Note that in the outer membrane leaflet lipid mixing occurs while inner leaflet mixing only takes place after HD rupture (shown in Bc).

Hemifusion turned out to be a key intermediate not only in protein-free model membrane systems but also in the biological fusion pathways of viral fusion (L. V. Chernomordik and Kozlov, 2003; L. V. Chernomordik *et al.*, 1998; Armstrong *et al.*, 2000; Kemble *et al.*, 1994; Melikyan *et al.*, 1999; Nussler *et al.*, 1997; Cleverley and Lenard, 1998), intracellular fusion

(Liu *et al.*, 2008; Hofmann *et al.*, 2006; Jahn and Scheller, 2006; Lu *et al.*, 2005; Reese *et al.*, 2005; Xu *et al.*, 2005; Giraudo *et al.*, 2005; L. V. Chernomordik *et al.*, 1993; Rizo, 2006; Yoon *et al.*, 2006; Jun and Wickner, 2007) and recently also in developmental fusion (Podbilewicz *et al.*, 2006) evidence for a hemifusion intermediate was found.

1.2.1.1 Characteristics of the fusogens

The hydrophobic effect driving the self-assembly of lipids provides membranes with an immense stability (Tanford, 1980). Eventually, membrane merger is thermodynamically favourable, but on this way a huge energy barrier has to be overcome (Harrison, 2008). Since membrane merger requires rearrangement of lipids, it is not surprising that this remodelling of the bilayer needs energy input without which bilayers would not fuse even upon long-lasting and close contact (L. V. Chernomordik *et al.*, 2006). In protein-free model systems membrane fusion could be triggered by dehydration using ions or synthetic fusogenic molecules bringing the bilayers into very close apposition separated by less than 1 nm (Yang and Huang, 2003; Lentz, 2007; Chanturiya *et al.*, 1997). Lowering the energy barrier for fusion of biological membranes by generating bilayer stresses (Graham and Kozlov, 2010; Kozlov *et al.*, 2010), membrane merger can be accomplished by fusogenic proteins (L. V. Chernomordik and Kozlov, 2008; Jahn *et al.*, 2003) using either a hairpin or a zipper like mechanism in the viral or intracellular fusion pathway, respectively.

1.2.1.2 Viral fusion pathway

Influenza virus hemagglutinin (HA) is the best characterized biological fusogen to promote membrane fusion (White, 1995). Influenza virus itself is usually spherical with 80-120 nm in diameter. HA and neuraminidase are the two glycoproteins embedded in the viral lipid envelope surrounding the nuclear capsid formed by the matrix protein M1. The capsid holds the genetic material embedded in eight viral ribonucleoprotein (vRNP) complexes. The structure of HA in the pre-fusion state in progeny virus particles was solved in 1981 (Wilson *et al.*, 1981). Organized in a homotrimeric form the HA precursor protein (HA0) is proteolytically cleaved in the trans-Golgi network during transport to the plasma membrane providing two still disulfide-linked subunits, HA1 and HA2 (Eckert and Kim, 2001). In the first step of cell entry the globular domain of HA1 (50 kDa) interacts with sialic acids of the

cell-surface receptors, glycolipids or glycoproteins, on the target cell (Weis *et al.*, 1988) bringing the two membranes into close proximity.

Since parts of the plasma membrane are constantly taken up via endocytosis, a special signal might not be required for the endocytotic uptake of the virus into an endosome (Harrison, 2008). Large-scale conformational changes of HA2 (26 kDa) are triggered upon endocytic uptake of the virus and acidification (pH~5) in the endosome. A major conformational change within the protein is a loop-to-helix transition where the loop connecting the two α-helices folds into a helix (Fig. 2 Bc) forming an extended triple-stranded coiled-coil structure (spring-loaded mechanism) (Carr and Kim, 1993) resulting in the exposure of the first 20-25 membrane-interacting amphiphilic residues of the N-terminus of the HA2 that were buried in a pocket inside the HA trimers until then (Skehel and Wiley, 1998). For other viral fusion proteins like gp41 of HIV, this characteristic conformational change is caused by receptor binding at the plasma membrane. The formation of the extended coiled-coil intermediates was also found for gp41 of HIV (Weissenhorn *et al.*, 1997; Chan *et al.*, 1997; Tan *et al.*, 1997) and SIV (Malashkevich *et al.*, 1998; Caffrey *et al.*, 1998), GP2 of Ebola virus (Weissenhorn *et al.*, 1998; Malashkevich *et al.*, 1999), F protein of paramyxovirus SV5 (Baker *et al.*, 1999), F protein of Human respiratory syncytial virus (Zhao *et al.*, 2000) and gp21 from human T cell leukemia virus (Kobe *et al.*, 1999),

The drop in pH in the endosome leads to a protonation of HA1 causing repulsion between the HA1 subunits in the trimeric HA and a partial opening of the distal HA1 parts. In a computational approach the interactions between HA2 and water molecules, now able to enter the generated void, have been shown to be the major driving force for the loop-to-helix transition of HA2 (Q. Huang *et al.*, 2009). These findings are in line with the experimental results that the HA2 coiled-coil structure is stably formed at neutral pH as well and, hence, does not require an acidic pH. Caused by the conformational change the N-terminus of HA2, the so called fusion peptide, is now able to interact with the apposed target membrane (Eckert and Kim, 2001; Jahn *et al.*, 2003; Skehel and Wiley, 2000). It was shown that the peptide is not inserted trans-membrane through the target membrane, but is positioned deeply at the interface between the acyl chains and the polar heads of the lipids (Fig. 2 Bd). Combining nuclear magnetic resonance (NMR) and electron paramagnetic resonance (EPR) data, it was found that at pH 5, a realignment of charged residues within the peptide perturbs the lipid packing and might thus facilitate the lipid mixing between the fusing membranes (Han *et al.*, 2001).

The major step in the conformational changes of HA is the reorientation of the C-terminal region with the transmembrane anchor of HA2 folding back to become parallel to the trimeric coiled-coil at the N-terminal part with the fusion peptide to form a hairpin structure. This refolding of HA1 leads to the post-fusion conformation of HA (Bullough *et al.*, 1994) and completes the fusion bringing fusion peptide and transmembrane peptide together in the same, now merged membrane (Fig. 2 Be) (Wharton *et al.*, 1995). In this step the three-fold symmetry of the C-terminus must be broken (Weissenhorn *et al.*, 2007).

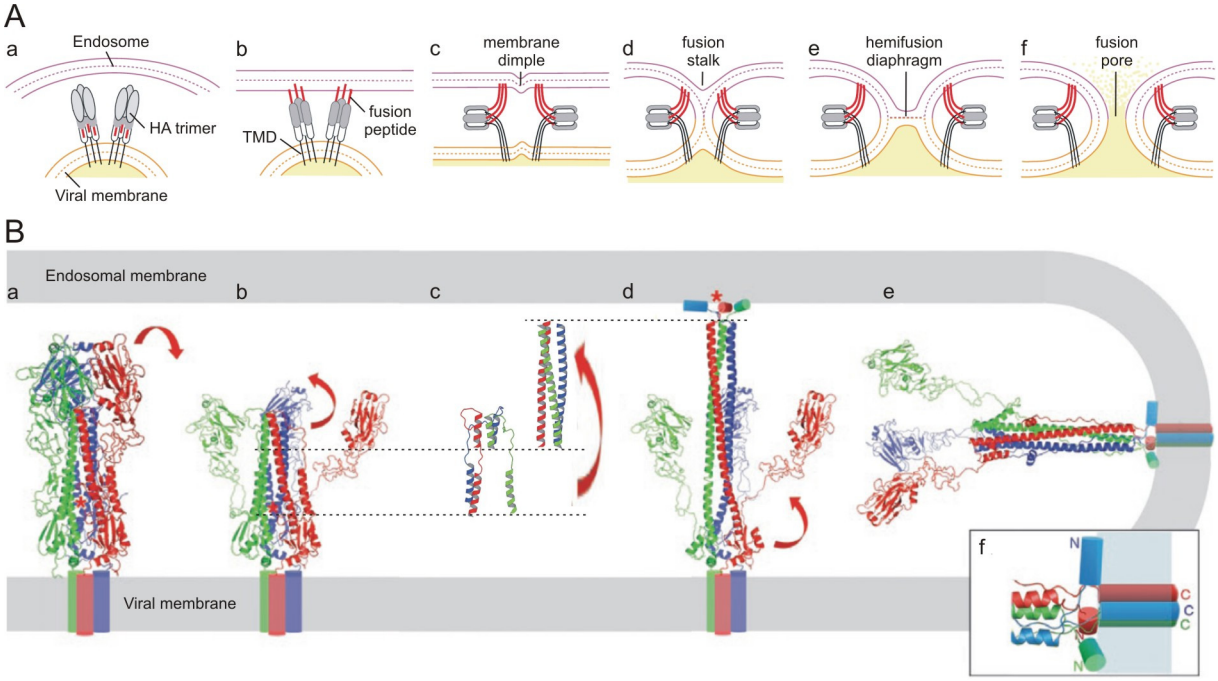

Fig. 2: HA fusion. (**A**) Sequence of events in fusion of viral and host cell membranes. HA trimer in pre-fusion conformation, with the fusion peptide (red) buried in the trimeric structure (**a**). Extended intermediate of HA with the fusion peptide inserted into the endosomal membrane (**b**). Collapse of extended conformation deforming the membrane (**c**). Connection of the membrane dimples forming a hemifusion stalk (**d**). Expansion of the stalk leads to the formation of a hemifusion diaphragm (**e**) within which a fusion pore opens up (**f**). (**B**) Proposed sequence of conformational changes with influenza virus hemagglutinin (HA): Pre-fusion conformation of the HA trimer (**a**). After receptor binding the HA1 subunits dissociates (**b**) allowing for the loop-to-helix transition to form the coiled-coil structure within HA2 (**c**) causing the insertion of the N-terminal fusion peptide of HA2 into the target membrane (**d**). Refolding of the HA2 subunit into a hairpin like structure (**e**) brings fusion peptides and transmembrane anchors together in the same membrane forming an N-cap structure (**f**). This interaction is supposed to support the opening of a fusion pore. Figures adapted from: Expert reviews in molecular medicine, 2001 and (Harrison, 2008).

1.2.1.3 Secretory fusion pathway

Based on current knowledge, membrane fusion of all steps of the intracellular pathway like the synaptic vesicle exocytosis are mediated by a specialized set of SNARE proteins (for detailed reviews see (Jahn and Scheller, 2006; Sudhof and Rothman, 2009)). SNARE mediated fusion employs three different proteins located in both opposing membranes destined to fuse. For example, for synaptic vesicle exocytosis syntaxin and SNAP-25 are located in the cell membrane, whereas synaptobrevin (or VAMP) is anchored in the vesicular membrane. Interaction of SNARE proteins leads to the formation of a ternary SNARE docking complex followed by a zipper like mechanism leading to a stable four-helix bundle that brings the two membranes together. The free energy released in the formation of the helix bundle is a significant step to enable membrane fusion (Sutton *et al.*, 1998). These binding energies in between the four-helix bundle were recently determined to be about 35 k_BT for an intermediate SNARE complex, which was only assembled over about 60 % - 80 % of its full length. This almost corresponds to the energy that is necessary to initiate the fusion of the outer lipid leaflet, i.e. hemifusion (F. Li *et al.*, 2007; Rizo and Dai, 2007).

1.2.1.4 Developmental fusion pathway

The situation in the developmental fusion pathway is much less clear than in viral or intracellular membrane merger and the players are much harder to identify compared to the simple viral systems with only a few proteins in total. However, in the nematode *C. elegans* for example, a set of developmental fusogens that must be present in both of the cell membranes destined to fuse could be identified (Mohler *et al.*, 2002; Sapir *et al.*, 2007), for a review see (Oren-Suissa and Podbilewicz, 2007; E. H. Chen and Olson, 2005). From fusion failure phenotypes of *C. elegans* the FF proteins could be identified as essential for organogenesis of e.g. epidermis and uterus. They display key structural elements similar to SNAREs or viral fusogens with a long extracellular part followed by a predicted transmembrane segment and a short intracellular tail at the C-terminus (Sapir *et al.*, 2007). Although the exact conformational pathway is not clear yet, a similar zipper-like mechanism as in viral or SNARE-mediated fusion was proposed (Sapir *et al.*, 2007; Oren-Suissa and Podbilewicz, 2007) and indications for a fusion pathway including a hemifusion intermediate were found, characterized by membrane merger without mixing of the cytoplasmic content (Podbilewicz *et al.*, 2006).

1.2.2 Lipidic character of membrane fusion

With formation of their hairpin or zipper-like motif fusion proteins have the ability to provide the energy for membrane fusion by structural rearrangements within the protein triggering a lipid rearrangement that finally results in the formation of a stalk. Anchored in both opposing membranes, the fusion proteins probably cause a dimple-like membrane bending towards the juxtaposed bilayer providing a protein free spot, accumulating bending energy and primed for fusion (Kozlov and Chernomordik, 1998; Kuzmin *et al.*, 2001; L. V. Chernomordik and Kozlov, 2003; L. V. Chernomordik and Kozlov, 2008). As reviewed in detail by Chernomordik and Kozlov (L. V. Chernomordik and Kozlov, 2003), the energy required for stalk formation is dependent on the lipid composition of the fusing membrane leaflets. In the contacting monolayer inverted-cone-shaped lipids like lysophosphatidylcholine (LPC) with a positive spontaneous curvature arching in direction of the lipid headgroup when forming a lipid monolayer were found to inhibit fusion (Fig. 1 Ba) of protein-free bilayers (L. V. Chernomordik and Kozlov, 2003) and of biological membranes in viral (L. V. Chernomordik *et al.*, 1993; Yeagle *et al.*, 1994; Gaudin, 2000; Melikyan *et al.*, 2000; Russell *et al.*, 2001) and intracellular fusion (L. Chernomordik, 1996) as well as in a reduced SNARE-like model system (Robson Marsden *et al.*, 2009).

In contrast, cone shaped lipids with a negative spontaneous curvature like phosphatidylethanolamine (PE) arching towards the lipid fatty acids in a lipid monolayer are promoting the formation of the hemifusion intermediate in the contacting membrane leaflets (Fig. 1 Ba) in protein-free (L. V. Chernomordik and Kozlov, 2003) as well as in biological membrane fusion events (Gaudin, 2000; L. Chernomordik, 1996; L. V. Chernomordik *et al.*, 1997). Interestingly, PE was very recently found to reduce the number of SNARE complexes needed to support membrane fusion to only three, although the probability of fusion was reduced in the model system with reconstituted SNAREs observing single-vesicle fusion events (Domanska *et al.*, 2010).

For the formation of a fusion pore within the HD, which is lined with polar lipid headgroups, (L. V. Chernomordik *et al.*, 1987) the lipid profile properties are reversed. Here, the inverted-cone-shaped LPC was found to promote the pore opening when incorporated into the distal monolayer (Fig. 1 Bc) in viral fusion of HA (L. V. Chernomordik *et al.*, 1998; Melikyan *et al.*, 1997; Razinkov *et al.*, 1998) and G protein (Gaudin, 2000) and in case of SNARE-mediated fusion (Grote *et al.*, 2000; Amatore *et al.*, 2006).

Another player driving the membrane fusion is membrane tension as shown in experiments (Cohen *et al.*, 1980; L. V. Chernomordik *et al.*, 1987; Ohki, 1982; Nikolaus *et al.*, 2010b) and simulations (Shillcock and Lipowsky, 2005; Katsov *et al.*, 2004). Lateral membrane tension tries to reduce the membrane area. Simulations show that increasing tension reduces the energy barrier for fusion which increases the frequency of fusion events in turn (Grafmuller *et al.*, 2009). Fusion of two bilayers is not the only possibility to relax tension. Besides hemi- and full fusion, bilayer rupture is an alternative pathway for relaxation of induced tension (Shillcock and Lipowsky, 2005). In experiments, it was observed that addition of e.g. divalent cations to protein-free, negatively charged bilayers creates an additional lateral tension within the membrane by selectively reducing the outer monolayer area of vesicular bilayers (Ohki, 1982; Sinn *et al.*, 2006). HD formation meets with this requirement as the merger of the outer leaflets during HD formation compresses the outer contacting monolayer area (Grafmuller *et al.*, 2009). In biological membrane fusion, lateral tension drives stalk expansion (Katsov *et al.*, 2004) as well as opening and expansion of a fusion pore within the forming HD (L. V. Chernomordik *et al.*, 2006; L. V. Chernomordik and Kozlov, 2003). Fusion proteins are able to generate tension (Y. A. Chen and Scheller, 2001; L. V. Chernomordik and Kozlov, 2003; Zimmerberg and Chernomordik, 1999).

1.2.3 Alternative fusion pathways

Given the findings that both, protein-free and biological membrane fusion, probably proceed through the same stalk – hemifusion – fusion pore intermediates and that it can – depending on the contacting or distal monolayer – be either inhibited or promoted by lipids with a nonzero curvature, respectively, implies that the forming pore is lipid-lined having a rim with a very high curvature in the monolayer forming the lipid pore (L. V. Chernomordik *et al.*, 1998; L. V. Chernomordik and Kozlov, 2008). Thus, although fusion proteins must be present in proximity to the emerging fusion pore, their membrane anchors are not exclusively lining the pore edges. The fusion pore connecting the two membrane enclosed compartments was found to be dominated by lipids (lipidic pore model, see above). To give a more complete overview, other proposed membrane fusion models will be introduced shortly. Lipid lining of the pore is in contrast to the proposed proteinaceous fusion pore model, where the entire connection between to fusing bilayers is established by transmembrane proteins. These proteins would form a pore in each of the juxtaposed membranes that subsequently align to

establish a channel-like gap junction connecting both luminal reservoirs (Fig. 3 A) (Tse *et al.*, 1993; Lindau and Almers, 1995; Jackson and Chapman, 2006). The edges of the pore would first be lined by proteins and only in a second step lipids would invade the area in between the protein subunits and remodel the two bilayers into one. The question of how lipids could enter this arrangement and how the double ring of proteins forming the gap junction-like pore would disassemble is not solved yet (Jahn and Scheller, 2006). Problematic about this model is also that either entirely hydrophobic transmembrane domains would be exposed on one side to an aqueous polar environment in the open channel-like ensemble or an amphiphilic protein segment would be buried in the hydrophobic lipid environment before channel formation. Both situations would be energetically unfavourable. EPR data, however, showed that the transmembrane helix resides in the nonpolar bilayer environment (Xu *et al.*, 2005). Chimera fusion proteins with swapped transmembrane domains are still able to mediate fusion thus also contradicting the hypothesis of protein-lined fusion pores. The finding that TMDs with a wide range of sequences are still able to mediate fusion argues against the possibility that the TMD lines an aqueous pore, where, as outlined above, a rather specific arrangement of polar and apolar residues would be necessary to face the water filled pore and the hydrophobic lipid membrane, respectively (Melikyan *et al.*, 1999). Besides the latter considerations it has been found that GPI-anchored hemagglutinin without the transmembrane domain is still able to induce small non enlarging fusion pores (Markosyan *et al.*, 2000).

Another fusion pathway leading to fusion through hemifusion is the extended lipid conformation where each acyl chain of a phospholipid is embedded in each of the contacting outer monolayer of two juxtaposed membranes leaving the lipid headgroup in the interface acting as an amphiphilic zipper on the way to hemifusion without a stalk intermediate (Fig. 3 B) (Kinnunen, 1992; Kinnunen and Holopainen, 2000). So far, no lipids were found in the extended conformation by coarse-grained and all-atom molecular dynamics simulation (Smeijers *et al.*, 2006; Ohta-Iino *et al.*, 2001; Kasson *et al.*, 2010).

In yet another pathway, fusion is promoted around a vertex ring in vacuole fusion (Fig. 3 C) (Jun and Wickner, 2007), where proteins regulating the fusion process assemble. On the way to fusion a ring-shaped HD would occur at the vertex protein ring leaving an intraluminal vesicle inside the fused vacuole lumen.

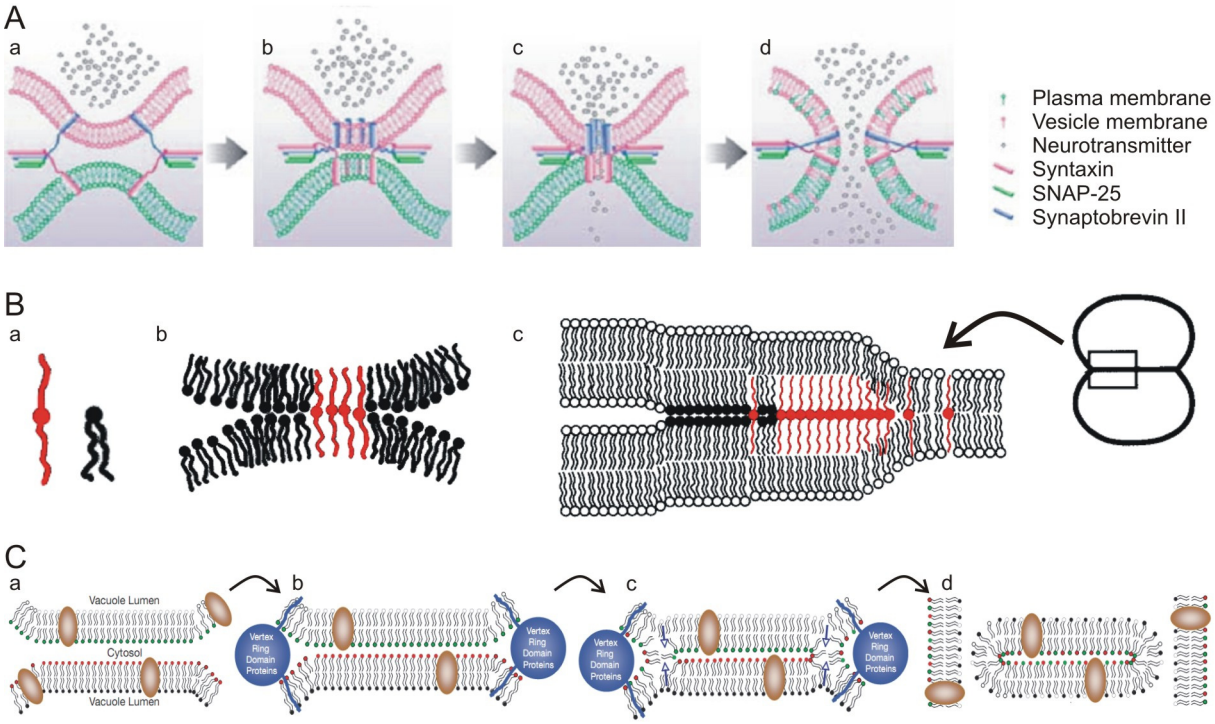

Fig. 3: Alternative fusion pathways. (**A**) In the protein-pore model the fusion pore is formed by transmembrane anchors of fusion proteins e.g. SNAREs (**a** - **c**). Upon expansion of the pore the TM anchors separate laterally and lipids are incorporated into the pore leading to bilayer merger (**d**). (**B**) Fusion model using lipids in the extended conformation (**a**) stretching an acyl chain into each of the contacting bilayers (**b**) finally leading to merging of two bilayers into one (**c**). (**C**) Upon close approach (**a**) a vertex ring of proteins (**b**) promotes the formation of a hemifusion intermediate around a vertex ring (**c**). Full fusion then results also in the formation of intraluminal membrane vesicle (**d**). Figures adapted from: (Jackson and Chapman, 2006; Kinnunen, 1992; Kinnunen and Holopainen, 2000; Jun and Wickner, 2007).

1.2.4 Role of the transmembrane membrane anchor

Stable transmembrane anchoring of the fusion proteins in the membranes is crucial for their functionality. Indeed, all fusion proteins are anchored in the juxtaposed bilayers destined to fuse. Trans-SNARE pairs are both anchored in the opposed bilayers by transmembrane domains. Viral fusion proteins are anchored transmembrane in the viral envelope and establish the contact to the endosomal membrane of the target cell by insertion of the fusion peptide (see below). Replacing the TMD by a more flexible lipid anchor like geranylgeranyl or glycosylphosphatidylinositol (GPI) residing only in the contacting monolayer mostly allows only for lipid mixing but impedes fusion pore formation. These observations suggest that the fusion pathway is arrested in the hemifusion intermediate. It was found for biological fusion

in the viral (Weiss and White, 1993; Salzwedel *et al.*, 1993; Kemble *et al.*, 1994; Melikyan *et al.*, 1995; Tong and Compans, 2000) and intracellular fusion pathways (Y. Wang *et al.*, 2001; Grote *et al.*, 2000) and also in model systems for reconstituted SNAREs (McNew *et al.*, 1999). Bilayer contact and HD formation might be driven by SNARE protein induced bending stresses transmitted by a linker region from the four-helix bundle to the transmembrane anchor within the membrane. Note that fusogens can only do so if their bending rigidity exceeds the rigidity of the bilayer that has to be bent in order to establish membrane contact. Typically, lipid bilayer bending rigidity is in the order of 10 kcal/mol (L. V. Chernomordik *et al.*, 2006), whereas protein stiffness could not been measured. By molecular dynamic simulations the connecting linker between the SNARE zipper region and the transmembrane anchor could be shown to be rigid enough to transmit the energy to disturb the bilayer integrity and to increase the fusion rate by two to five orders of magnitude (Knecht and Grubmuller, 2003). Also mutation of semiconserved residues or shortening of the TMD below a critical length that ensures contact with both bilayer leaflets inhibits fusion (Schroth-Diez *et al.*, 1998; Melikyan *et al.*, 1995; Melikyan *et al.*, 1999; Kozerski *et al.*, 2000; Armstrong *et al.*, 2000; Cleverley and Lenard, 1998; Cleverley *et al.*, 1997).

Additionally to mere anchoring leading to an apposition of the membranes destined to fuse evidence is accumulating that the membrane anchors also ensure a destabilisation of the bilayers (McNew *et al.*, 2000; Kesavan *et al.*, 2007; Siddiqui *et al.*, 2007; Abdulreda *et al.*, 2008) facilitating lipid rearrangement on the way to fusion pore formation. Isolated peptides derived from the transmembrane domain of SNARE proteins alone also promoted fusion (Langosch *et al.*, 2001; Hofmann *et al.*, 2006; Siegel *et al.*, 2006). Insertion of the TMDs in a 35° to 55° angle relative to the membrane normal depending on the lipids in the bilayer might account for the lipid mixing activity (Bowen and Brunger, 2006; Thomas and Brasseur, 2006). Studies using model transmembrane peptides of influenza HA showed an increased acyl chain ordering associated with a dehydration of the bilayer surface (Tatulian and Tamm, 2000; Tamm, 2003) as it was also shown for the fusion peptide of HA (Han *et al.*, 1999). Bilayer surface dehydration might facilitate the onset of a hemifusion intermediate as it reduces the hydration repulsion between the apposing bilayers (Tamm, 2003). Finally, SNAREs seem to recruit certain lipids like DAG interrupting the bilayer integrity or phosphoinositides and phosphatidic acid (PA) for synergetic assembly of the fusion competent SNARE complexes (Das and Rand, 1984; Siegel *et al.*, 1989; Vicogne *et al.*, 2006; Mima *et al.*, 2008)

Furthermore, in most viral families the short cytoplasmic tail (CT) being C-terminal of the TMD does not seem not to be required for fusion (Melikyan *et al.*, 1999, detailed review see Schroth-Diez *et al.*, 2000).

1.2.5 Role of the viral fusion peptide

In viral fusion the contact to the target cell membrane is established by insertion of the fusion peptide, a 10-30 amino acid long protein part, located either N-terminally or within a protein loop. For influenza HA the fusion peptide was found in a predominantly helical, amphipathic structure with a kink at the polar Asn-12 residue. It is located at the interface between the lipid headgroups and the hydrophobic hydrocarbon region (Han *et al.*, 2001; Q. Huang *et al.*, 2004; Vaidya *et al.*, 2010). As the N-terminus of HA2 is one of the most conserved regions of HA, it is not surprising that its kinked structure is intimately involved in the fusion process. A linear mutant was found to abolish fusion (Y. Li *et al.*, 2005). Binding energy of the HA fusion peptide at neutral pH was determined to be ~15 kT resulting in a force of ~20 pN to pull back a peptide of ~3 nm length (Kozlov and Chernomordik, 1998; Ishiguro *et al.*, 1996). This provides a sufficient attachment of the viral fusion proteins for downstream fusion processes. Intercalation of the hydrophobic residues of the amphipathic fusion peptide into the contacting juxtaposed monolayer (Gibbons *et al.*, 2004; Roche *et al.*, 2006; Heldwein *et al.*, 2006) probably introduces membrane curvature bending the membrane towards the viral membrane similarly to curvature mediated by BAR (Bin/Amphiphysin/Rvs) domains (Zimmerberg and Kozlov, 2006). Assuming a ring-like alignment of several fusion protein trimers many fusion peptides are plunged into the target membrane interface upon activation causing the formation of a dimple stressed at its tip (Weissenhorn *et al.*, 2007; L. V. Chernomordik and Kozlov, 2005; Gibbons *et al.*, 2004; Kozlov and Chernomordik, 1998).

An oblique insertion angle between 25 and 38° relative to the membrane normal was found for the HA fusion peptide by NMR and EPR (Han *et al.*, 2001; Y. Li *et al.*, 2005; Macosko *et al.*, 1997) agreeing well with a coarse-grained MD simulation finding an orientation of ~30° (Vaidya *et al.*, 2010; Lague *et al.*, 2005). It should be pointed out that the oblique insertion angles of the fusion peptide are matching those found for the transmembrane anchors emphasising a possible similarity in function of inducing curvature and thus bending the membrane dimples towards one another.

When the structural rearrangement within e.g. the trimer of HA is completed, the linker regions of the fusion peptides to the coiled-coil and N-terminus of the TMD interact and form a N-cap structure (Fig. 2 Bf) (Harrison, 2008; J. Chen *et al.*, 1999; Borrego-Diaz *et al.*, 2003; H. E. Park *et al.*, 2003). This interaction of transmembrane anchor and fusion peptide is supposed to support the hemifusion to fusion transition and open up an expanding fusion pore (Qiao *et al.*, 1999; Weissenhorn *et al.*, 1997; Melikyan *et al.*, 2000).

1.2.6 Taking a glance at hemifusion – simulation and visualization

Beginning in the 1980s, membrane fusion was explored using classical physics in a continuum approach based first on the elastic model (Kozlov and Markin, 1983; Kozlovsky *et al.*, 2002; Kozlovsky and Kozlov, 2002) and later on the self-consistent field theory of membrane sheets (Katsov *et al.*, 2006; Marrink and Mark, 2003; J. Y. Lee and Schick, 2007). The aim was to find the lowest energy transition state leading to the stalk model in the fusion through hemifusion pathway. As computing power went up, *in silico* experiments enabled visualization of the fusion process up to atomic details (reviewed in (L. V. Chernomordik and Kozlov, 2008)). Computer simulations of membrane fusion were performed from Brownian dynamics (Noguchi and Takasu, 2001) and coarse-grained molecular dynamics (MD) (Marrink and Tieleman, 2002; Marrink and Mark, 2003; Stevens *et al.*, 2003; Smeijers *et al.*, 2006; Kasson *et al.*, 2006; Kasson *et al.*, 2007) to dissipative particle dynamics (DPD) (Grafmuller *et al.*, 2007; Shillcock and Lipowsky, 2005; D. W. Li and Liu, 2005) and atomistic MD (Knecht *et al.*, 2006; Knecht and Marrink, 2007; Kasson *et al.*, 2010). In the different simulation methods, fusion through the hemifusion intermediate is observed.

The hemifusion intermediate resembles two membrane enclosed compartments separated only by a single bilayer formed by the two formerly inner leaflets with the outer leaflets fused. Whereas the definition of hemifusion is quite simple and each step in the fusion through hemifusion pathway can be analyzed in great detail in computer simulations, the direct experimental verification and characterization of the HD turned out to be difficult due to its normally transient nature and very small size. Experimental verifiable criteria for a hemifusion intermediate are lipid mixing before content mixing, redistribution of outer leaflet lipids before inner ones, dependence on lipids with an certain intrinsic curvature and a sequestering of transmembrane proteins upon formation of an HD (Fig. 1). Especially in biological membrane fusion, HD detection is difficult. Lipid mixing can, for example, be

restricted by a fence of fusion protein membrane anchors leading to a so called “restricted” hemifusion intermediate as found in case of the viral fusion protein HA of influenza virus. Here, although a continuous connection is established, no lipid mixing occurs (L. V. Chernomordik *et al.*, 1998). On the contrary, hemifusion is difficult to detect when HD and fusion pore form very quickly one after the other. To slow down the transition from hemifusion to complete fusion and thus increasing the chance for the observation of the hemifusion intermediate, the number of fusion proteins can be reduced, the membrane anchor can be modified, or the temperature can be reduced (L. V. Chernomordik *et al.*, 2006).

Artificial membrane systems seem to offer an easier way to control the parameters influencing the fusion pathway such as lipid composition, membrane curvature, lateral membrane tension and intermembrane distance. In biological membrane fusion, however, a direct membrane contact is prevented by membrane proteins covering the bilayer surface keeping the lipid bilayers at a distance of 10-20 nm (L. V. Chernomordik *et al.*, 2006). Only after sequestering of these obstacles, some of these proteins are probably involved in membrane binding and fusion, the two apposing now protein-free membrane spots can bulge towards each other, probably mediated by the fusion protein transmembrane anchors. This dimple-like membrane bending towards the juxtaposed bilayer accumulates bending energy and charges the bilayer for fusion stalk formation (Kozlov and Chernomordik, 1998; Kuzmin *et al.*, 2001; L. V. Chernomordik and Kozlov, 2003; L. V. Chernomordik and Kozlov, 2008).

The existence of hemifusion intermediates in biological and model membrane fusion is supported by a number of observations. Formation of a fusion stalk-like structure was found after reducing the hydration from a stack of parallel phospholipid bilayers as judged by the electron density distribution from X-ray diffraction (Yang and Huang, 2002; Yang and Huang, 2003). A non-lamellar stalk structure was also proposed (Leikin *et al.*, 1987) supported by experiments using planar lipid bilayers (reviewed in (L. V. Chernomordik *et al.*, 1987)). Fusion of planar lipid membranes with liposomes was already demonstrated in 1980 (Cohen *et al.*, 1980; Zimmerberg *et al.*, 1980), whereas only later also the hemifusion intermediate could be detected using an advanced experimental setup combining simultaneous electrical and fluorescence measurements (Chanturiya *et al.*, 1997). Redistribution of lipids between two hemifused membranes can be followed experimentally by a fluorescence dequenching assay (Struck *et al.*, 1981). This assay can, however, only provide indirect evidence for a transient hemifusion intermediate (Langosch *et al.*, 2001). Incorporation of cone-shaped LPC in the outer membrane leaflet blocks hemifusion (cf. section 1.2.2). Addition of LPC was

indeed found to reversibly inhibit liposome fusion in a dose-dependent manner (L. Chernomordik *et al.*, 1995). Successive formation of aggregated vesicles and hemifusion intermediate was also found in liposome-liposome fusion of small unilamellar vesicles mediated by PEG (J. Lee and Lentz, 1997). Hemifused bilayers have also been found as metastable or stable intermediates in fusion of large unilamellar vesicles (LUVs) (Kuhl *et al.*, 1996 and ref. therein). A very recent study on LUV fusion comprising reconstituted SNAREs could not only identify lipid merger without content mixing and thus hemifusion, but was also able to show that the SNARE proteins alone were able to expand the fusion pore within the HD to a size large enough to transmit ~11 kDa cargo reporter molecules (Diao *et al.*, 2010). Additional incorporation of a water soluble dye into a liposome enables to determine that lipid mixing (redistribution of lipid-bound fluorophores) precedes content mixing (Wilschut *et al.*, 1980; J. Lee and Lentz, 1997). Using such an assay detecting lipid mixing and content release, it could recently be shown in a single-vesicle fusion assay driven by reconstituted SNAREs that even very fast fusion events, previously thought to result from prompt full fusion, are in fact productive hemifusion events thus proceeding through a hemifusion intermediate (T. Wang *et al.*, 2009). Fusion in biological systems was investigated using similar lipid mixing assays studying fusion between viruses and liposomes (Stegmann *et al.*, 1985), fusion protein (e.g. HA) expressing cells and red blood cells (RBCs) (Kemble *et al.*, 1994; Melikyan *et al.*, 1995; L. V. Chernomordik *et al.*, 1997; Frolov *et al.*, 2000) and cell-cell fusion (Cleverley and Lenard, 1998). An elegant lipid mixing assay was used by Nüssler *et al.* (Nussler *et al.*, 1997) to show hemifusion between HA expressing cells and RBCs by specifically labelling the inner and outer membrane leaflet of RBCs solely with different fluorescent lipid analogues thus able to determine hemifusion by an exclusive movement of the outer leaflet dye. Observation of single virus particles fusing to larger and therefore flat membrane patches provided information about distinct fusion intermediates like the time points of HD and fusion pore formation, but still not able to visualize the HD itself (Melikyan *et al.*, 2005; Imai *et al.*, 2006; Floyd *et al.*, 2008; Joo *et al.*, 2010). A first observation of a hemifusion intermediate in biological fusion was reported by Zampighi *et al.* (Zampighi *et al.*, 2006) using conical thin sectioning and electron tomography analysis of cortical synapses. A drawback of this method, which provides a high optical resolution, is that no kinetic information can be obtained.

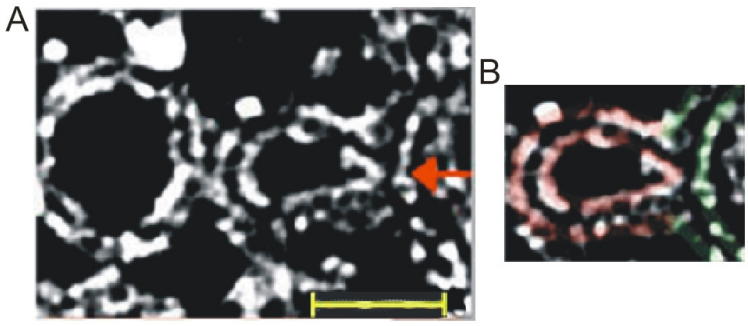

Fig. 4: Synaptic vesicle hemifused to the plasma membrane. Thin sectioning and conical electron tomography was used to determine the 3D structure of vesicles at the active zone. (**A**) Individual plane of hemifused vesicle (middle) with the plasma membrane (right). A second vesicle is only attached to the docked vesicle (left). (**B**) Illustration of small region of the active zone (green lines) and the docked vesicle (red lines) showing the HD. Bar corresponds to 50 nm. Image modified form (Zampighi *et al.*, 2006).

1.2.7 First direct visualization of protein-free HD formation

To demonstrate for the first time the displacement of transmembrane proteins within the fusion through hemifusion pathway and to use a well visible fluorescently labelled transmembrane marker to gather information about the kinetics of HD formation we devised a model system using giant unilamellar vesicles (GUVs). The size of this vesicle type turned out to be very useful to visualize the fusion process by fluorescence microscopy as shown previously (Lei and MacDonald, 2003; Lei and MacDonald, 2008; Pantazatos and MacDonald, 1999; Heuvingh *et al.*, 2004). This is to the best of our knowledge the first time extended protein-free HDs have been observed in a vesicle based system.

Adhesion and fusion of GUVs containing fluorescently labelled transmembrane peptides of fusogenic proteins in the presence of divalent cations was studied. To this end, tetramethylrhodamine (Rh)-labelled synthetic low-complexity hydrophobic model sequences (Rh-LV-Rh) that were designed to mimic the TMDs of SNARE proteins (Langosch *et al.*, 2001; Hofmann *et al.*, 2004) with a 16 amino acid hydrophobic core of leucine and valine flanked by lysine tripletts (Rh-LLV16-Rh: Rh-KKKKWLLVLLVLLVLLVLLVLKKKK-Rh; Rh-LV16-G8P9-Rh: Rh-KKKKWLVLVLVLGPVLVLVLVKKKK-Rh) and a 28 residues peptide (Rh-HA-TMD) corresponding to the TMD of influenza HA (strain A/Japan/305, Rh-ßA-ILAIYATVAGSLSLAIMMAGISFWMCSNKKK) were used. Additionally, a new type of synthetic stiff stick was used to demonstrate the structure independent principle of this assay.

1.3 Lipid domain specific protein sorting

1.3.1 Lipids – bilayer building blocks

As pointed out in the first part of the introduction, membranes are separating different compartments that enable a living cell to locally interrupt the development towards generally growing entropy and thus allow the cell to store information and energy e.g. in form of a proton gradient and to provide a restricted volume for certain chemical reactions. The main structural components within the membrane are lipids, amphiphilic molecules comprising a polar lipid head group and the hydrophobic fatty acid tails. Lipid self assembly, governed by the hydrophobic effect (Tanford, 1980), leads to the formation of spherical micelles or rather flat bilayers with the hydrophobic tails forming the core shielded from water, whereas the hydrophilic head groups face the aqueous surrounding. Besides compartmentalization, lipids like the phosphoinositides serve as second messengers in signal transduction processes and lipids also function as energy storage buffering e.g. triacylglycerols and steryl esters, therefore also providing fatty acids for new biosyntheses.

The lipid membrane functions as a platform for sorting membrane proteins. To understand the sorting ability of the membrane, one must consider its lipid components first. Three main classes of lipids are found in the eukaryotic membranes: glycerolipids, sphingolipids and sterols.

Glycerol forms the backbone of glycerolipids with two fatty acid chains ester-bound at position sn-1 and sn-2 (Fig. 5 A). The fatty acid in position 2 is often kinked due to a cis double bond decreasing the lipid packing density. Phosphatidic acid (PA) is formed by a phosphate at position sn-3, which can form further phosphate ester bonds with different head groups like choline (yielding phosphatidylcholine, PC), ethanolamine (phosphatidylethanol-amine, PE) and the negatively charged serine (phosphatidylserine, PS) and inositole (phosphatidylinositole, PI).

Sphingosine is the backbone for the second major class of lipids, the sphingolipids (Fig. 5 B). An amide linked fatty acid at the nitrogen yields ceramide (Cer). Cer with a phosphocholine head group becomes sphingomyelin (SM). Glycosphingolipids are created by addition of glucose to form glucosylceramide (GlcCer) and/or other monosaccharides. The tails of sphingolipids are commonly saturated allowing for a tighter packing and thus an increased lipid density.

Finally, sterols like the mammalian cholesterol (Fig. 5 C) with its planar four-ring structure and a tiny head group of only a hydroxyl group are able to incorporate in between the other lipids.

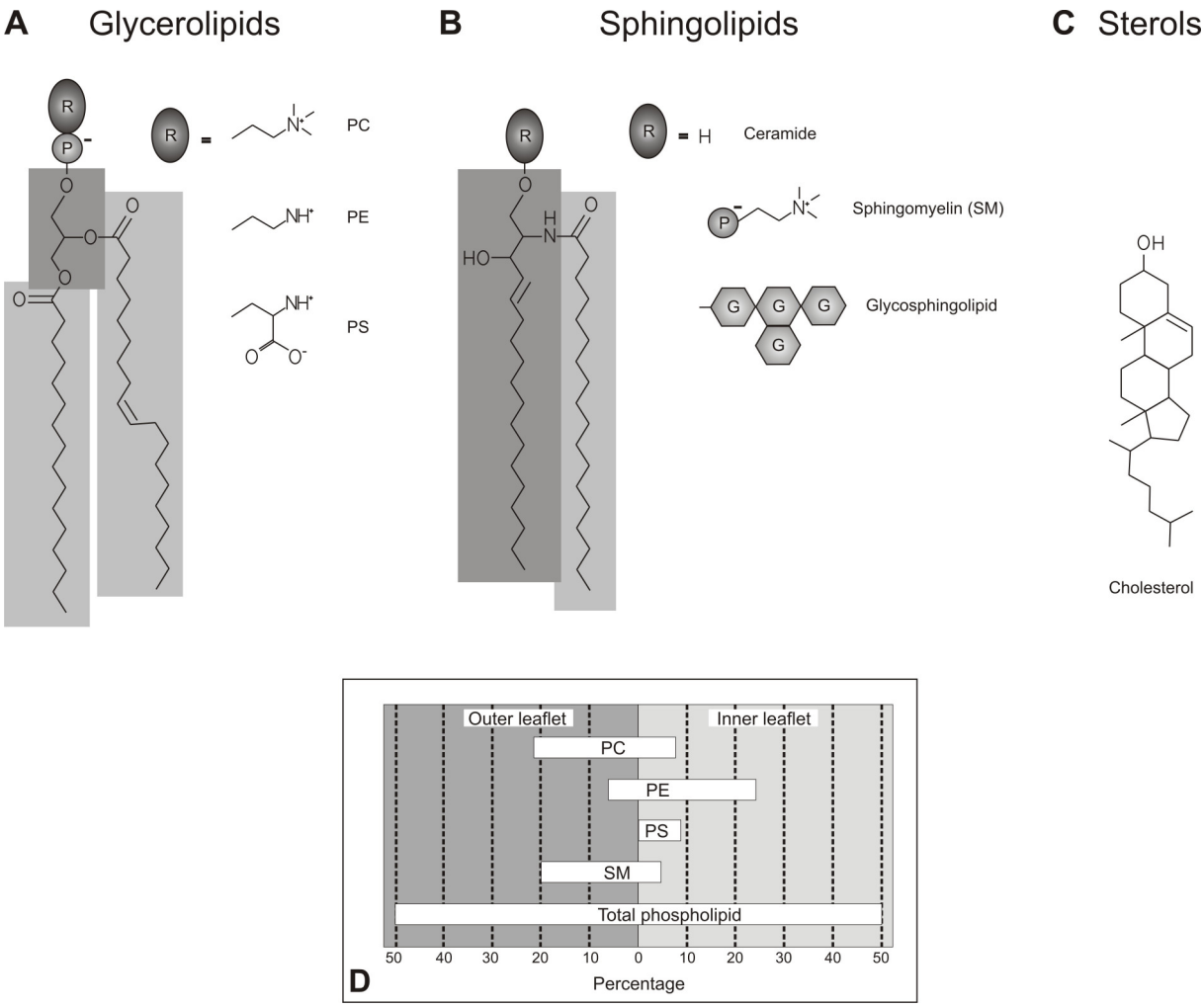

Fig. 5: Mammalian membrane lipid structures. Most common lipids in eukaryotic membranes are glycerophospholipids, sphingolipids and cholesterol. (**A**) Glycerol (dark grey shading) is the backbone within glycerolipids with fatty acids (light grey) ester-bound at position sn-1 and sn-2. A double bond in the sn-2 chain is common. Different head groups coupled at a phosphate at position sn-3 yield the most abundant zwitterionic phospholipids phosphatidylcholine (PC) and phosphatidylethanolamine (PE) or phosphatidylserine (PS) with an acidic net charge. (**B**) Sphingolipids are based on a sphingoid base (dark grey) with a saturated fatty acid (light grey) bound via an amide bond. A phosphocholine head group produces sphingomyelin (SM). A wide range of glycosphingolipids result from binding of one or more saccharides. (**C**) Four planar rings are the basic structure of sterols like cholesterol. (**D**) Asymmetric transbilayer lipid distribution in a cellular membrane on inner and outer bilayer leaflet, in mol%. Figure modified from (Rothman and Lenard, 1977).

The large variety of different building blocks for lipid head groups and tails results in a huge number of up to 500 lipid species in a cellular membrane (Poveda *et al.*, 2008). Given the possibility of a transbilayer and lateral asymmetric arrangement of different lipids, the cell puts a lot of energy into maintenance of this condition. A loss of asymmetry for PS in the plasma membrane, for example, which is present only on the inner membrane leaflet of viable cells due to sequestering by an aminophospholipid translocase (Holthuis and Levine, 2005), is recognized as an apoptosis signal when presented on the outer monolayer. In Fig. 5 D the asymmetric transbilayer lipid distribution of a eukaryotic plasma membrane is shown with negatively charged PS and PI as well as PE predominantly localized in the inner membrane leaflet, whereas PC and SM decorated with large glycosylated headgroups are found predominantly in the external leaflet. Additional 30-40 mol% of cholesterol (Holthuis and Levine, 2005) are distributed more within the external leaflet due to its higher affinity for SM due to its favourable packing ability (Pomorski *et al.*, 2001).

1.3.2 Biological membranes function as protein sorting platforms

Beside the transmembrane asymmetry, a lateral separation of lipids was found (Tillack *et al.*, 1983; van Meer *et al.*, 1987). In 1974, a change in the surface organization of plasma membrane lipids upon cooling was found (Petit and Edidin, 1974). Soon evidence started to accumulate that especially lipids like saturated long chain sphingolipids that have high melting temperatures would be organized in lateral domains. This developed further the concept of the fluid mosaic model of a cell membrane proposed by Singer and Nicolson (Singer and Nicolson, 1972), where membrane proteins were believed to be embedded in a homogeneous matrix of lipids. Proteins and lipids were thought to be randomly distributed. Simons and van Meer (Simons and van Meer, 1988) reported a distinct lipid composition in the apical and basolateral membranes in epithelial cells. The sorting of lipids together with membrane proteins already in the trans-Golgi network induced by a sorting signal was proposed. This signal would direct the transport vesicle toward their destined membrane. GPI-anchor and N-glycans or O-glycans attached to the proteins as well as lipid modifications and protein oligomerization are thought to act as an apical targeting signal (Lisanti *et al.*, 1989; Rajendran and Simons, 2005; Schuck and Simons, 2004). A basolateral transport might therefore take place in the absence of an apical signal (Simons and van Meer, 1988) or depend on di-leucine or tyrosine motifs as basolateral targeting signals (Rajendran and Simons,

2005). A lateral separation of lipids, so called lipid microdomains or lipid rafts, was proposed to be the foundation of these sorting processes.

1.3.3 Lipid rafts in biological membranes

Reminiscent of a wooden raft floating on water, lipid rafts were supposed to be afloat, freely diffusing and stable within a sea of the surrounding lipids. Rafts are enriched in sphingolipids and saturated phospholipids as well as cholesterol filling the interstices between the straight long saturated lipid tails below the lipids larger head groups, which was referred to as the umbrella model (J. Huang and Feigenson, 1999). Due to their saturated chains raft lipids lead to a thicker membrane width compared to the unsaturated acyl chains in the circumfluent nonraft membrane parts generating the raft-like image. Saturated lipids and cholesterol within rafts exhibit a higher degree of order compared to the unsaturated acyl chains in the nonraft bilayer (see below and cf. Fig. 7). As mentioned above, the main lipid constitutes of rafts, namely sphingolipids and cholesterol, are predominantly found in the exoplasmic membrane leaflet (Fig. 5). However, it has been hypothesized that a transbilayer coupling between the plasma membrane leaflets could induce a domain formation within the cytoplasmic leaflet and first experimental evidence in cells and in model systems point in that direction (Harder *et al.*, 1998; Gri *et al.*, 2004; Kusumi *et al.*, 2004; Collins and Keller, 2008; Kiessling *et al.*, 2006; Kiessling *et al.*, 2009). Whether the transbilayer coupling is generated by proteins (Devaux and Morris, 2004) or enabled by lipid interactions and interdigitation is still under discussion.

But what do rafts do? By including or excluding specifically certain proteins, rafts are able to locally change the protein concentration thus facilitating protein-protein interactions and functioning as transient signalling platforms (Varma and Mayor, 1998; Brown and London, 2000; Dykstra *et al.*, 2003; Sharma *et al.*, 2004; Holowka *et al.*, 2005; Sengupta *et al.*, 2007). Protein sorting is another field of duty for lipid rafts either in endocytic and exocytic pathways in trafficking (Schuck and Simons, 2004; Simons and Ikonen, 1997) or in the enrichment of viral proteins for the budding process of progeny virus particles as will be discussed later on (Luan *et al.*, 1995). Interestingly, rafts also seem related to membrane fusion (Rogasevskaia and Coorssen, 2006; Salaun *et al.*, 2004; Luan *et al.*, 1995). To what extend lipid-lipid and protein-lipid interactions are contributing to lipid raft formation is still under discussion (Poveda *et al.*, 2008).

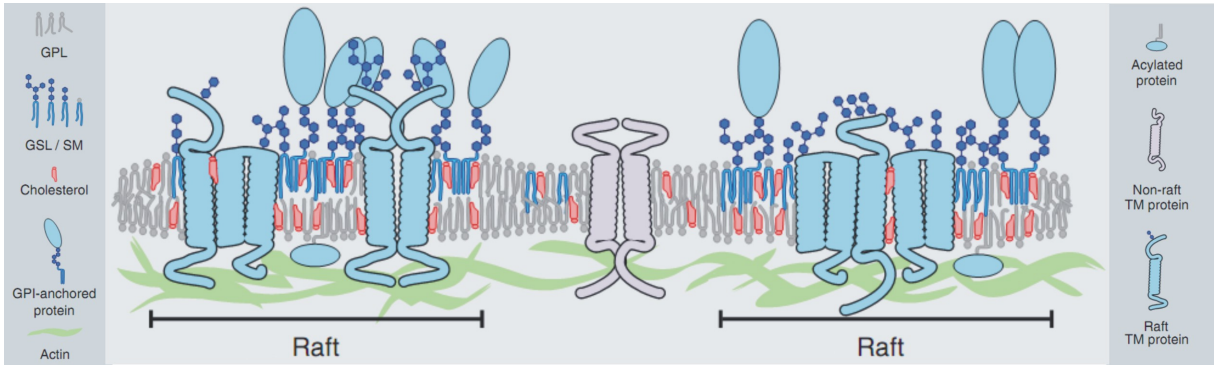

Fig. 6: Biological membrane rafts. Rafts enriched in cholesterol and glycosphingolipids (GSL) in the external and glycerophospholipids (GPL) with longer acyl chains predominantly on the cytoplasmic membrane leaflet. Integral raft associated transmembrane proteins partition into these domains accompanied by peripheral GPI-anchored and acylated proteins in the outer and inner leaflet, respectively. Shorter GPLs comprise the main component of the nonraft membrane areas including nonraft proteins. Anchoring of TM proteins to the actin cytoskeleton meshwork limits free protein and therefore also lipid diffusion. Figure is modified from (Lingwood and Simons, 2010).

1.3.4 Detection of lipid rafts in biological membranes

Lipid raft domains were first defined by their ability to resist treatment using non-ionic detergent like Triton X-100 at low temperatures (4°C) (Brown and Rose, 1992; Simons and Ikonen, 1997; London and Brown, 2000) and were therefore termed detergent resistant membranes (DRMs). Meanwhile, the detergents itself are under suspicion to induce lipid domains within the membrane as an artefact (Heerklotz, 2002; Munro, 2003; Lichtenberg *et al.*, 2005).

As membrane rafts are small in the range of 10-200 nm (Pike, 2006), direct visualization by conventional fluorescence microscopy is not possible. Therefore, various sophisticated biophysical techniques have been employed to study domain formation in cellular systems by observing either proteins or lipids. Fluorescence correlation techniques like FCS (fluorescence correlation spectroscopy) could show complex formation and that domain association of proteins is sensitive to cholesterol depletion and cytoskeleton meshwork detachment (Larson *et al.*, 2005; Wawrezinieck *et al.*, 2005; Lenne *et al.*, 2006). Single particle tracking (SPT) could demonstrate that lipids are confined to a limited area for a certain time (Kusumi and Suzuki, 2005; Dietrich *et al.*, 2002). And also by homo and hetero FRET (Förster resonance energy transfer) GPI-anchored proteins were found in nanoclusters consisting of only four or

less proteins (Meyer *et al.*, 2006; Mayor and Riezman, 2004; Sharma *et al.*, 2004; Kenworthy and Edidin, 1998; Varma and Mayor, 1998). Using FRET between carbocyanine lipids, nanoscopic laterally segregated ordered and disordered membrane domains have been identified that are sensitive to cholesterol variations (Sengupta *et al.*, 2007). Cholesterol sensitive protein clustering with established raft marker proteins was also found by fluorescence lifetime dependent FLIM-FRET measurements on hemagglutinin protein after depletion of the plasma membrane of living cells using methyl-β-cylodextrin (Engel *et al.*, 2010; Scolari *et al.*, 2009). As compared to the latter method probing protein clustering, the FLIM technique could also be applied recently to demonstrate domain formation for lipids (Stockl *et al.*, 2008; Stockl and Herrmann, 2010; Owen *et al.*, 2006; Margineanu *et al.*, 2007). Moreover, emerging super resolution microscopy technology like stimulated emission depletion (STED) pushing down Abbe's resolution limit of about 200 nm (Egner and Hell, 2005) could be used to finally visualize that GPI-anchored proteins are confined within less than 20 nm together with sphingolipids, but not with phospholipids, in a cholesterol sensitive way (Eggeling *et al.*, 2009).

1.3.5 Phase separation in model membrane systems

As the plasma membrane is complex and cellular rafts are transient, highly dynamic and small (Pike, 2006), their detection is difficult. They are, however, lipid bilayers and therefore insights are expected also from studying membrane model systems. As lipids differ in their head group as well as their tail length and saturation, they have different chemical and physical properties including their intrinsic curvature (cf. section 1.2.2) and melting temperature (T_m). Heated beyond their specific T_m phospholipids undergo a phase transition from a gel or solid ordered (S_o) phase to a fluid liquid disordered phase (Ld) (Fig. 7)(Gennis, 1989; Hancock, 2006). This behaviour at a given temperature is crucial for lipid domain formation since lipid acyl chains are tightly packed together in a rigid and straight conformation below T_m in the S_o phase and the lateral lipid mobility is highly restricted. Above T_m lipids are no longer restricted, but diffuse freely within the bilayer and their acyl chains become disordered and thus less densely packed due to trans-to-gauche isomerization introducing kinks to their structure. Due to this change the surface area of the lipid is increased, whereas the bilayer thickness is decreased by 10 to 15 %.

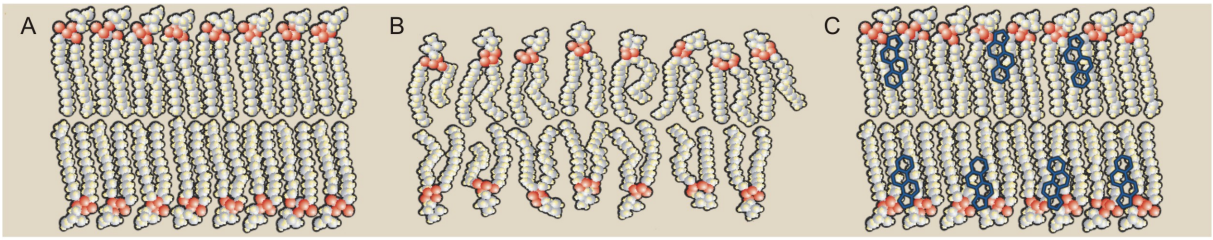

Fig. 7: Lipid phases in membranes. Membrane lipids shown in three different phases. (**A**) Rigid solid ordered phase, (**B**) Liquid disordered and (**C**) liquid ordered phase. For more information see text. Adapted from (Divito and Amara, 2009).

By introducing sufficient amounts of cholesterol to the bilayer, cholesterol moderates between the two phase regimes introducing a new liquid ordered phase (Lo) characterized by a high degree of order in the lipid tails, but with lateral mobility of the lipids themselves (Fig. 7 C). Due the very small, polar head compared to the four hydrophobic rings of cholesterol, it is not able to form bilayers by itself, but is therefore very well suited to incorporate into membranes. Cholesterol positions its polar OH-group at the interface between lipid headgroups and hydrophobic acyl chains, where it is able to form an H-bond with the amide carbonyl group of the SM head group (Bittman *et al.*, 1994). The image of cholesterol clenched under the larger polar head groups of sphingomyelin led to the so called umbrella model (J. Huang and Feigenson, 1999). Tight packing of cholesterol to the acyl chains leads to a condensing effect in the surrounding lipids (McConnell and Radhakrishnan, 2003), where the tails become straightened displaying a higher degree of order. Therefore, cholesterol is likely to enrich in phases with saturated phospho- and sphingolipids (Gennis, 1989). The function of cholesterol is twofold. It keeps the membrane more fluid at temperatures below T_m preventing an ordered packing of the lipid tails thus increasing their freedom of motion rendering the membrane more fluid and permeable. Whereas at temperatures beyond T_m the rigid structure of cholesterol decreases the freedom of lipid acyl chains thus also decreasing fluidity and permeability. In ternary lipid compositions comprising certain mixtures of unsaturated phospholipids, sphingomyelin and cholesterol these phases are found to coexist (de Almeida *et al.*, 2003; Mouritsen and Zuckermann, 2004; Veatch and Keller, 2002). Raising the temperature in the sample of such a lipid mixture beyond the T_m of the lipid with the highest melting point results in a phase transition for all components and leads to a homogenously distributed liquid disordered phase.

1.3.6 Detection of domains in model membrane systems

Many findings concerning phase separation and domain formation were discovered in model systems as lipid domains in the artificial systems were found to be larger in size and more stable in time than in biological membranes. Whereas in the cellular plasma membrane free diffusion of proteins and lipids is hindered beyond an approximately 30-250 nm radius by proteins bound to components of the actin cytoskeleton meshwork, this restraint is nonexistent in model membranes. These ideas are corroborated by experimental results (Kusumi *et al.*, 2004; Kusumi and Suzuki, 2005; Dietrich *et al.*, 2002) as well as by computer simulations (Yethiraj and Weisshaar, 2007). Interestingly, also the plasma membrane forms micrometer-sized domains when it is detached from the cytoskeleton (Baumgart *et al.*, 2007a; Lingwood *et al.*, 2008).

Several experimental setups and techniques are employed to investigate domain formation in model membrane systems comprising a ternary lipid mixture. An unsaturated phospholipid (e.g. DOPC) forming the Ld phase is mixed with saturated phospholipids (e.g. DPPC) or sphingolipids (e.g. SSM) and cholesterol to enrich in the Lo phase. Tapping mode AFM and fluorescence microscopy are used to study separation of lipids and also proteins in planar membrane structures (monolayer, bilayer and supported bilayer), respectively. Separation can be followed by domain specific partition of fluorescent lipid-conjugated dyes or by differences in the height profile of the lipid or protein domains (Shaw *et al.*, 2006; Weise *et al.*, 2009a; Vogel *et al.*, 2009). Techniques like ^{2}H-NMR and EPR spectroscopy as well as small angle X-ray scattering have the ability to analyse the order parameter and phase behaviour of membranes and are not limited by the lipid domain size (Eisenblatter and Winter, 2006; Kurad *et al.*, 2004; Vogel *et al.*, 2009; Bunge *et al.*, 2008). Besides the planar membrane systems also vesicular lipid model membranes were intensively used to study lipid domain formation, namely giant unilamellar vesicles (GUVs), which are easily observable by light and fluorescence microscopy. As in planar membranes partition of fluorescent probes indicates domain formation (Korlach *et al.*, 1999; Dietrich *et al.*, 2001; Veatch and Keller, 2003; Veatch and Keller, 2005; Bagatolli, 2006; Baumgart *et al.*, 2007b). These can also be identified by their domain shape as solid ordered phases exhibit elongated irregular forms, whereas the liquid domains are characterized by circular shapes, which recover rapidly after mechanical distortion, trying to minimize the boundary length indicating the presence of line tension at the domain interface (Garcia-Saez *et al.*, 2007). It is suspected that cholesterol might reduce the line tension between liquid domains (Hancock, 2006). The mobility of lipids

or membrane anchored proteins is different within the different lipid domains. This mobility can be assessed by single molecule methods like single particle tracking (SPT) (Douglass and Vale, 2005) or fluorescence correlation spectroscopy (FCS) (Korlach *et al.*, 1999; Kahya *et al.*, 2004; Korlach *et al.*, 2005) and by studying the fluorescence recovery in membrane spots after photobleaching (FRAP).

Optical microscopy is limited by Abbe's resolution limit of about 200 nm and lipid domains smaller than this cannot be observed directly. However, fluorescence based methods are able to report on domain formation below the optical resolution. FRET between two fluorescent probes will increase (decrease) if the both are found in the same (different) domains, given that small domains of sub-resolution size are present (Silvius, 2003; de Almeida *et al.*, 2005; Heberle *et al.*, 2005; Silvius and Nabi, 2006). Besides FRET also fluorescence lifetime imaging microscopy (FLIM) is able to detect the existence of lipid domains that are not revealed by fluorescence intensity patterns. Here, the fluorescence lifetime of the probe reports on the order in the surrounding lipid environment (de Almeida *et al.*, 2007; Margineanu *et al.*, 2007; Stockl *et al.*, 2008; Stockl and Herrmann, 2010; Nikolaus *et al.*, 2010a).

As the three concepts of DRMs, rafts in biological membranes and Lo phases in model systems have been introduced at this point, their crucial differences shall be highlighted ones more. DRMs are the result of treating membranes with different detergents. They only exist because of this treatment and are in the end the result of an incomplete solubilization due to thermodynamic or kinetic aspects (Heerklotz, 2002; Munro, 2003; Lichtenberg *et al.*, 2005; Brown, 2006). Membrane rafts are transient, highly dynamic and small domains *in vivo* enriched in sphingolipids, cholesterol and certain proteins (Pike, 2006), but they should not be equated with Lo domains in model systems in equilibrium where they refer to accurately measurable parameters like lipid order influencing lateral diffusion and acyl chains conformations (Munro, 2003; Simons and Vaz, 2004; Lingwood and Simons, 2010).

1.3.7 Protein sorting

Sorting of integral and peripheral proteins to raft and nonraft nanoclusters and domains in membranes is believed to be crucial for protein sorting and transport between the different cellular organelles as well as for signalling processes. As mentioned above, proteins

presumably possess different sorting signals directing them to e.g. the apical or basolateral surface in polarized cells. Apical protein sorting may be governed by lipid-protein and lipid-lipid interaction, thus by a possible interaction of proteins with rafts, since the apical membrane is enriched in sphingolipids and cholesterol (Schuck and Simons, 2004). This view is supported by indirect findings that depletion of sphingolipids and cholesterol affects apical sorting (P. Keller and Simons, 1998; Hansen *et al.*, 2000; Mays *et al.*, 1995). Coalescence of raft nanoclusters and cargo proteins in the Golgi membrane forming larger domains that might reach a critical size beyond which a transport carrier vesicle buds off and takes its protein cargo to the apical plasma membrane. This domain induced budding was first generally postulated on a theoretical basis to be driven by line tension (Lipowsky, 1993), but was later supported by studies on model membranes (Baumgart *et al.*, 2003; Bacia *et al.*, 2005). In these publications it was described that domains in GUVs can spontaneously undergo budding and fission and thus separation from the rest of the vesicle. Budding out from the surrounding bilayer will reduce the line tension of the domain by decreasing the length of the interface between the two domains (Schuck and Simons, 2004). However, the situation in a cellular membrane comprising a lipid mixture with a much greater variety of lipids compared to the model system will most likely be much more complex. The line tension here is probably affected by proteins acting as surfactants at the domain boundary (see Discussion).

But what mechanisms drive the coalescence of raft nanoclusters and what causes the partition of proteins to rafts? Raft clustering is driven by line tension and oligomerization of raft components (see Discussion, section 5.2.7 and 5.2.8) (Kusumi *et al.*, 2004). The formation of larger and more stable rafts upon clustering of raft associating proteins could be shown (Harder and Simons, 1999; Janes *et al.*, 1999; Holowka *et al.*, 2000; Lingwood and Simons, 2010). Besides the above mentioned GPI-anchor also transmembrane domains were found to mediate raft association in cellular membranes. The mechanism of transmembrane protein association with rafts is not fully understood. However, the hydrophobic length of the transmembrane segments was proposed by Bretscher and Munro (Bretscher and Munro, 1993) to be one factor. The hydrophobic matching between the transmembrane segment of the protein and the width of the hydrocarbon core of the bilayer could determine the protein partition. Bretscher and Munro found that proteins retained in the Golgi have significantly shorter TMDs (~15 aa) than proteins destined to be sorted to the plasma membrane (~20 aa). Together with the observations that first, the thickness of the bilayer is increased by cholesterol (Nezil and Bloom, 1992) and second, the cholesterol content increases in cellular

membranes along the secretory pathway, a protein sorting mechanism dependent on the hydrophobic matching was proposed (Kandasamy and Larson, 2006). The Golgi and plasma membrane were found to be thicker than the ER membrane by 2 and 5 Å, respectively (Mitra *et al.*, 2004). Studying the energetic feasibility of this cholesterol-dependent partition by using the theory of elastic liquid crystal deformations Lundbaek *et al.* could show that a greater membrane width, but even more the changes in the physical properties of the bilayer upon increasing cholesterol content allow for an effective partition of proteins comprising longer TMDs into membrane domains enriched in cholesterol (Lundbaek *et al.*, 2003). Thus, proteins destined to remain in the Golgi would partition to thinner nonraft domains, whereas hydrophobic matching with the width of the membrane domains enriched in cholesterol would serve as a sorting mechanism.

Acylation, i.e. the attachment of fatty acids, is a common modification of eukaryotic proteins (Smotrys and Linder, 2004). The focus will be placed on the post-translational thioester linkage of a saturated palmitic acid (C16:0) to cysteine residues here. For soluble proteins the primary function of the palmitoylation is to enhance the affinity of the protein to the membrane (Shahinian and Silvius, 1995). For transmembrane proteins it was speculated that palmitoylation might facilitate TMD reorientation and tilting to minimize a hydrophobic mismatch (Greaves *et al.*, 2009). This idea was supported by investigation in a model system (Joseph and Nagaraj, 1995). A positive mismatch of the TMD can alternatively be alleviated by sorting the palmitoylated protein to more ordered and therefore thicker membrane domains (as discussed above) (Greaves and Chamberlain, 2007). Several examples of palmitoylated proteins support the hypothesis that acylation with saturated lipid anchors targets transmembrane (but also peripheral) proteins to raft domains (e.g. HA, gp160, LAT, CD4, CD8, PAG1; summarized in Levental *et al.* (Levental *et al.*, 2010), also see (Epand, 2008; Chakrabandhu *et al.*, 2007)). Short unsaturated and/or branched lipid modifications in contrast have been shown to exclude proteins from partitioning to ordered and more tightly packed raft domains (reviewed in (Levental *et al.*, 2010)).

A protein segment that is located at the protein membrane interface and capable of binding cholesterol was also proposed to mediate the partition of proteins to cholesterol rich raft domains. This so called CRAC (cholesterol recognition/interaction amino acid consensus) motif is defined as an amino acid sequence of L/V-X_{1-5}-Y-X_{1-5}-R/K with X representing arbitrary amino acids (Epand, 2008). CRAC domains have inter alia been described adjacent

to the single TMD of the fusogenic protein gp41 of HIV as well as for caveolin (Epand, 2008). Both proteins have been reported to partition to rafts.

1.3.8 Examples for protein sorting

The formation of progeny enveloped viruses might serve as an example for raft dependent protein sorting. Lateral sorting of viral proteins is thought to be raft mediated leading to assembly and budding of new viral particles of influenza (Scheiffele *et al.*, 1997), HIV (Campbell *et al.*, 2001) and Ebola virus (Bavari *et al.*, 2002). The transmembrane spike glycoproteins of influenza, HA and NA, were shown to be enriched in raft domains, first by resistance to detergent (Scheiffele *et al.*, 1997; Kundu *et al.*, 1996; Barman and Nayak, 2000), but also by more sophisticated methods (Pralle *et al.*, 2000; Hess *et al.*, 2007; Scolari *et al.*, 2009; Engel *et al.*, 2010; also see Discussion). The three acylations of HA (with two palmitic and a stearic acid, see (Kordyukova *et al.*, 2008 and section 5.2.5) was found to be important for raft association (Takeda *et al.*, 2003; Scolari *et al.*, 2009; Engel *et al.*, 2010) as well as in the assembly of progeny viruses (B. J. Chen *et al.*, 2005). Also the oligomerization of HA and NA to its trimeric and quatromeric forms, respectively, will probably favour the raft association of these proteins (cf. Simons and Vaz, 2004). The influenza virus M2 protein bears a CRAC domain and is also palmitoylated. In a model it was proposed by C. Schroeder *et al.*, 2005 that the CRAC domain binding cholesterol and the palmitoylation could direct the M2 protein to the raft domain boundary assisting to pinch of the budding virus particles from the plasma membrane.

The Ras family proteins are small GTPases critically involved in signal transduction. They are peripheral membrane proteins attached to the membrane via lipid modifications. The different Ras isoforms (K-, N- and H-Ras) are highly homologous proteins differing only at the C-terminus comprising different membrane anchors (Plowman *et al.*, 2005). All Ras isoforms are farnesylated. Additional membrane anchoring is achieved by a positively charged polylysine stretch and one or two palmitic acids for K-, N- and H-Ras, respectively (Fig. 8). Whereas the double palmitoylated GDP-bound form of H-Ras strongly clusters in cholesterol-sensitive rafts domains, the activated GTP-bound form is excluded from these domains (Prior *et al.*, 2001). K-Ras proteins are only found in cholesterol-insensitive nonraft domains since the branched, unsaturated isoprenyl group is not able to partition to the more tightly pack domains alone. GTP- and GDP-loaded K-Ras isoforms were found to partition into spatially

distinct nanoclusters in an actin dependent manner (Prior *et al.*, 2003; Plowman *et al.*, 2008). Interestingly, the palmitoylated and farnesylated N-Ras was found to partition to the domain interface in studies using purely synthetic model membranes (Weise *et al.*, 2009a; Weise *et al.*, 2009b). It was speculated that at the boundary between the two domains the N-Ras could have a stabilizing effect on the domains as the proteins would function as a surfactant (Trabelsi *et al.*, 2008).

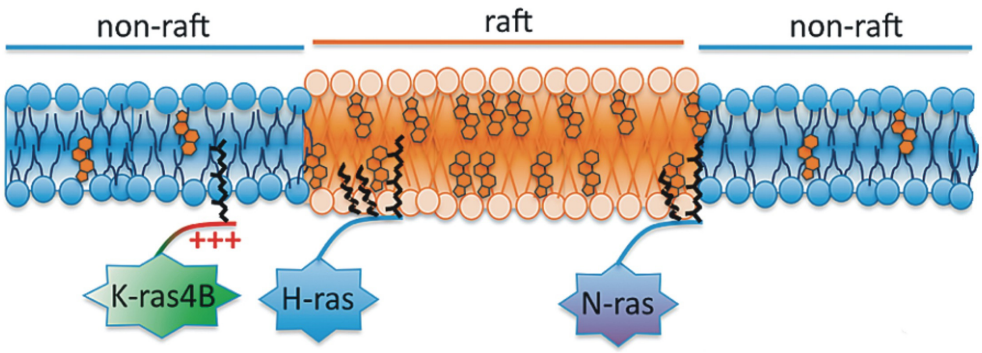

Fig. 8: Domain partition of the different Ras isoforms. Depending on the type of membrane anchor the different isoforms of Ras partition to different lipid domains of nonraft, raft and domains interface for K-Ras, GDP-loaded H-Ras and N-Ras, respectively. For details see text. Figure is modified from (Levental *et al.*, 2010).

„Wenn du eine weise Antwort verlangst,
musst du vernünftig fragen."

Johann Wolfgang von Goethe (* 28.08.1749; † 22.03.1832)

2 Aim of the study

Due to the diffraction limit and their very small size, virus or synaptic vesicle fusion with a target membrane can only be followed by indirect, fluorescence based methods to gather information about the process and its intermediates. Therefore, this study wants to establish a method that allows for the direct visualization of lipid bilayer fusion. The GUV model system is used here, as the GUV membrane is easily visible by optical microscopy. Incorporation of fluorescently labelled transmembrane markers allows for the first time to visualize and characterize the formation of large and protein-free hemifusion intermediates in membrane fusion. Using this system, the influence of e.g. lipid curvature and membrane tension can be studied and kinetic data can be obtained. Experimental results are used to formulate an analytical model of membrane fusion that will in turn encourage new experiments.

This study also aims at the characterization of the lateral sorting of transmembrane and lipid anchored proteins to better understand the mechanism and conditions leading to partition of proteins into laterally separated lipid domains. Again the model systems of GUVs, but also GPMVs resembling a biological membrane will be employed to gain new insights into the determining factors for lateral partition from model peptides to full length proteins like HA and Ras. Confocal fluorescence and lifetime microscopy will be used to study domain partition, but also the physical properties of the lipid environment within the membrane.

" Method is much, technique is much,
but inspiration is even more."

Benjamin Nathan Cardozo (* 24.05.1870; † 09.07.1938)

3 Material and Methods

3.1 Material

3.1.1 Chemicals

Phospholipids and fluorescent lipid analogues were purchased from Avanti Polar Lipids Inc. (Birmingham, AL, USA) and used without further purification. Lipid stock solutions were stored in chloroform at -20°C. C6-NBD-PC, 1-palmitoyl-2-[6-[(7-nitro-2-1,3-benzoxadiazol-4-yl)amino]hexanoyl]-*sn*-glycero-3-phosphocholine; N-NBD-PE, N-(7-nitro-2,1,3-benzoxadiazol-4-yl) hexadecylphosphatidylethanolamine; DOPC, di-oleoyl-phosphatidylcholine; POPC, 1-palmitoyl-2-oleoyl-phosphocholine; DOPE, di-oleoyl-phosphatidylethanolamine; DOPS, di-oleoyl-phosphatidylserine; SSM, N-stearoyl-sphingosylphosphorylcholine. Cholesterol and Annexin V-Cy3 were obtained from Sigma-Aldrich (Taufkirchen, Germany). Solvents used for vesicle preparation were of the purest grade available. Indium tin oxide (ITO) coated glass slides were supplied by Präzisions Glas & Optik GmbH (Iserlohn, Germany). 2.0 mm thick titanium foil for the custom-built GUV chambers was obtained from Alfa Aesar (Karlsruhe, Germany).

3.1.2 Buffers

Phosphate buffered saline (PBS) was used in various concentrations (10x to 0.001x PBS) was diluted from 10x PBS (40 g NaCl, 1 g KCl, 7,1 g Na_2HPO_4 $2H_2O$, 1 g KH_2 PO_4 in 500 mL ddH_2O) and pH was adjusted to 7.4.

For GUV preparation and microscopy sucrose buffer (250 mM sucrose, 15 mM NaN_3, osmolarity of ~280 mOsm/kg) and glucose buffer (250 mM glucose, 11.6 mM potassium phosphate, 5.8 mM of Na_2HPO_4 and NaH_2PO_4 each, osmolarity of ~300 mOsm/kg, pH 7.2) was used, respectively. For microscopy at high ionic strength a NaCl buffer (140 mM glucose, 11.6 mM potassium phosphate, osmolarity of ~300 mOsm/kg, pH 7.2) was used.

Giant plasma membrane vesicles (GPMVs) were prepared in 2 mM $CaCl_2$, 10 mM Hepes, 0.15 M NaCl, 25 mM formaldehyde, 2 mM DTT, pH 7.4.

3.2 Methods

3.2.1 Preparation of viruses

The influenza A virus strains A/PR/8/34 and Japan/305/57 were grown and purified as described in (Krumbiegel *et al.*, 1994) by Gudrun Habermann and Christian Sieben. In short, virus was grown for 48 h in 10 day old embryonated hen eggs. The allantoic fluid of the eggs was collected, and cell debris was removed by a low speed spin. The virus was pelleted by spinning the allantoic fluid with 90,000 x g for 50 min. The pellet was homogenized with a Teflon-coated homogenizer.

3.2.2 Viral lipid extraction

Lipids from influenza A virus strains A/PR/8/34 and Japan/305/57 were extracted by organic solvents according to Bligh and Dyer (Bligh and Dyer, 1959) by Sabine Schiller. In short, 3 mL chloroform:methanol (1:2) was added to the virus sample, vortexed and incubated for 30 minutes at 25°C. Addition of 1 mL chloroform is followed by addition of 1 mL acetic acid (40 mM). After centrifugation at 1000 g for 10 minutes the lower phase was collected and transferred to another glass vial. After addition of 2 mL chloroform to the remaining aqueous phase and centrifugation the lower phase was again collected and pooled with the first sample.

Phospholipid quantification was done from a dried lipid sample that was solved in 50 µL H_2O. 300 µl of 70 % perchloric acid were added and the sample was heated at 180°C for 1 h. After addition of 1 mL H_2O, 0.4 mL ammonium molybdate (1.25 %, w/v) and 0.4 mL ascorbic acid (5 %, w/v) the mixture was heated to 100°C for 10 minutes and subsequently allowed to cool to 25°C. Absorbance was measured at 797 nm and compared with a KH_2PO_4 standard calibration.

3.2.3 Peptide synthesis

Rhodamine-tagged LV-peptides (Rh-LV-Rh) with a 16 amino acid long hydrophobic core of leucine and valine residues flanked on both termini by lysines (Amino acid sequences: Rh-LLV16-Rh: Rh-KKKKWLLVLLVLLVLLVLLVLKKKK-Rh; Rh-LV16-G8P9-Rh: Rh-KKKKWLVLVLVLGPVLVLVLVKKKK-Rh) were synthesized by Boc chemistry (PSL, Heidelberg, Germany). The Rh-label was added by coupling of a lysine derivative (Fmoc-Lys(Dde)-OH) to the C- and N-termini during synthesis. Reaction of the peptide with 5-(and-6)-carboxytetramethylrhodamine succinimidylester (TAMRA, SE) (Invitrogen, Paisley, United Kingdom) yielded Rh-labelled peptides.

Rh-HA, containing 28 amino acid residues of the TMD of HA (strain Japan/305/57, H2; Rh-HA: Rh-ßA-ILAIYATVAGSLSLAIMMAGISFWMCSNKKK) was synthesized together with Ines Kretzschmar and Christiane Landgraf in the group of Rudolf Volkmer (iMi, Charité, Berlin) using Fmoc-chemistry performed on the TentaGel S RAM resin (0.25 mmol/g; Rapp Polymere, Tübingen, Germany) using the multiple peptide synthesizer (SYRO II, MultiSynTech GmbH, Witten, Germany). The coupling reagent (Benzotriazol-1-yloxy)tripyrrolidinophosphonium hexafluorophosphate (PyBOP) and N-Methylmorpholine (NMM) were used for activation and Fmoc-deprotection was achieved with 20 % piperidine in DMF. Dye-labelling was achieved by coupling TAMRA at the N-terminus via a ß-alanine by PyBOPB/NMM activation. The C-terminal end is flanked by three lysine residues. The presence of terminal lysines is a common approach to enhance the peptide solubility and to promote an insertion into the membrane (Hesselink *et al.*, 2005). Raw products were purified by preparative HPLC up to >90 % pureness measured by analytical HPLC and the peptide identity was judged by mass spectrometry.

Concentration of chloroform stocks of unlabelled peptides was determined from the UV absorbance at 280 nm in MeOH using a molar extinction coefficient $\varepsilon = 6990\ M^{-1}\ cm^{-1}$ ($\varepsilon_{Trp} = 5500\ M^{-1}\ cm^{-1}$; $\varepsilon_{Tyr} = 1490\ M^{-1}\ cm^{-1}$). For rhodamine-labelled peptides the concentration was determined by absorbance at 541 nm using $\varepsilon = 93\ 000\ M^{-1}\ cm^{-1}$.

3.2.4 Efforts to synthesize palmitoylated peptides

The efforts to yield a triple palmitoylated peptide comprising the TMD and cytoplasmic tail (CT) of HA unfortunately failed (also see Discussion 5.2.5). Already the synthesis of the longer TMD plus CT peptide with 39 residues was not possible with good yields using solid phase peptide synthesis (SPPS) and palmitoylation of the three C-terminal cysteines failed for this peptide. The desired sequence of the peptide (from influenza strain A/FPV/Rostock/34) was TMD: KDVILWFSFGASCFLLLAIAMGLVFI**C**^{551}V + CT: KNGNMR**C**^{559}TI**C**^{562}I. For the palmitoylation reaction a cysteine with a special monomethoxytrityl- (Mmt-) protecting group was used allowing a deprotection under weakly acidic conditions. For the formation of the thioester linkage of palmitic acids two protocols were tested. First, Yousefi *et al.* (Yousefi-Salakdeh *et al.*, 1999) used 100 % trifluoroacetic acid (TFA) for 10 minutes at room temperature to activate the palmitoylchloride. The second protocol from the Waldman lab was published originally for the palmitoylation of Ras peptides where S-palmitoylation was achieved after removal of the Mmt group by addition of palmitoylchloride in the presence of 1-Hydroxybenzotriazole (HOBt) and triethylamine for 16 hours (Ludolph *et al.*, 2002).

To avoid the ineffective synthesis of the entire peptide the idea was to divide the sequence into three shorter peptide fragments that will be palmitoylated and finally ligated (KDVILWFSFGASCFLLLAIAMG + LVFI**C**^{551}VKNG + NMR**C**^{559}TI**C**^{562}I). Both protocols were tested using the C-terminal fragment first. Only for the protocol proposed by Ludolph *et al.* (Ludolph *et al.*, 2002) the corresponding peptide mass could be detected in a Maldi-TOF mass spectrometry analysis, but at very low yields (<1 %). To exclude a steric hindrance of the resin for the palmitoylation reaction a linker (hydroxylmethylphenoxy acetic acid) was introduced between the peptide and the resin (TentaGel AM HMPA resin; Rapp Polymere, Tübingen, Germany), but the reaction could not be improved.

3.2.5 Preparation of lipid membrane vesicles

3.2.5.1 Preparation of large unilamellar vesicles (LUVs)

In a first step, multilamellar vesicles (MLVs) were prepared from the desired lipid mixture dissolved in chloroform with 1 mol% of the respective fluorescent lipid analogue. For incorporation of the respective transmembrane peptide dissolved in TFE the desired quantity was added to the lipid mixture. Ablating the solvent under a stream of nitrogen while rotating the conical test tube yielded a thin lipid film. About 5 µl ethanol (max 1 % of the final amount of buffer) were added to partially dissolve the lipid film from the glass surface. Buffer solution at $T > T_m$ was added to hydrate the lipid film, which was then vortexed for a time sufficient to generate MLVs (~ 5 min).

Applying five freeze-thaw cycles to MLVs and extruding the solution ten times through 200 nm polycarbonate membrane filters (Nuclepore, Whatman Schleicher & Schuell, Dassel, Germany) at a temperature above the phase separation temperature of the lipid mixture yielded large unilamellar vesicles (LUVs). LUVs were stored at 4°C and used within one week after preparation.

3.2.5.2 Preparation of giant unilamellar vesicles (GUVs)

Giant unilamellar vesicles (GUVs) were prepared from dried lipid films using the electroformation method established by (M. Angelova *et al.*, 1992) and (Mathivet *et al.*, 1996). Lipid mixtures along with 1 mol% of the respective lipid analogue were made from stock solutions in chloroform. Solvent was ablated and finally 100 nmol of lipids were dissolved in 80 µl trifluoroethanol (TFE). For incorporation of the respective transmembrane peptide or molecular rod dissolved in TFE or chloroform/methanol (1:1, v/v), respectively, the desired quantity was added. The lipid/peptide solution was spotted onto two ITO-coated slides that were placed on a hotplate at 50-60°C immediately thereafter to evaporate the solvent and thus to ensure a homogenous distribution of the lipid films at a temperature above T_m. Remaining traces of solvent were removed under high vacuum <10 mbar for at least 1 hour. Lipid-coated slides were assembled with a 1 mm silicone spacer (Fig. 9). This electroswelling chamber was filled with 1 mL prewarmed (50-60°C) sucrose buffer (250 mM sucrose, 15 mM NaN_3, osmolarity of 280 mOsm/kg) and sealed with plasticine. An alternating electrical field of 10 Hz rising from 0.02 V to 1.1 V in the first 54 minutes was applied for 2.5 hours at 50°C

followed by 30 minutes of 4 Hz and 1.3 V to detach the formed liposomes. GUVs were stored at ambient temperatures, shielded from light and used within one week after preparation.

In another approach GUVs were generated in a chamber made from two hollowed titanium plates (Fig. 9) instead of ITO-coated glass slides due to a possible peroxidation at lipid double bonds of SM and unsaturated phospholipids as reported by (Ayuyan and Cohen, 2006). Results were found to be independent of whether GUVs were prepared on ITO slides or titanium plates.

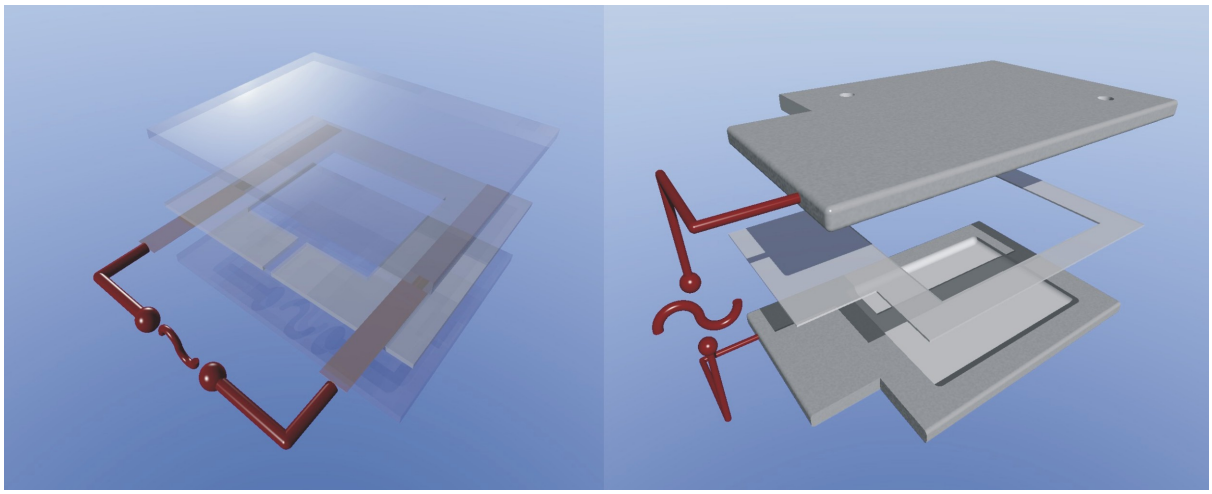

Fig. 9: Chambers for GUV preparation. Made from two Indium tin oxide coated glass slides and a 1 mm insulating layer of silicone with two conductive copper foils (left) or made from two hollowed titanium plates with a piece of Parafilm (Pechiney Plastic Packaging, Chicago, IL, USA) for insulation in between.

3.2.6 Tetramethylrhodamine labelling and reconstitution of hemagglutinin into GUVs

For the labelling and reconstitution of HA two slightly different protocols were applied. According to the first protocol HA was labelled with TMR (5/6-Carboxytetramethyl-rhodamine maleimid, emp Biotech, Berlin, Germany) on the intact virus particle, from which HA containing virosomes were generated to finally produce GUVs with reconstituted HA for the hemifusion experiments. In the second protocol the virus proteins were first isolated from the virus and subsequently labelled with TMR by Thomas Korte and Gudrun Habermann. Proteoliposomes were generated from labelled HA and subsequently used for GUV preparation for the lipid domain specific sorting experiments.

Protocol 1: Influenza virus strain X31 was preincubated for 2 h at RT in the dark with TMR, which readily reacts with the cysteine residues of HA and was added from a 5 mM Me_2SO stock to molar excess of 10 over HA. Uncoupled TMR was removed by washing labelled virus in phosphate buffered saline (PBS, pH 7.4) and harvested by centrifugation at 52 000 × g. SDS-PAGE analysis revealed that only influenza virus HA was labelled (data not shown).

Virosomes were prepared according to (Papadopulos *et al.*, 2007). Triton X-100 solubilized influenza virus with TMR-labelled HA was mixed with a Triton X-100 solubilized lipid mixture of DOPC:DOPE:DOPS (3:1:1, molar ratio) at a lipid/protein ratio of 20 (w/w) and incubated for 1 h. To remove detergent and to generate virosomes 1 g of SM2 BioBeads (Bio-Rad, Munich, Germany) per 70 mg of Triton X-100 were added and rotated at 4°C. After 12 h the same amount of BioBeads was added for another 4 h. The turbid suspension was withdrawn carefully from the beads and washed twice with PBS and collected by centrifugation (55 000 × *g*, 1 h, 4°C) to remove remaining detergent.

GUVs with reconstituted viral protein were generated according to (Girard *et al.*, 2004). Virosomes were diluted with distilled water to 0.4-0.8 mg/mL lipid, 0.02 g sucrose/g lipid was added to protect proteins during the following dehydration (Doeven *et al.*, 2005) and finally 50 µl of this suspension was deposited onto each ITO slide or titanium plate. Dehydration was achieved by placing the slides in a sealed chamber containing a saturated NaCl solution overnight. Thereafter, formation of GUVs followed the electroformation method described above.

Protocol 2: 20 mg virus protein from Triton X-100 solubilized influenza virus strain X31 was incubated for 2 h at RT in the dark with TMR, added from a 5 mM Me_2SO stock to molar excess of 10 over HA. Uncoupled TAMRA was removed by washing three times in phosphate buffered saline (PBS, pH 7.4) and harvested by centrifugation at 52 000 × g. The pellet was solubilized by adding 500 µl PBS, pH 7.4, containing 28 % (w/v) octylglycoside (Alexis, Lörrach, Germany) and gently shaken on ice in the dark for 1 h (Bottcher *et al.*, 1999). After centrifugation for 1 hour (100 000 × g, 4°C), the HA containing supernatant was purified by affinity chromatography on ricin A agarose (*Ricinus communis* lectin, Sigma-Aldrich, Munich, Germany). To remove detergent and galactose, 1 vol sample was dialysed against 500 vol PBS, pH 7.4. The purity of TMR-labelled HA was verified by SDS-PAGE.

Purified TMR-labelled HA was solubilized by Triton X-100 and proteoliposomes and GUVs were generated following protocol 1 with the exception that a Triton X-100 solubilized lipid mixture of DOPC:SSM:Chol (1:1:1, molar ratio) or virus lipid extracts from influenza virus strain A/PR/8/34 with 1 mol% C6-NBD-PC was used.

3.2.7 Preparation of giant plasma membrane vesicles

GPMVs were prepared by Silvia Scolari (Nikolaus *et al.*, 2010a) according to (Baumgart *et al.*, 2007a; Sengupta *et al.*, 2008), which is a modified protocol originally described by (Scott, 1976; Scott and Maercklein, 1979; Holowka and Baird, 1983). In short, GPMVs were generated from confluent CHO-K1 cells 24 h after transfection with HA-Cer, TMD-HA-YFP or GPI-CFP using Lipofectamine 2000 (Invitrogen, Karlsruhe, Germany). HA-Cer and TMD-HA-YFP are described in (Engel *et al.*, 2010) and (Scolari *et al.*, 2009), respectively. GPI-CFP has been kindly provided by Patrick Keller (P. Keller *et al.*, 2001). All fluorescent constructs contain the A206K mutation preventing their dimerization (Zacharias *et al.*, 2002). Cells grown in flasks were washed twice with GPMV buffer (2 mM $CaCl_2$, 10 mM Hepes, 0.15 M NaCl, pH 7.4). Then 1.5 mL of GPMV buffer containing 25 mM formaldehyde and 2 mM dithiothreitol (DTT) were added and flasks were incubated for 1 h at 37°C slowly shaking (60–80 cycles per minute). After incubation, detached GPMVs were gently decanted into a conical glass tube. GPMVs were allowed to sediment for 30 min at 4°C. For microscopy 30 µl of GPMVs were labelled with a 20 µM R18 (Octadecylrhodamine-B-chloride, Invitrogen, Karlsruhe, Germany) solution. Images of the equatorial plane of the GPMVs were taken at 10°C.

For fluorescence lifetime imaging (see below section 3.2.12) GPMVs as well as intact CHO-K1 cells were labelled with C6-NBD-PC as described in (Stockl *et al.*, 2008). Aliquots of C6-NBD-PC were ablated in a glass tube and resolved in buffer. GPMVs were incubated for some minutes at a final concentration of 2 µM at room temperature. CHO-K1 cells were first washed with cold PBS. Labelling was performed for 20 min on ice at a final concentration of 0.5-1 µM C6-NBD-PC. Subsequently, cells were intensively washed with PBS (25°C) and imaged immediately to ensure a labelling primarily of the plasma membrane.

3.2.8 Preparation of red blood cells and incorporation of the molecular rod

For the incorporation of the molecular rod in biological membranes human red blood cells (RBCs) and RBC ghosts were used. Blood stabilized by citrate was provided by the blood bank Berlin-Lichtenberg, Germany. Buffy coat of the erythrocytes was removed and RBCs were washed twice in HBS buffer at 4°C. RBC ghosts were obtained according to (Dodge *et al.*, 1963). Rh-Rod-Rh was added to RBC and RBC ghost membranes from a stock solution dissolved in DMSO and incubated for 0.5 to 4 hours at a final concentration of 10-20 µM. For the addition of Rh-Rod-Rh to GUV membranes a similar protocol was used.

3.2.9 Ras protein synthesis and membrane binding experiments

Bodipy-labelled full length N-Ras and K-Ras4B proteins were provided by Gemma Triola and Herbert Waldmann (MPI Molecular Physiology, Dortmund) and syntethized as described before (Bader *et al.*, 2000; Vogel *et al.*, 2009; Y. X. Chen *et al.*, 2010; Weise *et al.*, 2010). In short, lipidated N- and K-Ras peptides were synthesized and subsequently ligated with the respective purified C-terminally truncated wild type Ras protein expressed and purified from *E. coli*. SDS-PAGE and MALDI-TOF MS were used to analyze the proteins. Proteins were added to GUVs and GPMVs to yield a final concentration of about 2 µM and incubated at room temperature for the indicated time.

3.2.10 Fluorescence microscopy

Images of the equatorial plane of GUVs and GPMVs were taken with an inverted confocal laser scanning microscope FluoView 1000 (Olympus, Hamburg, Germany) with a 60× (N.A. 1.35) oil-immersion or a 60× (N.A. 1.20) water-immersion objective. If necessary, a custom built temperature chamber was used together with µ-Slide VI chamber (ibidi, Martinsried, Germany) allowing cooling or heating the sample in a range of 4°C to 37°C. Cover slips were used for microscopy at room temperature except for long-lasting experiments, where poly-L-lysine-coated glass bottom culture dishes (MatTek Corporation, Ashland, MA USA) were used. GUVs were added to glucose buffer (250 mM glucose, 11.6 mM potassium phosphate, pH 7.2) with an osmolarity of 300 mOsm/kg at a ratio of 1:1 to 1:3. Prior to microscopy GUVs were given some minutes to settle down on the cover slip due to the higher density of

the sucrose buffer in the GUVs compared to the glucose buffer on the outside. The difference in the refractive indices between the two buffers also allows for a better visualization of the GUV membranes in differential interference contrast (DIC) microscopy (Sinn *et al.*, 2006). The slightly hypertonic pressure due to the slight difference in buffer osmolarity allows originally spherical GUVs to undergo shape changes, e.g. those associated with adhesion, due to an altered surface to volume ratio (Papadopulos *et al.*, 2007).

3.2.10.1 Confocal laser scanning microscopy (CLSM)

The CLSM setup described above was used to acquire images with a size of 512×512 pixel in a sequential scanning mode. An Argon ion and a Helium–Neon laser (both from Melles Griot, Bensheim, Germany) as well as a 440 nm laser diode (PicoQuant, Berlin, Germany) were used for excitation. For a detailed list of fluorophores, lasers and filters see Tab. 1.

Tab. 1: List of fluorophores, lasers and filters used in this work. WL: wavelength; DM: dichroic mirror; Ar-ion: Argon ion laser; He-Ne: Helium-Neon laser.

Laser type	Fluorophore	Excitation WL / nm	DM / nm	Emission WL / nm
Confocal				
Laser diode	Cerulean	440	440/488/543	460-490
	CFP	440	440/488/543	460-490
Ar-ion	NBD	488	405/488/559/635	500-530
	BODIPY	488	405/488/559/635	500-530
	YFP	515	BS 20/80	530-545
He-Ne	TAMRA	559	405/488/559/635	570-670
	R18	559	405/488/559/635	570-670
FLIM				
Laser diode	NBD	470	405/458/515	520-560

3.2.10.2 Wide field microscopy – CCD camera

To image the fusion kinetics a high resolution digital B/W CCD camera (ORCA-ER, Hamamatsu, Herrsching, Germany) was used with an epifluorescence illumination. The filter combination used was either a 510/50 nm excitation filter in combination with a >590 nm long pass emission filter or a 480/20 nm excitation filter together with a >510 nm long pass

emission filter. To trigger adhesion and fusion divalent cations were added from a 100 mM stock solution by a syringe. The images were edited with the Cell M software and intensity plots were created using FluoView FV 1000 software (both from Olympus, Hamburg, Germany).

3.2.11 Fluorescence recovery after photobleaching (FRAP)

FRAP measurements were performed with the same confocal setup as described above. Laser intensity was established at 488 nm to photobleach about 80 % of the fluorescence of the NBD lipid analogue. FRAP was performed in the equatorial plane of a GUV bleaching an upright membrane area of about 7 µm × 1 µm. Subsequently, scanning of the bleached area was continued with low laser intensity for about 90 seconds. Recovery kinetics was fitted to $F(t) = F_0\tau + F_\infty t / (t + \tau)$ which is an approximation of the theoretical recovery curve, where t is the time after bleaching, F(t) is the fluorescence as a function of time, F_0 is the fluorescence immediately after bleaching, F_∞ is the amount of fluorescence recovery, and τ is the time of half-maximal recovery (Axelrod *et al.*, 1976; Kwon *et al.*, 1994). Fitting procedures yield accurately fitted experimental curves. Calculation of the diffusion coefficient (D) was done using the equation: $D = (\gamma/4)\omega/\tau$ where γ is related to the bleaching depth and is approximately 1.45 under these experimental conditions (Yguerabide *et al.*, 1982), ω is the bleached area, and τ is the calculated time for half-maximal recovery. Performing FRAP in an upright membrane area may not necessarily be comparable with standard FRAP experiments on horizontal membranes, but it is appropriate for comparison of the two situations, the diffusion in the contact region (HD) and outside of this region, respectively. The mobile fraction (M_f) was calculated using: $M_f = (F_\infty - F_0)/(1 - F_0)$.

3.2.12 Fluorescence lifetime imaging microscopy (FLIM)

Data acquisition of FLIM images was done using an inverted confocal laser scanning microscope IX81 equipped with a 60× oil-immersion objective (N.A. 1.35) and a FluoView FV 1000 scan head (Olympus, Hamburg, Germany). A pulsed diode laser with a pulse frequency of 10 MHz and a pulse width of 60 ps was used to excite the fluorophores at a wavelength of 470 nm. Fluorescence emission was detected using a 540/40 nm bandpass filter. FLIM images (512 × 512 pixels) were acquired with an FLIM upgrade kit (PicoQuant,

Berlin, Germany) with a PicoHarp 200 for time-correlated single photon counting (TCSPC) with picosecond resolution. In TCSPC the time difference between the laser pulse excitation and the single photon signal detected with the single photon avalanche diode (SPAD) is measured and the photon lag time is determined, which allows for the calculation of the fluorescence lifetime decay curve summarising over all detected photons. To avoid an overestimation of shorter lifetimes the laser intensity was adjusted to yield a maximum photon count rate of 1 % of the pulse rate (~2-4 x 10^4 counts/s). 60 frames were acquired for each image.

Fluorescence lifetimes were determined using the SymPhoTime and FluoFit software (PicoQuant, Berlin, Germany). The lipid bilayer of GUVs or the plasma membrane of living cells or GPMVs with the NBD lipid analogue was selected using an intensity based threshold that was refined manually. A fluorescence lifetime decay curve was calculated from the selected membranes for each image. A non-linear least squares iterative fitting procedure was applied to the 'tail' of the decay curve (tail-fit, ~3-80 ns after the pulse) that is not affected by the instrument response function (IRF) to calculate the fluorescence lifetimes of NBD (Stockl *et al.*, 2008; Nikolaus *et al.*, 2010a):

$$F(t) = \sum_i \alpha_i \exp(-t/\tau_i)$$

where F(t) is the fluorescence intensity at time t and α_i is a pre-exponential factor representing the fractional contribution to the time-resolved decay of the component with a lifetime τ_i such that $\Sigma_i \alpha_i = 1$. For the calculation of lifetime histograms the fitting procedure was performed for every pixel of a selected region of interest.

The number of lifetime components used for the fitting procedure was dependent on the lipid composition of the membranes. In single lipid systems (plus lipid analogue) or systems with defined large lipid domains - so within each of these domains - already two lifetime components yield sufficiently good fits, whereas in multilipid systems (GUVs from viral lipids or GPMVs) a fitting procedure with three different lifetimes was applied. The distribution of the residuals and the χ^2 value were used to judge the quality of the fit.

" The most exciting phrase to hear in science, the one that heralds new discoveries, is not 'Eureka!', but 'That's funny...'"

Isaac Asimov (* 02.01.1920; † 06.04.1992)

4 Results

The results obtained during this work will be presented following the steps of a viral replication cycle and focus on two important phases in this process: fusion and assembly. The fusion pathway of lipid membranes and an important intermediate herein will be investigated. Many of the obtained results are published in Nikolaus *et al*. (Nikolaus *et al.*, 2010b). This first section is followed by a second part, focusing on the sorting of viral proteins and the possible involvement of lipid domains. To characterize the properties of these possible sorting platforms, also non-viral proteins such as lipid anchored RAS come into play.

4.1 Direct visualization of large and protein-free hemifusion diaphragms

4.1.1 Giant unilamellar vesicles as a model system to study hemifusion

For the visualization of hemifusion between two lipid bilayers a model system of giant unilamellar vesicles (GUVs) is ideally suited. Due to their remarkable large size with a diameter of 1 – 100 µm (Walde *et al.*, 2010), giant vesicles are easily visible by light and fluorescence microscopy. The electroformation method is a reliable technique for the preparation of GUVs compared to others methods like gentle hydration (Rodriguez *et al.*, 2005) or rapid evaporation (Moscho *et al.*, 1996). Electroformation, using an alternating

electric field, was first described by Angelova and Dimitrov (M. I. Angelova and Dimitrov, 1986; M. Angelova *et al.*, 1992; Dimitrov and Angelova, 1987) and allows for the preparation of GUVs with a defined lipid composition with only slight variances of the used lipid mixture originally prepared in organic solvent (Veatch and Keller, 2003). For the hemifusion experiments GUVs were prepared from a mixture of unsaturated phospholipids DOPC:DOPE:DOPS (3:1:1, molar ratio). Similar results were observed when DOPC was replaced by POPC (not shown). The mixture resembles the major fraction of phospholipids in intracellular membranes, in particular of the Golgi, and in the cytoplasmic leaflet of the plasma membrane of mammalian cells, the major sites for fusion processes in the cell (Holthuis *et al.*, 2003; Holthuis and Levine, 2005). Furthermore, this lipid composition has been shown previously to be optimal for TMD peptide mediated fusion studies using smaller liposomes (Gurezka *et al.*, 1999; Hofmann *et al.*, 2004; Ollesch *et al.*, 2007). The correct incorporation of the anionic phospholipid DOPS was tested by incubation of GUVs with Annexin V-Cy3 in the presence of Ca^{2+}. Annexin V binds to membranes only in the presence of negatively charged lipids. A homogenous lateral distribution of DOPS was found (Fig. 10 B). The different rhodamine-tagged transmembrane peptides used in this part of the study and the fluorescent lipid analogue N-NBD-PE were reconstituted into the GUV membrane during vesicle preparation. The different peptides and the lipid analogue N-NBD-PE were homogenously distributed in the membrane of the respective GUVs (Fig. 10).

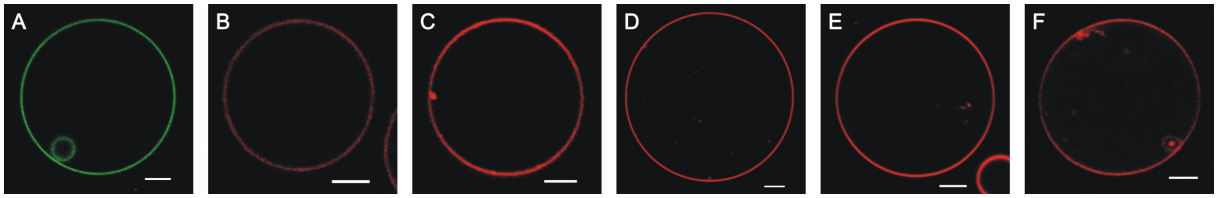

Fig. 10: Laser scanning confocal microscopy images of the equatorial plane of GUVs prepared from a lipid mixture of DOPC:DOPE:DOPS (3:1:1, molar ratio) including the green fluorescent lipid analogue N-NBD-PE (**A**) found in a homogeneous distribution. PS is evenly integrated in the bilayer indicated be a homogenous distribution of red fluorescent labelled PS-binding protein Annexin V-Cy3 (**B**). The rhodamine-labelled transmembrane peptides of HA Rh-TMD (**C**) and the model peptides Rh-LLV16-Rh (**D**) and Rh-LV16-G8P9-Rh (**E**) as well as the molecular oligospiroketal Rh-Rod-Rh (**F**) are all also homogenously incorporated in the GUV membrane as shown by detecting the homogenous red fluorescence. Images were taken at 25°C, Scale bar corresponds to 5 µm.

To test whether the reconstituted peptides were incorporated in a transmembrane manner during GUV formation and not just adhered to the bilayer by electrostatic interaction between

the negatively charged PS on the one side and the positively charged lysine residues of the peptide on the other side, the rhodamine fluorescence intensity at the GUV membrane was followed upon stepwise increasing the ionic strength of the buffer by addition of 100 mM NaCl solution. For Rh-LLV16-Rh a linear decrease of only ~8 % of the rhodamine fluorescence at the GUV membrane was detected upon doubling the ionic strength of the buffer, thus arguing for a transmembrane incorporation. A possible explanation for the slight decrease in fluorescence could be that few peptides are only peripherally attached to the membrane by electrostatic interaction, which dissociate upon shielding of the terminal lysine residues and PS by Cl^- ions, whereas the majority of peptides are well inserted across the bilayer. Transmembrane incorporation was also corroborated following the blue shift of the fluorescence emission of a Tryptophan residue placed in the centre of the HA-TMD due to the more hydrophobic environment close to the bilayers hydrophobic centre (not shown).

4.1.2 Formation and expansion of a hemifusion diaphragm

First, the interaction of N-NBD-PE labelled GUVs with GUVs containing Rh-LV-Rh peptides was studied. Previous observations showed that these peptides are able to trigger fusion between large unilamellar vesicles (Hofmann *et al.*, 2004; Ollesch *et al.*, 2007). Aggregation of GUVs was achieved at 2 mM Ca^{2+} or Mg^{2+} (Papahadjopoulos *et al.*, 1977; Papahadjopoulos *et al.*, 1990). When raising the Ca^{2+} concentration to 6 mM by injection of a 100 mM $CaCl_2$ solution via a pipette, typically the following sequence of events (Fig. 11) was observed: An area with significantly reduced fluorescence intensity emerged within the region of the initial contact between two GUVs approx. 5 seconds after the increase of Ca^{2+}-concentration. The first image corresponding to t = 0 refers to the last snapshot before alterations of the adhesion region between two GUVs were detected. A reduction of fluorescence in the adhesion region is essentially caused by sequestering of Rh-labelled peptides, but also due to displacement of N-NBD-PE (Fig. 13). A more detailed analysis (see below, section 4.1.3) revealed that sequestering of TMDs is due to formation of an HD.

The kinetics of the HD growth for the three GUV pairs is plotted in Fig. 11 D (assessed HD area vs. time). All three HD formations exhibit an almost linear evolution in time. These and the following results were also used to develop a quantitative analytical model, describing the kinetics and equilibrium of the HD formation on the pathway to full fusion by Jason M. Warner and Ben O'Shaughnessy (Columbia University, New York). In Fig. 11 D the short

time model prediction is plotted (solid line) which agrees well with the measured HD growth data (see Discussion). An HD growth rate between 22 and 34 $\mu m^2/s$ was measured which consistent with the analytical model predicting a linear short term HD growth rate of 24 $\mu m^2/s$ (Fig. 11 D, solid line).

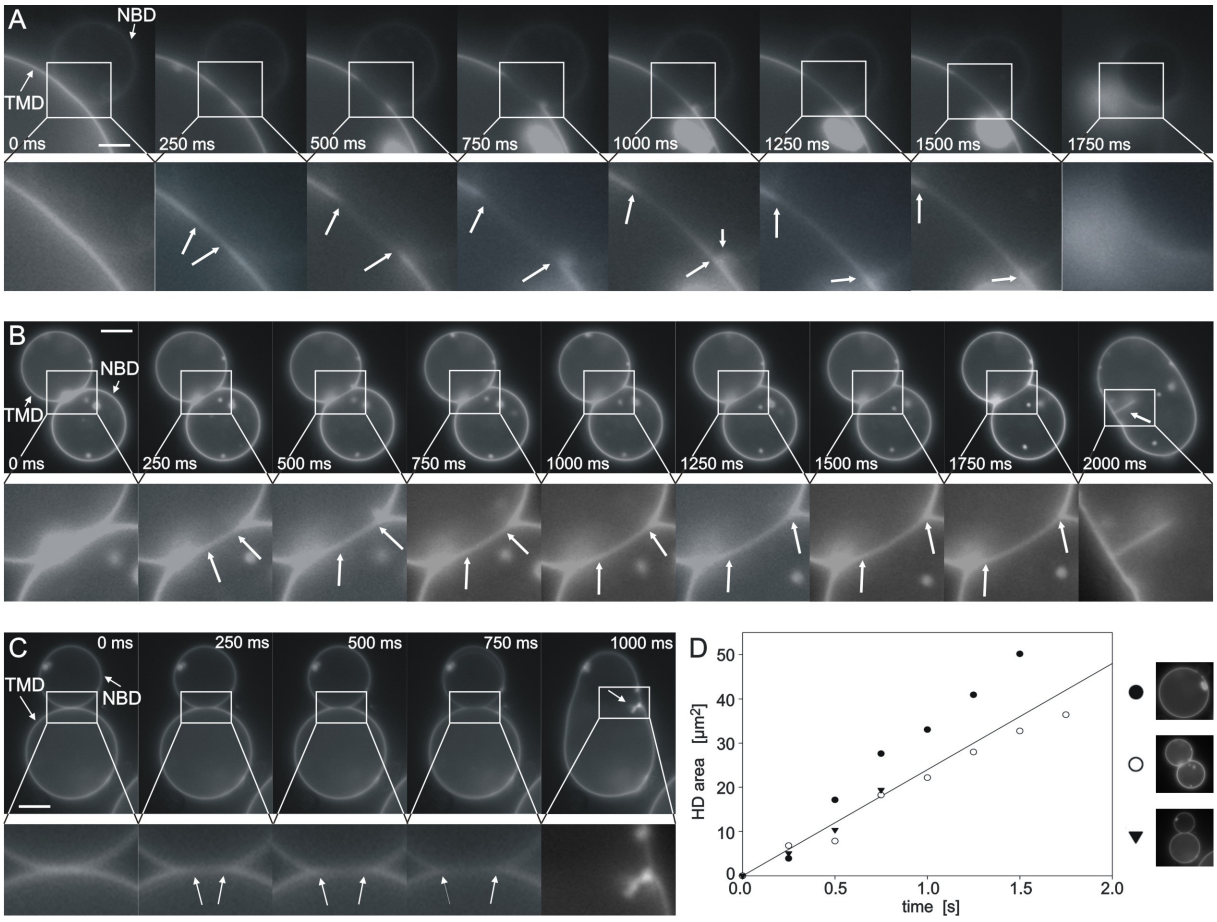

Fig. 11: Sequence of fusion between GUVs made of DOPC:DOPE:DOPS (3:1:1, molar ratio), containing either 1 mol% Rh-LLV16-Rh or 1 mol% N-NBD-PE (indicated by an arrow). Pairs of GUVs were imaged by fluorescence microscopy using the Olympus Cell^M software ((**A**) excitation filter 510/50 nm, emission filter >590 (long pass filter); (**B** and **C**) excitation filter 480/20 nm, emission filter >510 nm (long pass filter)) at 25°C. Arrows in the magnifications indicate the borders of the growing HD. (**A**) bright spot in the lower figure part corresponds to fluorescent aggregates inside the large GUV. In the last image the GUVs disintegrate. (**B** and **C**) In the last images the HD ruptures very likely at junction site of the three bilayers at the HD periphery and retracts to the opposite side (indicated by an arrow). Bar 5 µm. (**D**) shows HD area growth vs. time for the three depicted fusing GUVs. Solid line presents model prediction from Jason M. Warner and Ben O'Shaughnessy (Columbia University, New York).

Magnification of the HD region shows that a structure of rather high fluorescence intensity was formed at the rim of this region, which may correspond to transient enrichment of sequestered molecules (Fig. 12). Finally, the diaphragm ruptures, very likely at the junction site of the three bilayers at the HD periphery and retracts to the other side (Fig. 11 B and C).

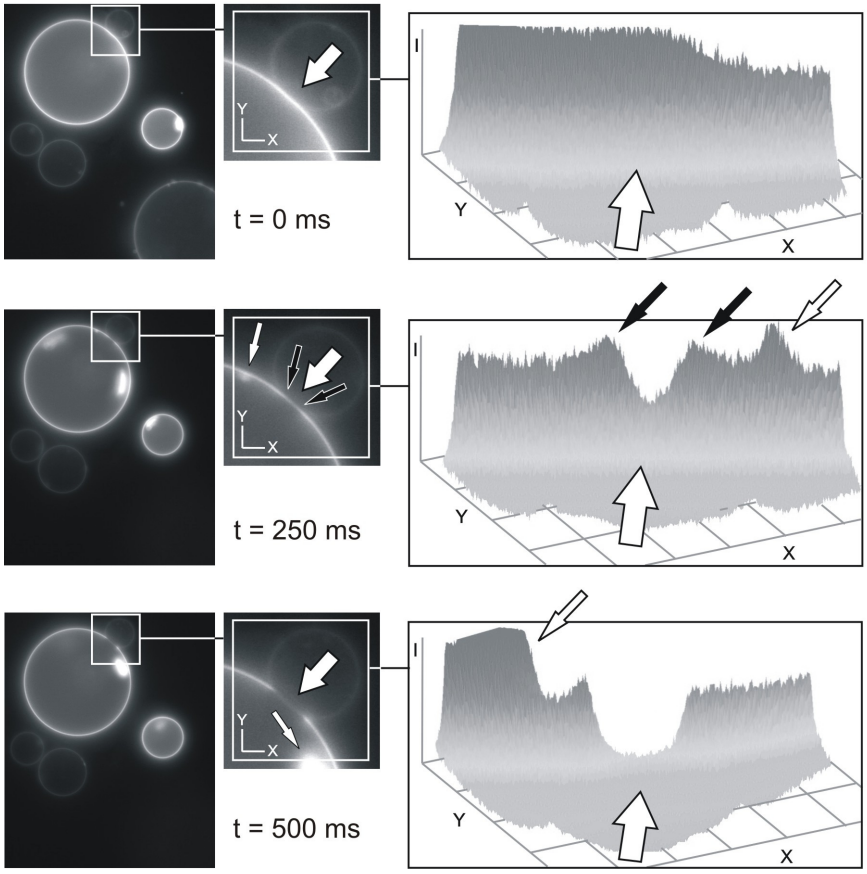

Fig. 12: **Temporary enrichment of TMD peptides at the rim of the forming HD**. CCD camera images of the fusion kinetic of Fig. 11 A are presented in an intensity plot showing the forming HD and its rim. Upon formation of the HD (see fluorescence decrease in the forming HD (large open arrow)) there is a temporary local fluorescence increase at the rim of the forming HD (see small solid arrows) as the TMDs get sequestered. The small open arrow marks structures in the GUV not related to fusion. Note, the large open arrow in the intensity plots indicates also the direction of view (from back to front).

4.1.3 Quantification of fluorescent analogues confirms HD formation

At 2 mM Ca^{2+} or Mg^{2+} GUVs attached, but did not fuse immediately or even remained unfused. Using these conditions the distribution of N-NBD-PE and Rh-LV-Rh could be visualized and quantified within the area of contact that was stable on a timescale of seconds

to minutes (Fig. 13). To mimic the TMD of a native fusogenic protein the peptide Rh-HA-TMD was also studied corresponding to the TMD of influenza virus hemagglutinin from strain A/Japan/305/57 (H2). The peptides differ not only in their amino acid sequence, but also in their secondary structure. Whereas Rh-HA-TMD and Rh-LLV16-Rh have been shown to be α-helical, Rh-LV16-G8P9-Rh exhibits a β-sheet structure (Tatulian and Tamm, 2000; Hofmann *et al.*, 2004; Ollesch *et al.*, 2007). For both types of peptides sequestering from the adhesion region was observed. For Rh-HA-TMD the peptide was sequestered in 77 out of 91 cases (85 %). Since both LV- and HA-TMDs were sequestered, displacement seems to be typical for TMD peptides and not related to a specific sequence. Rh-HA-TMD was not or only partially sequestered in the remaining cases. In this case no redistribution of N-NBD-PE to the peptide containing GUV was found (see below and Fig. 14). This observation also precludes that sequestering of TMD peptides is related to the rhodamine moiety due to e.g. steric hindrance, since peptides with the rhodamine moiety are for few cases also found at the site of two closely adhered membranes. Even for Rh-HA-TMD peptides, labelled with a rhodamine only at the N-terminus, with the rhodamine moiety facing towards the lumen of the GUV for presumably 50% of the Rh-HA-TMDs the peptide could still be located in the attachment site. With this orientation the TMD peptide would expose its three C-terminal lysine residues on the exterior of the GUV and they could in principle interact with the negatively charged head groups of DOPS in the outer leaflet of the opposite, attached GUV. Although in 14 out of 91 cases (15 %) attached GUV with TMD peptides in the adhesion region were observed, displacement of the TMD peptides for GUVs shown in Fig. 13 shows that any electrostatic interaction between lysine residues and PS was not sufficient to keep the peptides in the adhesion region. When both contacting GUVs contained peptides contact regions with sequestered peptides were also found (see below, Fig. 17), but less frequently.

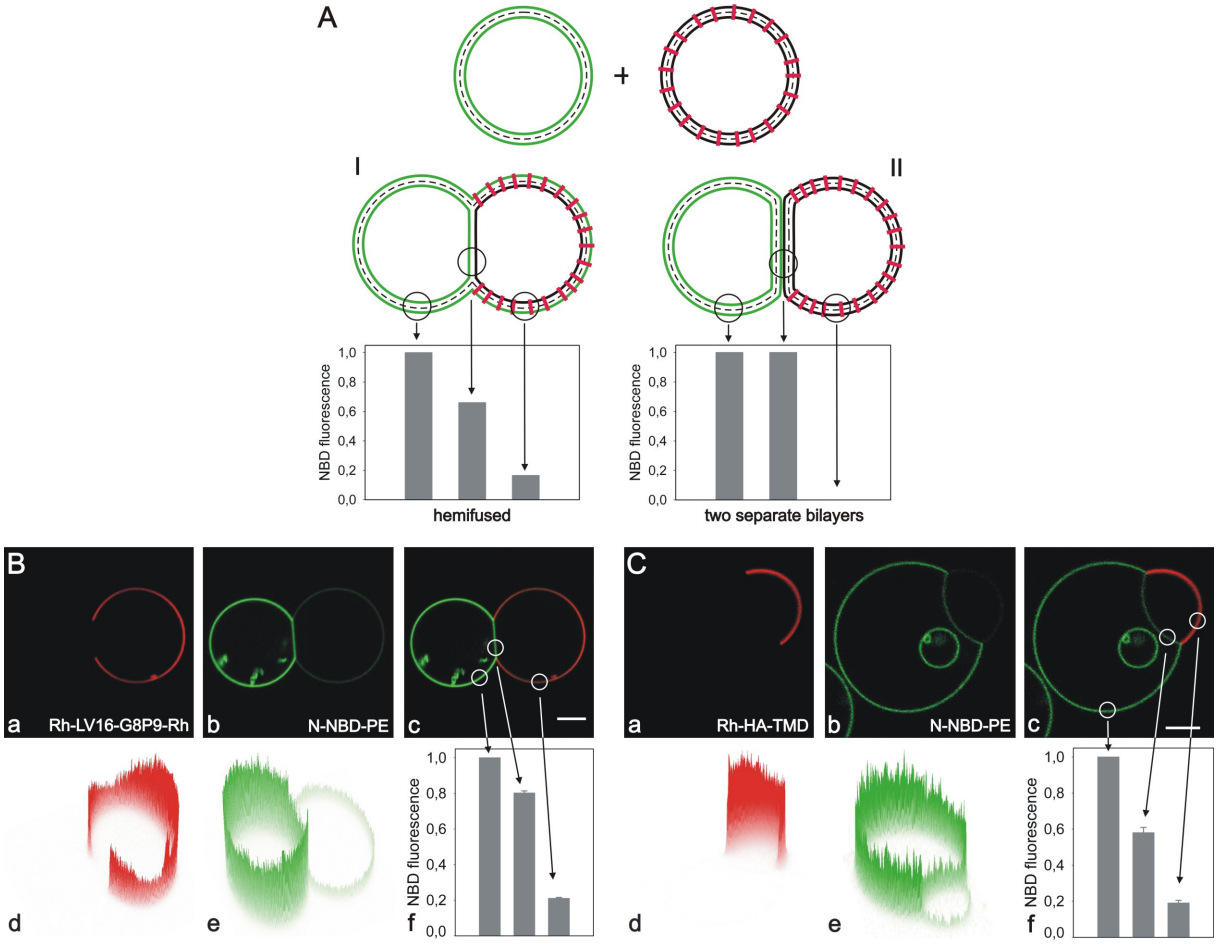

Fig. 13: Fluorescence intensity of fluorescent lipid analogues in the contact region. (**A**) Expected fluorescence intensity of N-NBD-PE in membranes of adherent GUVs (left GUV labelled with N-NBD-PE (green); right GUV with inserted peptide (red)). Intensity is shown for two possible different structures of the adhesion region: (**I**) HD; (**II**) two separate adherent bilayers. While for (**II**) no N-NBD-PE is found in the peptide-containing GUV, the outer leaflet of the peptide-containing GUV becomes labelled by the analogue for (**I**). However, NBD intensity is reduced by approximately about 50 % due to FRET from NBD to Rh-labelled peptides. (**B** and **C**) GUVs containing the peptide Rh-LV16-G8P9-Rh (**B**) or Rh-HA-TMD (**C**) and N-NBD-PE labelled GUVs were mixed. 2 mM Ca^{2+} or Mg^{2+} were added to trigger adhesion of GUVs. Distribution of Rh-labelled peptide (**a**); distribution of N-NBD-PE (**b**); overlay of a and b (**c**). Fluorescence intensity profiles of rhodamine (**d**) and NBD (**e**). N-NBD-PE fluorescence intensity in three different bilayer regions is given in (**f**): Region of the NBD-labelled GUV outside the HD (intensity was set to 100 %), HD, and region of the peptide-containing GUV outside the HD. Differences between (**B**) and (**C**) with respect to the relative intensities are due to the different sizes of GUVs.

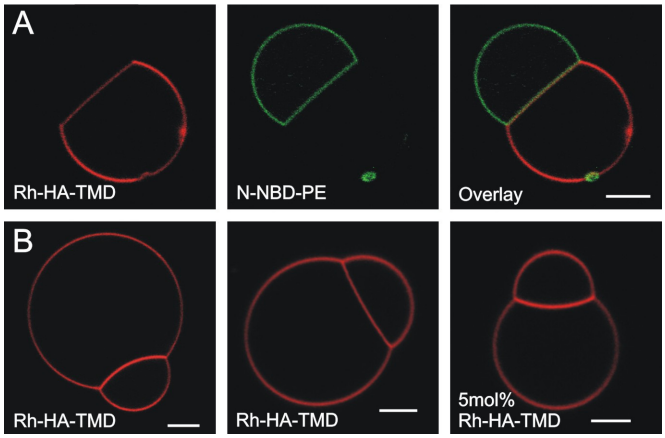

Fig. 14: Adhesion regions without sequestered peptides. GUV pairs for which Rh-HA-TMD peptides are not sequestered from the adhesion region. (**A**) Pair of N-NBD-PE labelled GUV and of peptide (1 mol%) containing GUV. Lateral distribution of Rh-labelled peptide Rh-HA-TMD, N-NBD-PE and overlay are shown. Note N-NBD-PE is not redistributed to the peptide-containing GUV (cf. Fig. 13). (**B** to **D**) Both GUVs contain 1 mol% (**B** and **C**) or 5 mol% peptide (**D**). Bar 5 µm.

A contact region devoid of TMDs could be indicative of an HD. To unravel the membrane organization in this region, the NBD fluorescence intensity was quantified. As illustrated in Fig. 13 A, NBD fluorescence allows to distinguish between adhered, yet unfused bilayers and an HD. For hemifusion two criteria can be identified: First, N-NBD-PE is expected to redistribute to the outer leaflet of the peptide-containing GUV. Note, that the intensity of N-NBD-PE (donor) in the outer leaflet of the peptide-containing GUV is decreased by Förster-Resonance-Energy-Transfer (FRET) to rhodamine (acceptor). Second, as a consequence of lipid analogue redistribution in the outer, but not in the inner leaflets between GUVs the NBD fluorescence intensity in an HD should be about two thirds of that found outside of this region in the GUV, originally labelled with N-NBD-PE. On the other hand, if the contact region still consists of two separate bilayers, the NBD fluorescence in and outside this region would be similar for the N-NBD-PE labelled GUV and N-NBD-PE would not redistribute to the apposed membrane of the peptide-containing GUV since the headgroup labelled N-NBD-PE is anchored to the lipid membrane leaflet by two long fatty acid chains (cf. Fig. 14 A). The NBD intensity pattern of images in figure Fig. 13 B and C indeed suggests that an HD has been formed. Further, the transmembrane incorporated peptide did not redistribute to the N-NBD-PE labelled GUV due to geometric restrictions by anchoring of the TMD in both bilayer leaflets, since only the outer leaflets are merged for the hemifusion intermediate, whereas a N-NBD-PE labelling of the GUV containing the peptide was found (see sketch Fig. 13 A I). N-

NBD-PE fluorescence is reduced by FRET. The latter would not be expected if two bilayers would form an adhesion region.

4.1.4 Further conformation of HD formation by fluorescent analogue addition

Further evidence for the formation of an HD was obtained by studying the contact region between Rh-HA-TMD containing GUVs and non-labelled GUVs (no N-NBD-PE present). To GUVs forming a contact region with sequestered peptides the short-chain lipid analogue C6-NBD-PC was added, which is known to insert rapidly into the exposed, outer membrane leaflet (see cartoon, Fig. 15 A). A rapid labelling of both GUV membranes except for the contact region was found (Fig. 15 B, C and D). The intensity profile of the analogue outside this region reveals that insertion of the analogue reached equilibrium within about 1 min (Fig. 15 Bc). Again, the NBD fluorescence in GUVs containing the TMD peptides is lower due to FRET (Fig. 15 Bc). This labelling pattern supports the existence of an HD since an adhesion region formed by two separate bilayers would be rapidly labelled by lateral diffusion of analogues. Assuming a typical lateral lipid diffusion rate of about 1 µm²/sec, an analogue would diffuse about 2 µm per sec, or migrate into a 10 µm wide contact region within 5 sec. However, weak NBD fluorescence was detected only after about 130 sec in the HD. Slow labelling of the HD is most likely due to redistribution of the short-chain analogues from the outer to the inner leaflet of GUVs caused by peptide mediated perturbations of the bilayer and/or by the membrane structure at the junction site of three bilayers at the HD periphery. The fluorescence in the HD slowly increased to a level comparable to that of the NBD intensity in the peptide-free GUV outside this region. The latter observation argues also for the formation of an HD. If this region would consist of two intact bilayers with only the outer leaflets labelled, the final fluorescence intensity would be twice as much as that observed outside this region. To verify that labelling of the HD is due to redistribution of analogues to the inner leaflet and not due to restricted diffusion of analogues between two adhered intact bilayers, fluorescence recovery after photobleaching (FRAP) measurements were performed in the equatorial plane of the GUVs after a constant fluorescence of C6-NBD-PC in the HD has been reached. The same recovery pattern in the HD and outside of this region was found (Fig. 16), which would not be expected in the case of restricted diffusion between two bilayers. Hence, neither the slow labelling kinetics nor the final fluorescence intensity and the

lateral diffusion of analogues are compatible with the presence of two intact separated bilayers in the adhesion region.

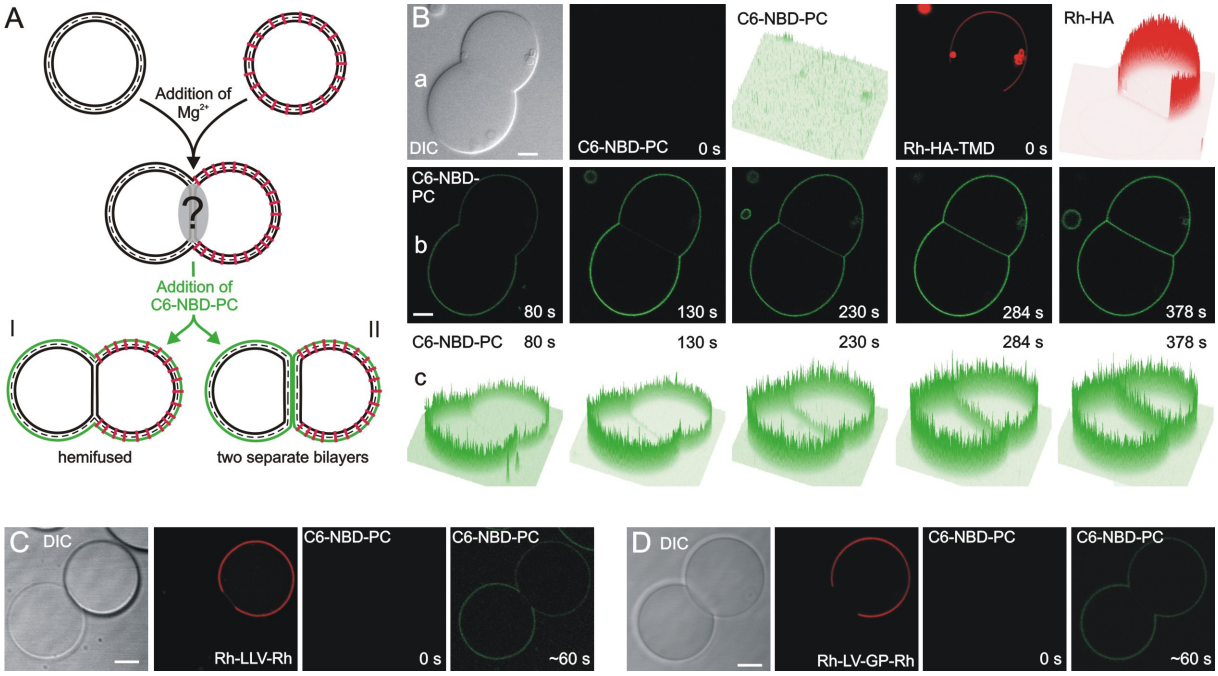

Fig. 15: Lipids in the outer leaflet cannot enter the HD. C6-NBD-PC was added to pairs of GUVs with sequestered Rh-TMD peptides. After insertion of the lipid analogue in the outer leaflet, labelling of the contact region was studied by following the lateral distribution of the NBD fluorescence. (**A**) Sketch of C6-NBD-PC localization. In case of HD formation no fast redistribution of the lipid analogue to the HD is observed (I) whereas the adhesion region becomes quickly labelled when it is formed by two separated bilayers (II). (**B**) Lateral distribution of C6-NBD-PC observed by confocal fluorescence microscopy. (**a**) Images of a GUV pair before addition of C6-NBD-PC (t = 0). From left to right: DIC; distribution of C6-NBD-PC (green); intensity profile of NBD fluorescence; distribution of Rh-labelled peptide (red); intensity profile of rhodamine fluorescence. Distribution of C6-NBD-PC (**b**) and corresponding intensity profile (**c**) at various times after addition of C6-NBD-PC. (**C** and **D**) Hemifused situation also shown for Rh-LLV16-Rh (**C**) and Rh-LV16-G8P9-Rh (**D**) before and ~60 seconds after C6-NBD-PC addition. Bar 5 µm.

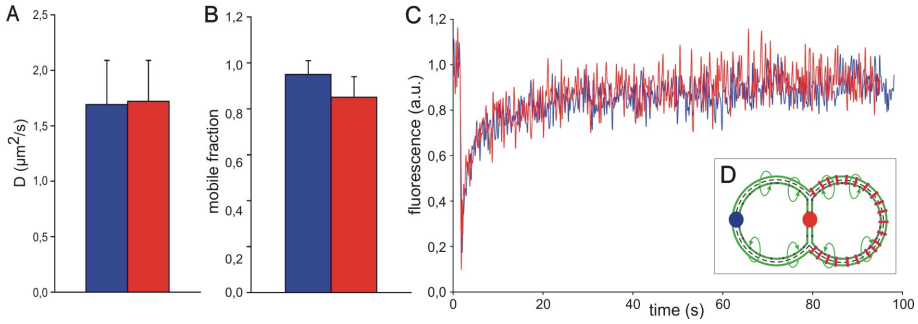

Fig. 16: Fluorescence recovery after photobleaching (FRAP) shows similar diffusion properties of fluorescent lipid analogue in the GUV membrane outside the HD (blue, n=22) and in the HD of two hemifused GUVs (red, n=14), respectively. For localization of bleached spots see (**D**). Diffusion coefficient D ($\mu m^2/s$) (**A**) and mobile fraction (**B**), for calculation see section 3.2.11 in Material and Methods. Bars represent the mean ± SD of at least 14 measurements. (**C**) Two selected fluorescence recovery graphs for FRAP measurements in GUV membrane outside the HD (blue) and within HD (red), respectively.

In another approach the outer leaflet of Rh-HA-TMD peptide-containing GUVs was labelled with C6-NBD-PC before allowing them to adhere. In the contact region of those GUVs both the peptide as well as the lipid analogue were displaced (Fig. 17). Again, the latter would not have been observed if this region would consist of two intact bilayers. Only after longer incubation labelling of the HD by C6-NBD-PC was observed very likely due to redistribution of analogues to the inner leaflet (see above). Both approaches gave the same results for GUVs without peptide (not shown). Based on these various observations it can be concluded that the contact region with sequestered peptides corresponds to an HD.

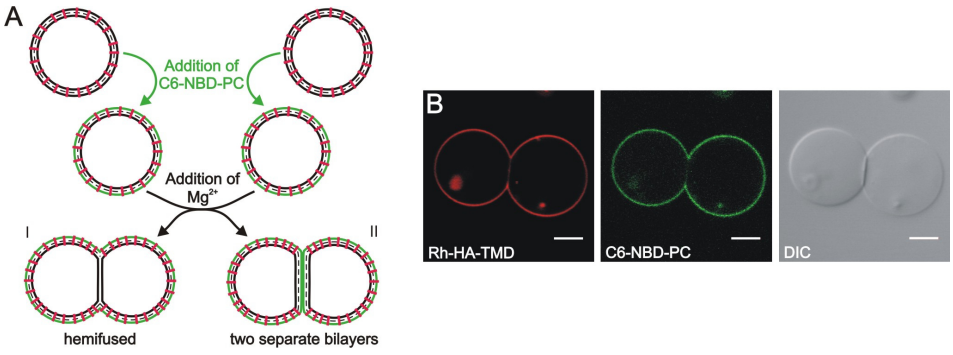

Fig. 17: Sequestering of C6-NBD-PC upon HD formation. Outer membrane leaflets of GUVs were labelled by addition of C6-NBD-PC prior to addition of Mg^{2+}. (**A**): Sketch of C6-NBD-PC localization. (**I**) If an HD is formed C6-NBD-PC is sequestered from the forming HD. (**II**) C6-NBD-PC remains in the adhesion region when it is formed by two separated bilayers. (**B**): Addition of 2 mM Mg^{2+} led to the adhesion of the GUVs with sequestered Rh-HA-TMD peptides. Images of rhodamine and NBD fluorescence of two attached GUVs, both contain Rh-HA-TMD peptide. Peptides as well as C6-NBD-PC are sequestered from the HD. Bar 5 µm.

4.1.5 Further parameters determining HD formation

Growth of an HD is expected to decrease the total membrane area, accompanied by a reduction of membrane tension. This reduction of tension is observable as an increase of the contact angle between GUV and cover slip upon which the GUV settles down (Radler *et al.*, 1995). Indeed, from Z-stack images (1 µm slices) (Fig. 18) it was found that the GUV-cover slip contact angle for hemifused GUVs (83 ± 9)° was much larger than for non-hemifused GUVs (35 ± 14)°.

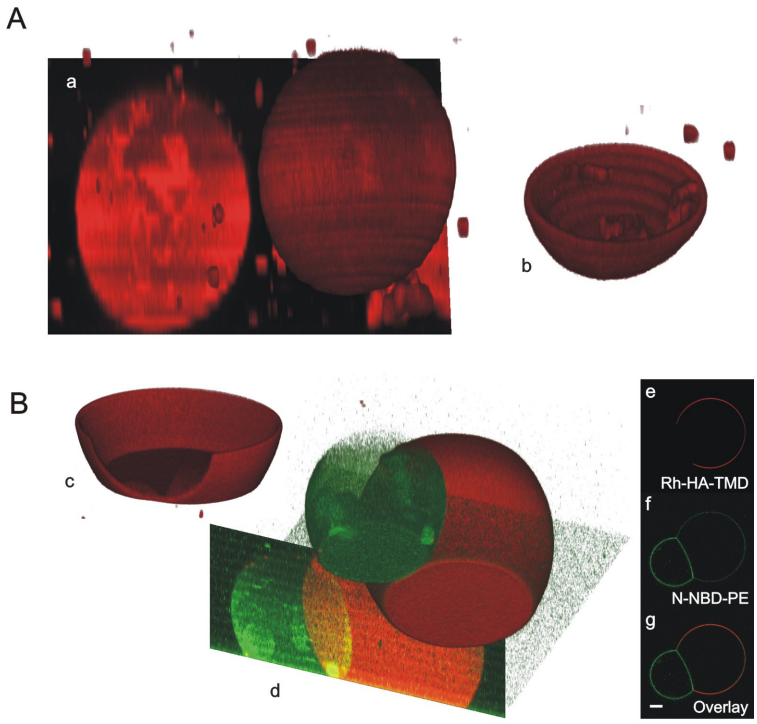

Fig. 18: **3D reconstruction from Z-stack images** of a round non-hemifused GUV with Rh-HA-TMD (**A**) and two flattened hemifused GUVs (**B**) with N-NBD-PE and Rh-HA-TMD. Complete GUVs are shown from below (**a, d**) and a look inside the sliced open GUVs is represented in (**b, c**). (**e-f**) images of the equatorial plane of the hemifused GUV. Bar 5 µm.

The size of the HD was dependent on the surface area of GUVs. An almost linear increase of the surface area of HD with that of the GUV pair was found (Fig. 19). Notably, reduction of phosphatidylserine (PS) from 20 to 10 mol% did not affect the linear dependence. Only in case that the size of the two hemifused GUVs was very different, a shallower dependence of HD size from that of GUVs was found (see Fig. 19). For a more detailed analysis see Discussion.

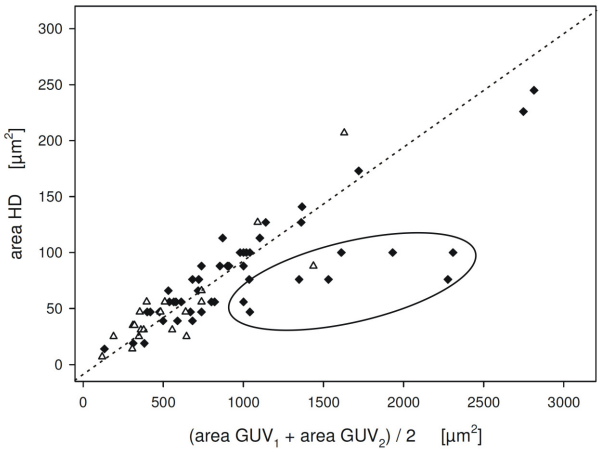

Fig. 19: **HD area vs. GUV surface area**. HD area plotted against the mean surface area of the two hemifused GUVs. Filled symbols - GUVs containing 20 mol% PS lipids; open symbols - GUVs with 10 mol% PS. A shallower dependence was observed in case the size of the two hemifused GUVs was very different (encircled, ratio of GUV diameters > 4.4). Dotted line shows the model prediction based on an analytical description of equilibrium HD size for GUVs with a ration of <4.4. For details see Discussion.

A dependence of the HD size on TMD peptide concentration was observed, i.e. for increasing peptide concentration a decreasing HD size was found (Fig. 20). When the peptide concentration was raised above 1 mol% only occasionally formation of HD was found not sufficient for statistics. At 5 mol% HD formation was never observed (Fig. 14 D). Very likely, the increased amount of TMD in the membrane outside the HD produces a surface pressure pressing on the HD boundary, thus resisting HD growth. When GUVs were prepared without DOPE no hemifused GUVs were observed.

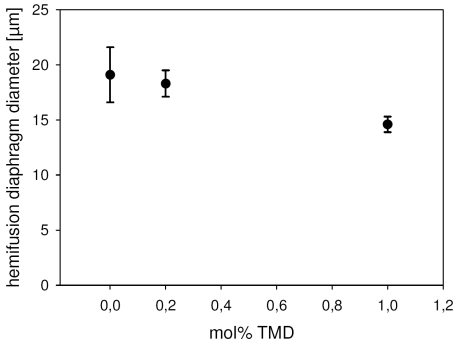

Fig. 20: Dependence of HD size on TMD concentration. For increasing Rh-HA-TMD peptide concentration in GUVs a decrease in the HD size was observed. Plotted values are diameter (mean ± SEM) of HD size versus mol% of TMD peptide concentration reconstituted into GUVs. 0 mol% TMD value stands for hemifusion of two GUVs both labelled with N-NBD-PE and without TMD peptides. In the latter case formation of HD was detected by measuring and comparing the fluorescence intensity of N-NBD-PE in the different GUV regions (see Results).

4.1.6 Sequestering of reconstituted full length hemagglutinin

To address whether full length HA is also sequestered from contact regions, full length HA protein was reconstituted into DOPC:DOPE:DOPS (3:1:1) GUVs containing 1 mol% N-NBD-PE according to protocol 1 (cf. section 3.2.6). Although rarely observed, HA was sequestered from the forming HD upon addition of 2 mM Ca^{2+} (Fig. 21). Unfortunately, at low pH conditions that are known to trigger a conformational change of HA leading to membrane fusion, the formation of an HD could not studied because GUVs became instable.

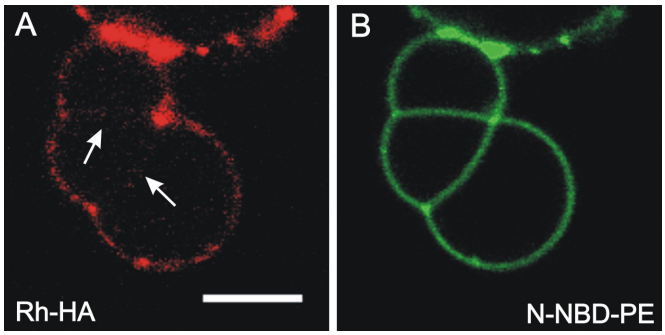

Fig. 21: Sequestering of full length HA from contact regions. Rhodamine-labelled full length HA (Rh-HA) was reconstituted into GUVs made of DOPC:DOPE:DOPS (3:1:1, molar ratio), containing 1 mol% N-NBD-PE. Upon addition of 2 mM Ca^{2+} adhesion of GUVs and formation of regions depleted of HA could be observed (arrows). (**A**) Rh-HA and (**B**) N-NBD-PE fluorescence. Bar 5 µm.

4.1.7 Sequestering of a Rh-labelled oligospiroketal rod

Besides transmembrane peptides with different secondary structures and the full length HA protein also the sequestering of a new synthetic molecular rod was observed. The hydrophobic molecular rod has a high conformational rigidity and proteolytic stability. The oligospiroketal backbone of the Rh-Rod-Rh is functionalized on both ends with a rhodamine-labelled pentapeptide comprising three lysine residues for a better transmembrane insertion (Hesselink *et al.*, 2005). It was reconstituted into GUVs in a same procedure as the TMD peptides. Mixed together with GUVs labelled with N-NBD-PE and addition of 2 mM Mg^{2+} the sequestering of Rh-Rod-Rd was found upon HD formation (Fig. 22).

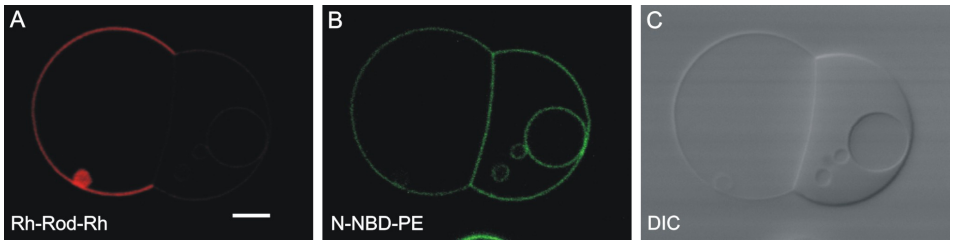

Fig. 22: Sequestering of Rh-labelled oligospiroketal rod. Pair of GUVs comprising either about 1 mol% Rh-Rod-Rh (**A**) and 1 mol% N-NBD-PE (**B**) showing sequestered Rh-Rod-Rh and redistributed N-NBD-PE to the GUV originally only containing Rh-Rod-RH. Hemifusion was triggered by addition of 2 mM Mg^{2+}. Differential interference contrast (**C**). Bar 5 µm.

4.1.8 On the dynamics of complete membrane fusion

As seen in the sequence of fusion kinetics (Fig. 11 B and C), a single HD first forms and subsequently expands over a large area as compared to the vesicle radius and finally ruptures, most likely, at its rim and pulls back to the opposite side (cf. Kozlovsky *et al.*, 2002). The formation of the larger HDs seemed most common in this system. However, the formation of smaller and fast evolving fusion pores was also observed, as can be concluded from Fig. 23. Here, several fusion events within the adhesion area lead to the formation of small vesicles probably comprising the contacting bilayer areas with the TMD peptides of the adhering GUVs membranes since these small internal vesicles show both Rh-TMD and N-NBD-PE fluorescence.

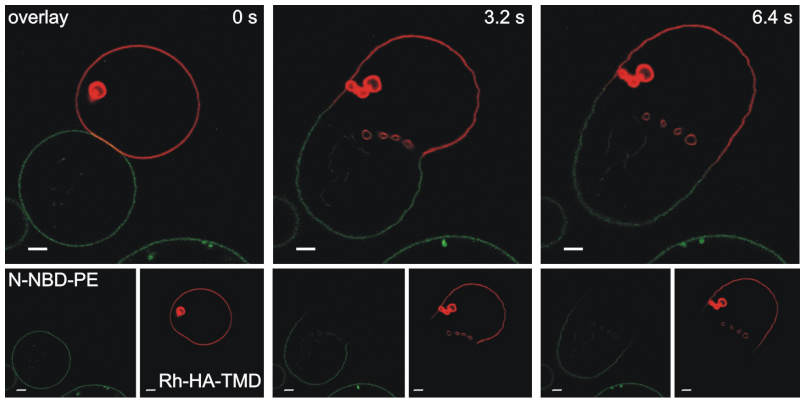

Fig. 23: Sequence of GUV fusion imaged by confocal laser scanning microscopy. Upper GUVs contains Rh-TMD of HA, lower GUVs is labelled by N-NBD-PE. GUV fusion probably proceeded via formation of several fusion pores indicated by the remaining small vesicles comprising both Rh-TMD and N-NBD-PE from both adhered GUVs (see 0 s). Fusion was triggered by 2 mM Mg^{2+} at 25°C. Time per image 3.2 seconds. Bar 5 µm.

Finally it should be mentioned that besides long-lasting hemifusion intermediates often also complete fusion of GUVs was observed in the presented model system indicated by GUVs having both N-NBD-PE and Rh-labelled peptide present in one membrane after GUVs of two separate preparations (N-NBD-PE only and Rh-TMD only) were mixed (cf. Ollesch *et al.*, 2007). Fusion of GUVs containing TMD peptides was not only found after the addition of divalent cations, but also after incubation at 37°C as previously described for a TMD containing model system of small unilamellar vesicles (SUVs) (Langosch *et al.*, 2001). Whereas besides in a fluorescence dequenching assay liposome fusion was also shown by the appearance of larger liposomes in electron microscopy images, this could not be shown for GUVs by fluorescence microscopy. Here, GUVs containing Rh-LLV16-Rh peptides and a control group only labelled with N-NBD-PE showed no difference in their size distribution ($n > 300$) after 3h incubation at 37°C (not shown). Also GUVs did fuse under these conditions, shown by mixing and fusion of only N-NBD-PE and only Rh-TMD labelled GUVs, size comparison of the giant vesicles is not able to detect this probably due to instability of very large GUVs.

4.2 Lipid domain formation and protein sorting

The understanding of the mechanisms underlying the sorting of lipids and proteins in lipid bilayers is crucial for the understanding of many cellular processes in signalling and sorting at the membrane. In this second part, the formation of lipid domains and the sorting of proteins within model and biological membrane systems was therefore investigated.

4.2.1 Lipid domain formation

The fluorescent lipid analogue C6-NBD-PC was established as a powerful tool to study lipid domain formation in model as well as biological membranes, as it could be shown in previous publications (Stockl *et al.*, 2008; Nikolaus *et al.*, 2010a). Partitioning and fluorescence lifetime analysis of C6-NBD-PC was also used here to investigate the physical properties of the membrane.

The properties of the membrane probe C6-NBD-PC at a concentration of 1 mol% was first characterized in GUV membranes. As for the visualization of a hemifusion diaphragm (see 4.1.1), GUVs are also a very suitable membrane model system to study domain behaviour due to their size and almost arbitrary lipid compositions (Veatch and Keller, 2003). A possible oxidation of unsaturated lipids using ITO coated glass slides for the preparation of GUVs was reported (Ayuyan and Cohen, 2006), leading to an unintended formation of lipid domains. Therefore, GUVs for sorting and partition experiments were mainly prepared on titanium plates (cf. Fig. 9). C6-NBD-PC was introduced already to the lipid mixture prior to spreading the lipids to form a film on the titanium slides. Electroformation (cf. section 3.2.5.2, M. I. Angelova and Dimitrov, 1986) yielded mostly unilamellar vesicles with a comparable amount of fluorophores incorporated in both membrane leaflets. Obviously, multilayer vesicles or GUVs with an unusual appearance were not used for analysis. However, GUVs including smaller internal vesicle not in contact with the membrane of interest where considered for evaluation. In an ensemble of vesicles exhibiting a certain characteristic at a certain temperature always the behaviour of the majority of vesicles in the population is described. Note that after preparation there is transbilayer lipid symmetry across the two membrane leaflets in model vesicle systems. Only recently a method was introduced by which a transbilayer lipid asymmetry can be achieved (Cheng *et al.*, 2009).

A lateral homogenously distribution of C6-NBD-PC is found in the vesicle membrane of the unsaturated phospholipid DOPC GUVs at 25°C being in an all liquid disordered (Ld) phase as T_m is -22°C (Weber *et al.*, 2005). This homogenous distribution demonstrates at least the absence of larger lipid domains that can be resolved by confocal microscopy above the diffraction limit. Measuring the fluorescence decay of the fluorophores and fitting of these decay reveals two lifetime components termed τ_1 and $\tau_{2,Ld}$ of 2.1 ± 0.1 ns and 6.7 ± 0.1 ns (as for all lifetimes in this study: mean ± SEM; here: n = 22), respectively. Comparable results were obtained in (Stockl *et al.*, 2008). The short lifetime τ_1 was found in all FLIM measurements of C6-NBD-PC to be approximately between 2 and 3 ns having a small (fractional) amplitude with a contribution of <10 %. It probably results from not incorporated lipid analogues in buffer and from a red edge excitation of fluorescence within the membrane (Stockl *et al.*, 2008; Chattopadhyay and Mukherjee, 1993).

The longer lifetime τ_2 was found to be sensitive to the lipid environment reporting on the physical properties of the membrane (Stockl *et al.*, 2008). This is the powerful advantage of the GUV model system being able to visualize micrometer scaled lipid domains and simultaneously determine the fluorescence lifetime of an incorporated lipid probe in the respective domain. This can later be used to report on domains not detectable by a visible domain separation. In GUVs of a DOPC:SSM:Chol (1:1:1, molar ratio) lipid composition at 25°C both microscopic visible Ld and Lo domains are present (Veatch and Keller, 2003; van Duyl *et al.*, 2002) identified by a preferential partition of C6-NBD-PC into the Ld domain (Shaw *et al.*, 2006) and also by co-staining this domain using other lipid Ld markers like N-Rh-DOPE (Baumgart *et al.*, 2007a) (not shown). Analysis of the fluorescence decays revealed different lifetimes of around 7 ns in the Ld, as in pure DOPC GUVs, and of around 11 ns in the Lo domain, comparable to GUVs of a DOPC:SSM:Chol (1:1:8, molar ratio) lipid mixture found to be in an all Lo lipid phase (cf. Stockl *et al.*, 2008) (Fig. 24 A and E). Similar results were obtained for POPC:SSM:Chol (1:1:1, molar ratio) at 25°C with a PC lipid having a saturated C16:0 acyl chain besides the C18:1 compared to the DOPC (di-C18:1PC). As expected for a lipid with one saturated acyl chain predominantly residing in the Ld domain, $\tau_{2,Ld}$ is significantly longer here (8.4 ± 0.1 ns, n = 21) compared to the DOPC mixture (7.4 ± 0.1 ns, n = 10) (Fig. 24 F). In GUVs prepared from virus lipid extracts of influenza A virus strain A/PR/8/34 measured at 10°C the difference between the two τ_2 lifetimes was similar (Fig. 24 B) with a tendency of both components to be shorter than in the synthetic lipid

mixtures. Finally it should be noted that not all the GUVs prepared from synthetic or viral lipids, respectively, did exhibit lipid domain formation.

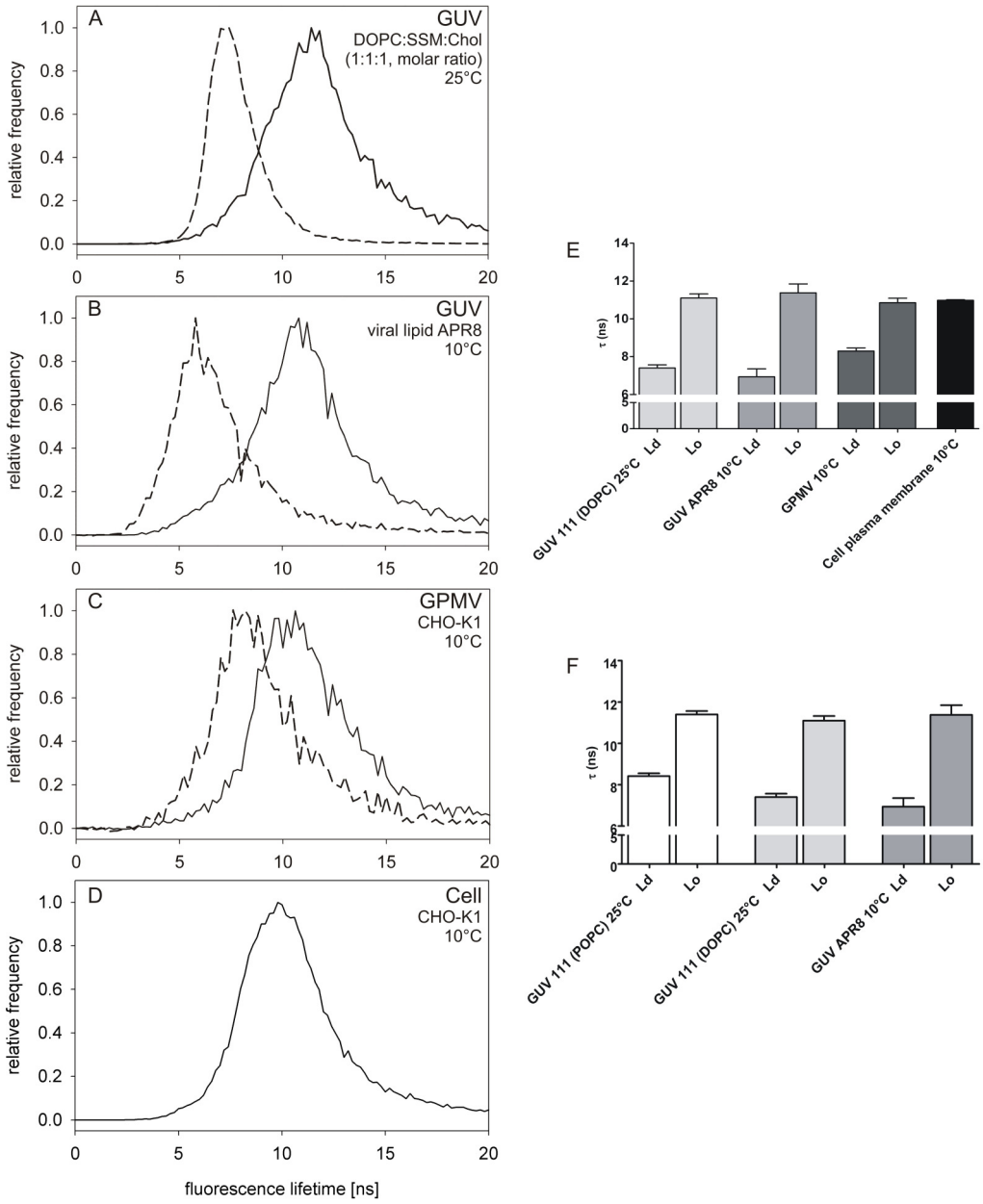

Fig. 24: Fluorescence lifetime of C6-NBD-PC in GUV, GPMV and plasma membrane. In the lipid domains C6-NBD-PC showed a double exponential fluorescence decay. Here, only the longer lifetime (τ_2) sensitive to the lipid domain is shown (Stockl *et al.*, 2008). Lifetime histograms of C6-NBD-PC are shown for Ld (*dashed line*) and Lo (*full line*) in GUVs prepared from DOPC:SSM:Chol mixtures (1:1:1, molar ratio) at 25°C (**A**), GUVs prepared from total lipid isolated from influenza A/PR/8/34 at 10°C (**B**), GPMVs prepared from CHO-K1 cells (**C**) and in the plasma membrane of CHO-K1 cells at 10°C (**D**). Histograms were normalized to 1. In (**E**) the fluorescence lifetimes are presented in a bar plot as average ± SEM of 9 to 16 GUVs, GPMVs and cells, respectively. In (**F**) the lifetimes of GUVs comprising a POPC:SSM:Chol mixtures (1:1:1, molar ratio) are shown in comparison to the mixtures indicated before.

However, for giant plasma membrane blebs (GPMVs) prepared from CHO-K1 cells labelled with C6-NBD-PC the difference between $\tau_{2,Ld}$ and $\tau_{2,Lo}$ was much smaller compared to the GUV model system of synthetic lipid mixtures or viral lipid extracts. The lifetime in the Ld domains of GPMVs was significantly higher as in GUVs, whereas the lifetime in the Lo domains was found to be slightly shorter even so measurements of GPMVs were performed at 10°C (Fig. 24 C and E). Note that at 10°C not all GPMVs did show domain formation. GPMVs for the measurement were provided by Silvia Scolari.

For CHO-K1 cells, a hamster ovary epithelial tissue cell line, microscopic visible domain formation was observed neither at 25°C nor at 10°C. Determination of the C6-NBD-PC lifetime in the plasma membrane of labelled CHO-K1 cells revealed besides the short τ_1 only one second lifetime of τ_2 ~ 10.8 ± 0.1 ns at 25°C and $\tau_{2,Ld}$ ~ 11.0 ± 0.1 ns at 10°C (Fig. 24 D und E) since two lifetimes provided accurate fits of the fluorescence decay curves. FLIM images of CHO-K1 cells were provided by Silvia Scolari. In contrast, for K562 cells, a human suspension myeloid leukemia cell line, only three exponential fits of the fluorescence decay curves of C6-NBD-PC yielded reasonably results. Lifetimes of τ_1 ~ 3.26 ± 0.88 ns, $\tau_{2,Ld}$ ~ 7.93 ± 0.27 ns and $\tau_{2,Lo}$ 11.63 ± 0.19 ns (n = 107) were obtained indicating the existence of submicroscopic lipid domains within the plasma membrane of K562 cells since also here no visible formation of lipid domains was observed. K562 cells were provided by Sebastian Riese (AG Dernedde/Tauber, FU Berlin). Whether raft domains are, as speculated, located in the microvilli structures on the cell surface could not be shown in this FLIM approach since the number of counts originating from the microvilli was too low for an accurate analysis of these structures alone (not shown).

4.2.2 Lipid domain partition of influenza virus hemagglutinin in model membranes

For the budding of progeny virus particles an efficient lateral sorting of newly synthesized viral proteins is necessary. To study possible sorting signals residing in the proteins the lateral partitioning was investigated in lateral lipid domain forming model systems of different complexity. In Fig. 25 an overview of the various constructs for studying the lateral partition among Ld and Lo domains of GUVs and GPMVs is shown.

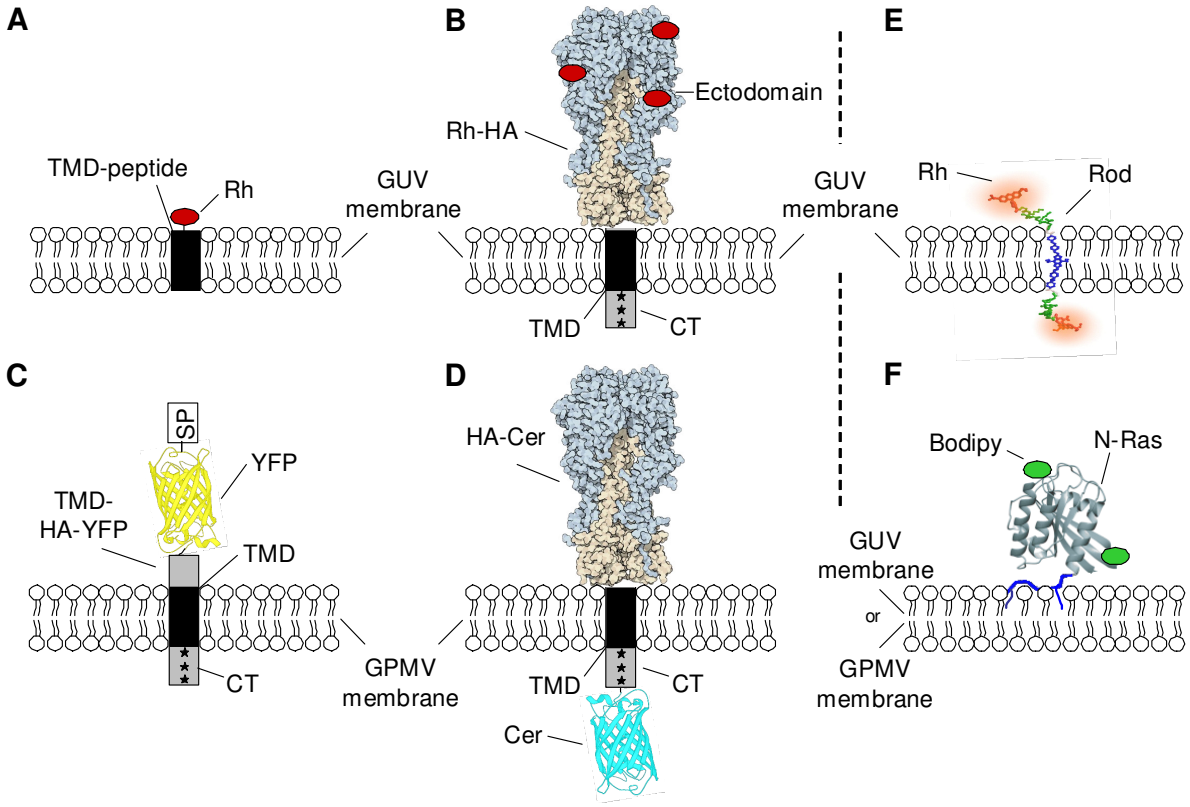

Fig. 25: Overview on different HA constructs, oligospiroketal rod and Ras-protein. (**A** and **B**) Rhodamine (TAMRA) labelled synthetic peptide (TMD peptide) corresponding to the transmembrane domain of influenza HA (**A**, Rh-HA-TMD) or full length HA (**B**, Rh-HA) were incorporated into GUVs of different lipid compositions. (**C** and **D**) HA fragment linked N-terminally to YFP and signal peptide (SP) (**C**, TMD-HA-YFP) or full length HA tagged C-terminally with Cerulean (**D**, HA-Cer) were expressed in the plasma membrane of CHO-K1 cells. Subsequently, GPMVs were generated and used for confocal scanning microscopy. (**E**) Oligospiroketal rod flanked on both ends by a rhodamine-labelled pentapeptide was incorporated into GUVs. (**F**) Bodipy labelled full length N-Ras protein was added to GUVs and GPMVs and anchored in the membranes via two lipid modifications. Rh – TAMRA; TMD – transmembrane domain; CT – cytoplasmic tail; * - palmitoylation site.

4.2.2.1 Lateral organisation of the TMD peptide of HA in GUVs

Influenza HA is anchored in the membrane via a single α-helical transmembrane anchor. Hydrophobic length and amino acid sequence of this TMD are two most obvious candidates for the determination of a certain domain partitioning. Therefore the lateral organisation of the tetramethylrhodamine-labelled peptide Rh-HA-TMD (Fig. 25 A) corresponding to the HA transmembrane domain sequence was studied. The peptide was incorporated into membranes during GUV preparation (1 mol%, see Material and Methods, section 3.2.5.2). While a

homogenous distribution in pure DOPC vesicles (Fig. 26 A) was found, Rh-HA-TMD strongly partitioned into the Ld domain of GUVs consisting of DOPC:SSM:Chol (1:1:1, molar ratio) (Fig. 26 B) as judged by comparison with C6-NBD-PC distribution being a marker for the Ld domain (Shaw *et al.*, 2006). To mimic a more native lipid environment Rh-HA-TMD was reconstituted into GUVs prepared from virus lipid extracts from influenza virus A strain A/PR/8/34 at 25°C and was also found in the Ld domain (Fig. 26 C), and also at 10 and 37°C (not shown).

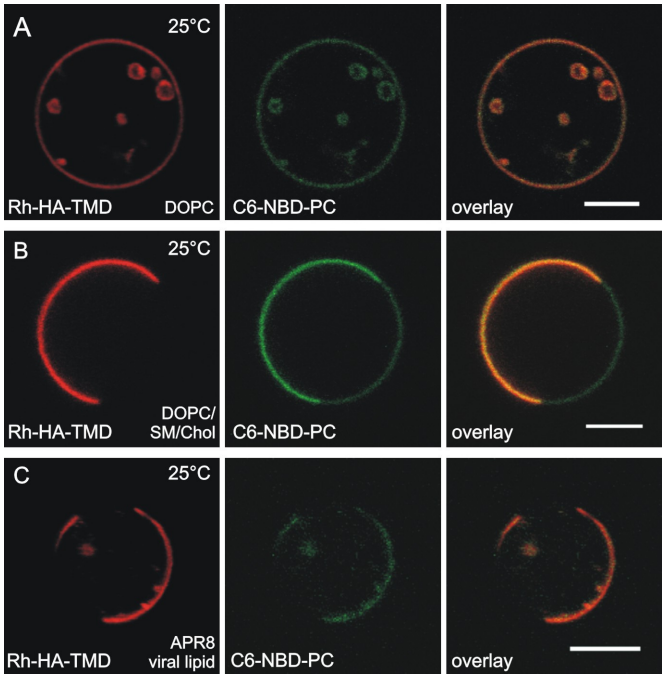

Fig. 26: Lateral organisation of transmembrane HA peptide in domain forming GUVs. Rhodamine (TAMRA) labelled synthetic peptide (Rh-HA-TMD) corresponding to the transmembrane domain of influenza virus hemagglutinin was incorporated into GUVs made from DOPC (**A**), DOPC:SSM:Chol (1:1:1, molar ratio) (**B**) or from influenza virus lipid extracts strain A/PR/8 (**C**). Rh-HA-TMD - Rhodamine fluorescence (red); C6-NBD-PC fluorescence (green) as marker for liquid-disordered domains; overlay. Bar 5 µm. Images were taken at 25°C.

Besides the Rh-HA-TMD comprising the amino acid sequence of the wild type TMD of HA (strain Japan/305/57 subtype H2 (Tatulian and Tamm, 2000)) also a mutation in the TMD sequence was tested. As the mutation GS520AA was found in detergent extraction experiments to alter the partition of full length HA expressed in BHK cell from DRMs to DSMs (Scheiffele *et al.*, 1997) also this TMD sequence was incorporated into GUV membranes of the different lipid compositions. The same results as for the Rh-HA-TMD comprising the 'wild type' sequence were obtained with a homogenous distribution in nonraft

GUV and a partition into the Ld domain in GUVs of the synthetic raft mixture DOPC:SSM:Chol (1:1:1, molar ratio) or GUVs prepared from virus lipid extracts from A/PR/8/34 (not shown).

To exclude the rather unlikely possibility that Rh-HA-TMD concentrated in the Lo domain would cause a self-quenching of the rhodamine fluorescence already at 1 mol% of incorporated TMD peptide also experiments at 0.1 and 0.01 mol% Rh-HA-TMD were carried out. The same partition behaviour as for 1 mol% Rh-HA-TMD was observed (not shown). Note, that also at low peptide concentration no enrichment of Rh-HA-TMD at the Lo/Ld domain boundary was found (cf. 4.2.4 and see Discussion).

Formation of GUVs from a DOPC:DSPS:SSM:Chol (1:1:1:1, molar ratio) lipid mixture results in a vesicles harbouring the di-C18:0PS in the Lo domain (Stockl *et al.*, 2008). With the Ld domain again identified by 1 mol% C6-NBD-PC it was tested whether electrostatic attraction of the negatively charged PS in the Lo domain could recruit the three positively charged terminal lysine residues of the Rh-TMD of HA. No partition of the TMD into the Lo domain was found (not shown), not even enrichment at the Lo/Ld domain boundary (cf. section 4.2.4.1).

4.2.2.2 Lateral organisation of reconstituted full length HA in GUVs

As the full length HA protein is expressed and transported to the apical plasma membrane it is modified during its passage through Golgi apparatus. Besides proteolytical cleavage the protein is glycosylated and acylated, which is, amongst other, responsible for trimerization (Copeland *et al.*, 1986) and plasma membrane targeting (Veit *et al.*, 1991) as well as for a possible lipid domain association, respectively. To determine whether these posttranslational modifications influence the domain partitioning viral full length HA was reconstituted in GUV membranes (Fig. 25 B). HA from X31 influenza virus labelled with TAMRA (Rh-HA) was reconstituted in GUVs according to the protocol adapted from (Papadopulos *et al.*, 2007; Girard *et al.*, 2004) (see Protocol 2, Material and Methods, section 3.2.6). To this end, HA was reconstituted into proteoliposomes from which GUVs were generated. While the Rh-HA was homogenously distributed in pure DOPC GUVs (not shown), a lateral inhomogeneous organisation of Rh-HA in lipid domain forming GUVs consisting of DOPC:SSM:Chol (1:1:1, molar ratio) (Fig. 27 A) and virus lipid extracts from A/PR/8/34 (Fig. 27 B) was observed at 25°C. The partition behaviour of intact full length Rh-HA in GUVs was very similar to that of

Rh-TMD as judged by comparison with the distribution of C6-NBD-PC (see above). Again, a preference of HA for the Ld domain was observed.

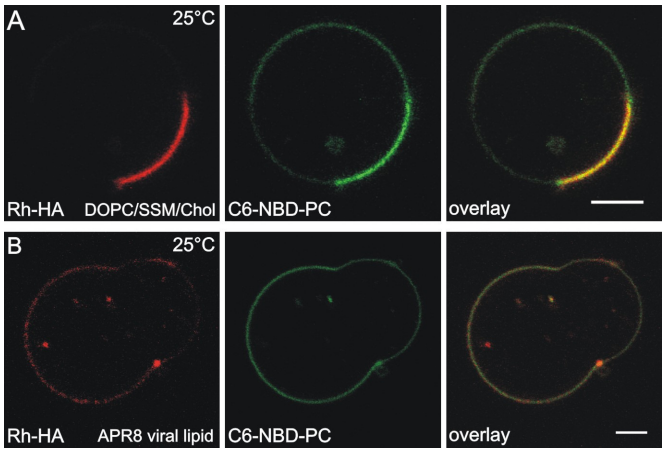

Fig. 27: Lateral organisation of full length HA in domain forming GUVs. Rhodamine (TAMRA) labelled full length HA (Rh-HA) was incorporated into GUVs made from DOPC:SSM:Chol (1:1:1, molar ratio) (**A**) or from influenza virus lipid extracts of A/PR/8/34 (**B**). Rh-HA - Rhodamine fluorescence (red); C6-NBD-PC fluorescence (green) as marker for liquid-disordered domains; overlay. Bar 5 µm. Images were taken at 25°C.

Addition of TMD peptides to preformed GUVs probably resulted in a homogenous distribution of the peptides as visible by fluorescence microscopy on GUVs (not shown). These results are supported by an AFM study measuring the force necessary to pull out an incorporated TMD peptide from the bilayer. Here also a so called 'snap-in' of TMD peptides back into the membrane could be observed after leaving the AFM tip hovering closely above a lipid bilayer (Goldenbogen and Herrmann, 2010, unpublished results). For full length HA protein having the cytoplasmic tail C-terminal of the TMD this situation is different. Addition of Rh-HA to GUVs prepared from DOPC:DOPE:DOPS (3:1:1, molar ratio) did exhibit red fluorescence at the GUV membrane in glucose microscopy buffer. But when the ionic strength of the microscopy buffer was increased by 150 mM NaCl no red fluorescence of Rh-HA was found at the bilayer (not shown). For GUVs comprising only DOPC or DOPC:SSM:Chol (1:1:1, molar ratio) no binding was found even in glucose buffer of low ionic strength. The Rh-HA binding to PS containing GUVs seemed thus only mediated by electrostatic interactions and whether a transmembrane incorporation of the membrane anchor of HA was achieved may be doubted. These results do not support a reconstitution protocol that overlays

purified Rh-HA rosettes, a ring-like assembly of 5-9 HA trimers, on a lipid film for GUV preparation.

4.2.2.3 Lateral organisation of fluorescent HA in plasma membrane blebs

In the literature the lipid domain specific sorting of HA has essentially been studied at the plasma membrane of mammalian cell expressing the full length protein. As lipid domains in living cell membranes are highly dynamic and of submicroscopic size (Pike, 2006) the HA partition cannot be observed directly. The recently published method to generate large bleb-like surface protuberances from the plasma membrane of cells (Baumgart *et al.*, 2007a) now offers the opportunity to directly visualize micrometer-scaled segregation of fluid phase lipid domains and the protein of interest in those GPMVs at lower temperature (10°C) by comparison with the partition of lipid domain markers. To avoid interference of fluorescence tags (Cer, CFP or YFP) of the respective proteins and the fluorescence of the lipid domain marker C6-NBD-PC, the red fluorescent lipid-like octadecyl rhodamine B chloride (R18) was used which is known to partition into the Ld domain (Baumgart *et al.*, 2007b).

The proteins of interest, GPI-CFP, the membrane anchored HA fragment TMD-HA-YFP and full length HA-Cer, are transiently expressed in CHO-K1 cell. These experiments were performed by Silvia Scolari, Stephanie Engel and Anna Pia Plazzo. The GPI-CFP construct is found on the outer plasma membrane leaflet. It is known to enrich in Lo domains and has been often used as a raft marker (P. Keller *et al.*, 2001). Indeed, GPI-CFP was excluded from R18 containing domains (Fig. 28 A). The full length HA-Cer (Fig. 25 D) was tagged at its cytoplasmic tail (C-terminus) with the fluorescent protein Cerulean, a variant of CFP with an improved quantum yield and a higher excitation coefficient (Rizzo *et al.*, 2004). The membrane anchored fragment TMD-HA-YFP (Fig. 25 C) consists of the TMD and the CT as well as a short sequence of the HA ectodomain. Essentially, the HA ectodomain was replaced by YFP. In contrast to HA-Cer, this construct circumvents tagging of the cytoplasmic tail which may interfere with its role in lateral organisation of the protein. Indeed, previous studies indicated that mutations in the TMD and the CT of HA reduce association with DRM fractions (Lin *et al.*, 1998; Scheiffele *et al.*, 1997; Zhang *et al.*, 2000; Takeda *et al.*, 2003). Apart from GPMVs with a homogenous distribution of R18 at 10°C also domain forming blebs were observed indicated by a heterogeneous distribution of the lipid domain marker. At 25°C domains were never found in blebs or the intact plasma membrane of CHO-K1 cells.

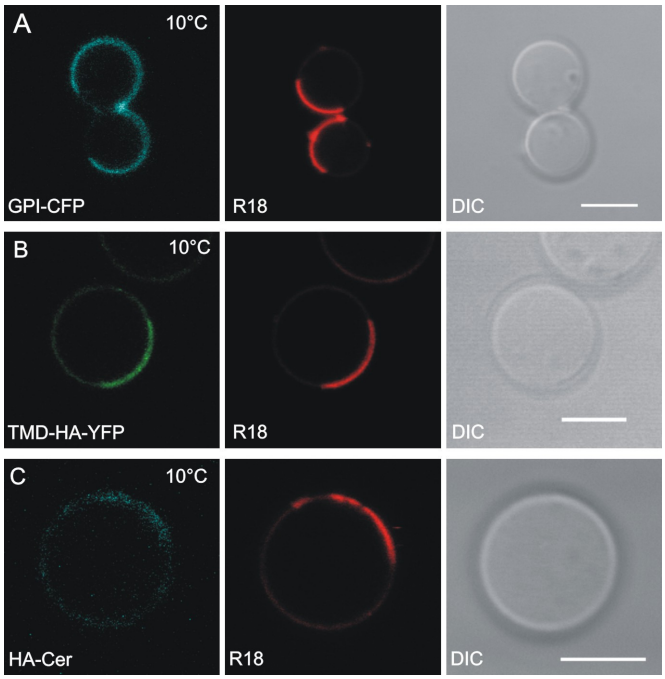

Fig. 28: Lateral arrangement of HA-Cer and TMD-HA-YFP in GPMVs. GPMVs were derived from CHO-K1 cells expressing Lo domain marker GPI-CFP (**A**), TMD-HA-YFP (**B**) or HA-Cer (**C**) in the plasma membrane. Confocal images were taken after cooling samples to 10°C. R18 fluorescence (red) as marker for liquid-disordered domains; DIC – differential interference contrast image. Bar 5 µm.

TMD-HA-YFP was found to partition preferentially to the Ld domain in GPMVs as indicated by colocalization with R18 (Fig. 28 B). HA-Cer also was enriched in Ld domains (Fig. 28 C). Note that the differences in partition of TMD-HA-YFP and HA-Cer between Lo and Ld domains is less pronounced compared to full length HA and TMD peptide of HA in GUVs prepared from synthetic or viral lipids. A quantitative analysis of the fluorescence intensities is provided in Tab. 2 giving the ratio of fluorescence intensity in the Lo and Ld domain in percent for each of the studied systems. On average the ratio is seven times higher in GPMV (0.266) as compared to the GUV system (0.039). At 25 or 37°C neither clustering for HA-Cer and TMD-HA-YFP nor lipid domain formation in the GPMV system (see above) was observed.

Tab. 2: Quantitative fluorescence intensity analysis of HA peptide and protein partitioning between Lo and Ld domains in GUVs and GPMVs. Table shows the ratio of the fluorescence intensity of the HA peptide or protein in the Lo and Ld domains, respectively. Average fluorescence intensities were determined at the membrane of the two distinct domains using Olympus FluoView 1000 software (Olympus, Hamburg, Germany). Average background fluorescence was subtracted prior to calculating the ratio of the fluorescence intensity (Lo/Ld). Note, the ratio refers to the fluorescence intensity, but not to the ratio of amount of HA protein or peptide in the two domains. n refers to the number of analyzed vesicle.

Vesicle	GUV				GPMV	
Protein	Rh-HA-TMD		Rh-HA		TMD-HA-YFP	HA-Cer
Figure	Fig. 26B	Fig. 26C	Fig. 27A	Fig. 27B	Fig. 28B	Fig. 28C
Lipids	DOPC/ SSM/Chol	APR8	DOPC/ SSM/Chol	APR8	CHO-K1	CHO-K1
Ratio	0.006	0.005	0.020	0.126	0.185	0.347
± SEM	0.016	0.018	0.027	0.016	0.023	0.057
n	11	7	8	7	12	6

4.2.3 Lipid domain partition of further transmembrane entities

4.2.3.1 Lateral organisation of SNARE derived LV model peptides in GUVs

The LV model peptides designed as membrane-spanning low-complexity models to mimic the transmembrane anchors of SNARE proteins introduced already in section 4.1.1 were found in a homogeneous lateral distribution in membranes of nonraft lipid mixtures (cf. Fig. 10 and Ollesch *et al.*, 2007). Two variants of the rhodamine-labelled LV-peptides, Rh-LLV16-Rh (Fig. 29 A,B) and Rh-LV16-G8P9-Rh (Fig. 29 C,D), were also incorporated into domain forming GUVs prepared from DOPC:SSM:Chol (1:1:1, molar ratio) and virus lipid extracts from influenza A virus strain A/PR/8/34. Here also a strong colocalization of the peptides and the NBD-lipid was found, showing the partition of both peptides into the liquid disordered domains of GUVs of either lipid preparation. As the two LV-peptides differ from the Rh-TMD of HA in their sequence, thus in hydrophobic length and secondary structure (cf. 4.1.3), sequence and hydrophobic mismatch seem not to be the dominating parameters in the lateral sorting process in artificial model membrane systems of GUVs (see Discussion).

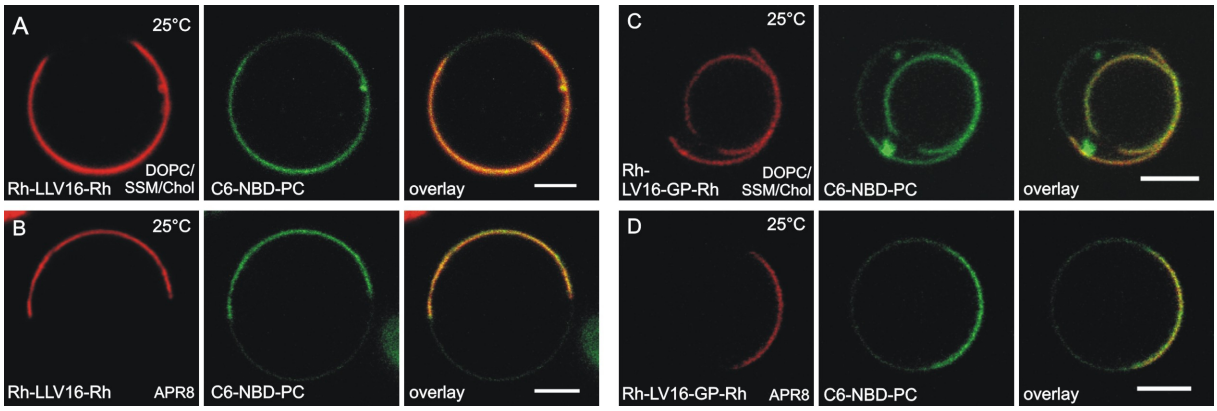

Fig. 29: Lateral organisation of transmembrane LV-peptides in domain forming GUVs. Rhodamine (TAMRA) labelled synthetic LV-peptides (Rh-LLV16-Rh and Rh-LV16-G8P9-Rh) were incorporated into GUVs made from DOPC:SSM:Chol (1:1:1, molar ratio) (**A,C**) or from influenza virus lipid extracts strain A/PR/8/34 (**B,D**). Bar 5 µm. Images were taken at 25°C.

4.2.3.2 Lateral organisation of a stiff molecular rod

Peptides in general, including the transmembrane peptides used here to study the lateral sorting in model membrane systems likely have a rather flexible structure concerning helix dynamics and backbone stability as well as amino acid side-chain mobility (Hofmann *et al.*, 2004; Ollesch *et al.*, 2007; Quint *et al.*, 2010). Therefore it is also interesting to investigate the lateral partition of the hydrophobic molecular rod (Fig. 25 E) based on spirocyclic joined saturated rings. This structure renders the rod with a high conformational rigidity. Functionalization of the oligospiroketal backbone with rhodamine-labelled pentapeptide allows for the observation of membrane incorporation (Muller *et al.*, 2009). The Rh-Rod-Rh is homogeneously distributed in nonraft forming GUVs prepared from DOPC, either added during GUV preparation (Fig. 30 A) or added to already formed GUV membranes (Fig. 30 B). After addition of Rh-Rod-Rh to human red blood cells (RBCs) (not shown) and RBC ghosts (Fig. 30 C) an insertion into these biological membranes was found (Muller *et al.*, 2009). Also here a homogenous lateral distribution was observed since RBCs are not known to exhibit microscopic visible lateral lipid domain formation (Sengupta *et al.*, 2007). Also GUVs prepared from RBC lipid extracts did not show any lipid domains formation (not shown). A partition of the Rh-Rod-Rh into the Ld domain of GUVs prepared from DOPC:SSM:Chol (1:1:1, molar ratio) was found for an incorporation of the rod during GUV preparation (Fig. 30 D) and also for an addition of rod to preformed GUVs (not shown).

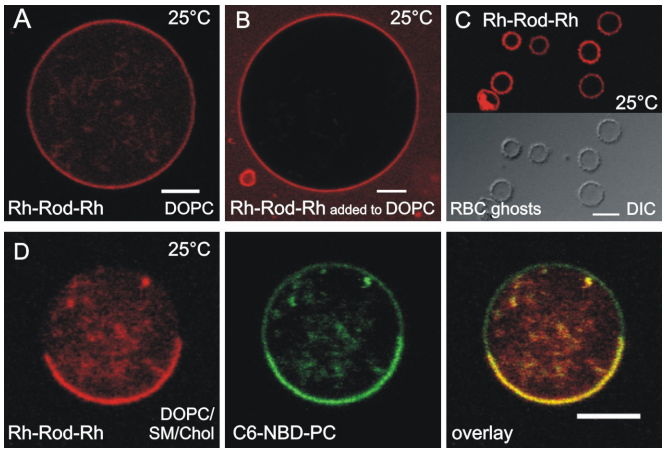

Fig. 30: Lateral organisation of Rh-Rod-Rh in GUVs and RBC ghosts. Rhodamine-labelled Rh-Rod-Rh was homogenously distributed in GUVs made of DOPC; rod present during GUV formation (**A**) and after addition to already formed GUVs (**B**) and to red blood cell ghost membranes (**C**). A partition of Rh-Rod-Rh into the Ld domain of GUVs made from DOPC:SSM:Chol (1:1:1, molar ratio) (**D**) was found indicated by colocalization with C6-NBD-PC as an Ld domain marker. Bar 5 µm. Images were taken at 25°C.

4.2.4 Lipid domain partition of lipid anchored Ras proteins

Besides the partition of transmembrane anchored membrane peptides and proteins also the sorting behaviour of soluble proteins bound to the membrane via lipid modifications was studied.

4.2.4.1 Domain specific binding of lipidated N-Ras protein

The lateral distribution of full length N-Ras protein, farnesylated and hexadecylated at Cys 186 and Cys 181, respectively, in domain forming GUVs and GPMVs was studied. Parts of the obtained results are published in cooperation with other groups as indicated below (Vogel *et al.*, 2009). For visualization N-Ras was Bodipy-labelled (Fig. 25 F). Labelled N-Ras was provided by Gemma Triola and Herbert Waldmann (MPI Molecular Physiology, Dortmund) (Bader *et al.*, 2000). In domain forming GUVs comprising the synthetic lipid mixture of POPC:DPPC:Chol (1:1:0.6, molar ratio) and PSM:DPPC:Chol (1:1:0.6, molar ratio) the N-Ras protein was found predominantly in the bulk of the Ld domain as indicated by colocalization with the Ld marker N-Rh-DOPE at 25°C (not shown). Note that not all GUVs did show lipid domain separation at 25°C. Imaging of GUVs at different temperatures of 4, 10, 20, 25, 30 and 37°C, respectively, revealed that for the POPC:DPPC:Chol (1:1:0.6, molar

ratio) system the number of GUVs displaying visible lipid domain separation strongly decreased at temperatures between 20 and 30°C. For GUVs made from POPC:PSM:Chol (1:1:0.6, molar ratio) lipid domains were observed in the majority of GUVs over the whole temperature range.

To mimic a more natural lipid mixture of a biological membrane GUVs were prepared from viral lipid extracts of influenza A virus strain A/PR/8/34. Small amounts of synthetic phospholipids (10 mol% POPC and 10 mol% PSM) were added to yield a membrane composition that was also suitable for ^{2}H NMR studies that were carried out in parallel by Alexander Vogel (Institute of Biochemistry, University Halle) and Daniel Huster (Institute of Medical Physics and Biophysics, University Leipzig). The viral lipid mixture was also checked for domain formation and shows a strong decrease in visible lipid domain separation between 20 and 30°C. Addition of N-Ras protein led to partition of the protein to the Ld domain as again indicated by N-Rh-DOPE at 4, 10, 20 and 30°C. After incubation for 24h or 48h at 20°C the N-Ras protein was enriched at the Lo/Ld domain boundary region (Fig. 31 A). From the fluorescence intensity profile of the image it is easily recognizable that only the N-Ras protein, but not the lipid domain marker is enriched in the boundary region (Fig. 31 B). Similar results were obtained by tapping mode AFM measurements of a planar supported bilayer probe incubated with unlabelled full length N-Ras protein (Fig. 31 G). The AFM experiments were performed by Katrin Weise (AG Roland Winter, Physical Chemistry I, TU Dortmund) (Vogel *et al.*, 2009). ^{2}H NMR results using deuterated POPC and PSM as marker lipids could clearly show a different hydrophobic thickness of the respective domains where POPC and PSM partition to. Using N-Ras protein with deuterated lipid modification a disordering of the N-Ras lipid modification was found being a strong indication for a partition of N-Ras in the Ld domain (Vogel *et al.*, 2009).

As for the experiments with HA protein also for N-Ras advantage was taken of the possibility to directly visualize lipid segregations of micrometer size of lipid bilayers derived from the plasma membrane of HeLa cells (Baumgart *et al.*, 2007a). GPMVs were prepared and Bodipy-labelled N-Ras protein was added. At 4°C phase separation was found as indicated by R18 (Ld domain marker – cf. 4.2.2.3). N-Ras was found predominantly in the Ld domain (Fig. 31 E).

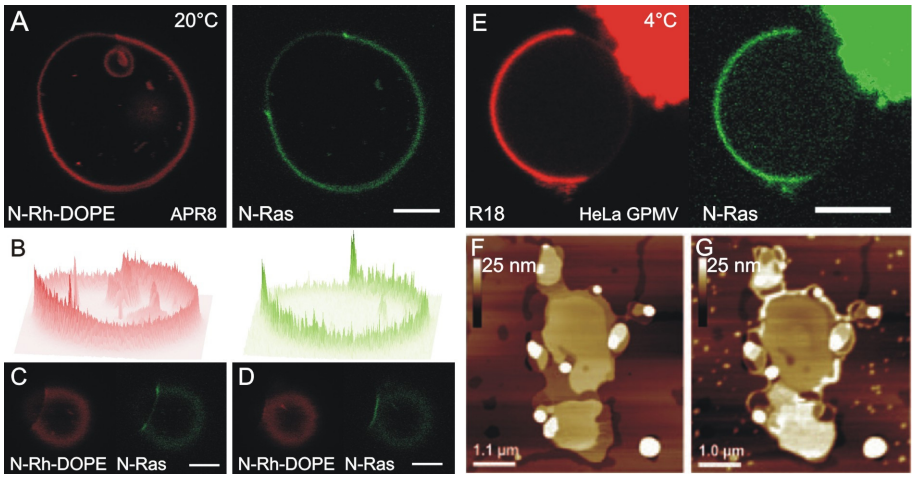

Fig. 31: N-Ras binds to the Ld domain. Bodipy labelled N-Ras incubated for 24h with GUVs prepared from influenza virus lipid extracts containing 10 mol% POPC, 10 mol% PSM and 1 mol% N-Rh-DOPE as Ld marker binds to the Ld domain and is enriched at the Ld/Lo domain boundary (**A**), as also clearly visible in the fluorescence intensity profiles (**B**) of the respective image. (**C** and **D**) display different confocal plane of (A) illustrating again the enrichment of N-Ras at the domain boundary. **(E)** GPMV prepared from HeLa cell exhibiting lateral lipid domains at 4°C with N-Ras protein colocalized with Ld marker R18. Bright fluorescence in the upper right corner is due to labelled cellular remains. Bar 5 µm. (**F** and **G**) AFM images of lipid bilayer of viral lipids before and after incorporation of N-Ras protein with a pronounced enrichment of N-Ras at the domain boundary (AFM images taken from Vogel *et al.*, 2009).

4.2.4.2 Domain specific binding of lipidated K-Ras protein

Whereas N-Ras membrane anchoring is mediated by an S-farnesylation and an S-palmitoylation, K-Ras anchoring is achieved instead by an additional polybasic stretch of six lysine residues besides a farnesyl lipid modification. The lateral distribution of K-Ras4B GDP and K-Ras4B GTP were studied on domain forming GUVs from viral lipid extracts (influenza A strain Japan/305/57). Bodipy-labelled K-Ras4B was supplied by Gemma Triola and Herbert Waldmann (MPI Molecular Physiology, Dortmund) (Y. X. Chen *et al.*, 2010). Unlike N-Ras which was found significantly enriched at the Lo/Ld domain boundary the K-Ras4B was observed only in the bulk Ld domains even after 48h incubation at 20°C for the GDP and GTP bound isoforms (Fig. 32). The Ld domain was identified by the lipid marker R18. These results are in line with AFM measurements performed by Katrin Weise (AG Roland Winter, Physical Chemistry I, TU Dortmund).

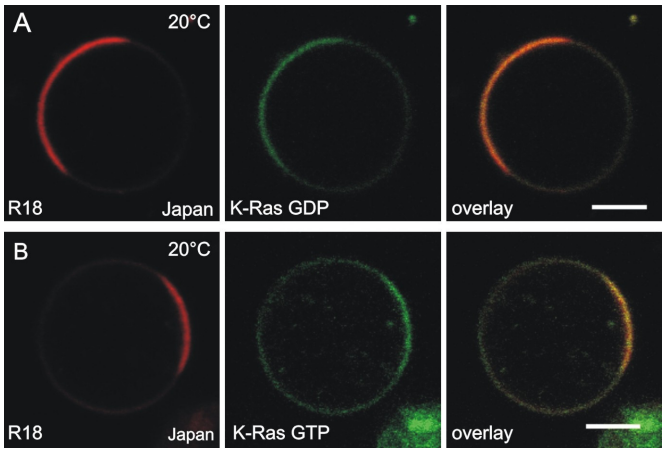

Fig. 32: K-Ras GDP and GTP bind to the Ld domain. Bodipy labelled K-Ras4B GDP (**A**) and K-Ras4B GTP (**B**) incubated for 12h at 20°C with GUVs prepared form influenza virus lipid extracts (strain Japan/305/57) binds to the bulk of the Ld domain as indicated by the Ld marker R18. Images were taken at 20°C. Bar 5 µm

„Das Schwierigste am Diskutieren ist nicht,
den eigenen Standpunkt zu verteidigen,
sondern ihn zu kennen."

Emile Herzog (* 26.07.1885; † 09.10.1967)

5 Discussion

The results will be discussed in two sections covering hemifusion in the first and domain specific sorting in the second paragraph.

5.1 The hemifusion intermediate in the pathway to fusion

5.1.1 Visualization of hemifusion

Their large size and direct visibility of the membrane make GUVs an ideal tool to study the fusion between lipid bilayers by light and fluorescence microscopy. Whereas fusion stalk and hemifusion intermediate are too small and transient to be resolved directly in biological membranes as well as in artificial model systems of small vesicles, GUVs have proven to allow for visualization of the fusion process as shown previously (Lei and MacDonald, 2003; Lei and MacDonald, 2008; Pantazatos and MacDonald, 1999; Haluska *et al.*, 2006; Heuvingh *et al.*, 2004). Full fusion between GUVs triggered either by fusogenic substances or by electroporation has been studied by using a high time resolution camera (50 µs/frame) (Haluska *et al.*, 2006). The opening kinetics of the fusion necks between GUVs was very fast with an expansion velocity of centimetres per seconds. Using this high-speed experimental setup Haluska *et al.* were unable to detect hemifusion in the prefusion stage probably due to

the limited overall recording time (2 sec) of the camera's internal memory. In another setup using lipids bearing DNA bases attached to their head groups to reduce the distance between the GUV membranes by complementary base paring and thus triggering fusion, Heuvingh *et al.* (Heuvingh *et al.*, 2004) were able to clearly observe a hemifused state of the vesicles with outer leaflets merged and the inner contents still separated. Also the group of R.C. MacDonald could show the existence of HDs in a system of positively and negatively charged GUVs using a fast camera setup (a few ms/frame). In our present study the organization of the contact region between TMD peptide-containing GUVs preceding divalent cation induced fusion was investigated. Here, divalent cations have two main functions. First, aggregation of GUVs comprising negatively charged lipids (PS) and second, inducing membrane tension driving membrane fusion (see below). For the first time, a reconstituted TMD peptide is used primarily as a marker to directly visualize the formation of an HD. In this region a sequestering of peptides as well as a significant depletion of fluorescent lipid analogues was typically observed in a microscopically visible structure. While the structure was short lived and followed by full membrane fusion, it was stable at lower divalent cation concentration and allowed to investigate its organization by fluorescence microscopy. At lower cation concentration less lateral membrane tension affects the bilayers and formation of a long-lived HD structure is more likely. Similar results were found in molecular dynamic simulations (Grafmuller *et al.*, 2009).

5.1.2 Evidence for the formation of a hemifusion diaphragm

Displacement of the different TMD variants and of the molecular rod as well as of the full length HA protein from the membrane contact region, and equally important the redistribution of lipid analogues between the contact region and the remaining membrane, provided strong evidence for the formation of an HD. For GUVs labelled on both leaflets with N-NBD-PE, a comparison of the fluorescence intensity of lipid analogues between the contact region and the membrane outside this region was consistent with hemifusion, but not with adhering non-hemifused GUVs (cf. Fig. 13). Obviously, lipid analogues of the outer leaflet, but not those of the inner leaflet were sequestered from this region. This was confirmed when membranes were labelled on the outer leaflet with C6-NBD-PC after preparation of GUVs. Upon adhesion, lipid analogues were sequestered from the contact region (Fig. 17). Furthermore, lipid analogues externally inserted into the outer leaflet could not rapidly enter the contact

region as it would be expected if this region would consist of two adhered bilayers (Fig. 15). It could be shown by FRAP measurements that slow migration of lipid analogues was not due to a restricted diffusion within the HD (Fig. 16).

Taken together these observations give strong evidence that the forming structure within the region of contact between the two GUVs corresponds to an HD. In the experiments within the model system, sequestering of peptides was independent of their amino acid sequence as well as secondary structure. While the only 23 amino acid long LV peptides display ~ 80 % α-helical and ~20 % ß-sheet structure in case of Rh-LLV-16-Rh, Rh-LV16-G8P9-Rh consist of ~20 % α-helical and ~80 % ß-sheet structure in membranes (Ollesch *et al.*, 2007). The 31 amino acid comprising HA peptide is essentially of α-helical structure (Tatulian and Tamm, 2000). Also the about 5 nm long rhodamine-labelled rod comprising a very rigid oligospiroketal backbone is sequestered in a similar way to the peptides. Taken together these results demonstrate that anchoring of a membrane spanning entity in the lipid head group regions of both membrane leaflets leads to an inevitable sequestering upon a remodelling of the membrane structure and the outward driven enlargement of the forming HD.

5.1.3 Forces driving hemifusion diaphragm formation

The formation of such large and protein-free HDs is remarkable and only observed in model systems. Whether a fusion stalk can expand to an HD has been the focus of many theoretical studies. HD growth increases the length of its rim, where monolayer curvature is large (Kozlov and Markin, 1983; L. V. Chernomordik and Kozlov, 2003; Kozlovsky and Kozlov, 2002; May, 2002;Kozlovsky *et al.*, 2004). This is energetically unfavourable unless the spontaneous lipid curvature is sufficiently negative to favour and drive HD growth (Kozlov and Markin, 1983; L. V. Chernomordik and Kozlov, 2003; Kozlovsky *et al.*, 2004). This is consistent with this report (Nikolaus *et al.*, 2010b) and previous observations (Pantazatos and MacDonald, 1999) that HD formation requires negatively curved lipids like DOPE (cf. 1.2.2).

In biological membrane fusion an external pulling force acting on the diaphragm rim is probably provided by a specialized set of membrane proteins like HA or SNAREs. In the GUV model system comprising TMD peptides, it is not obvious that the membrane incorporated TMDs alone could develop such a pulling force. However, TMD peptides have been shown to facilitate the fusion of model system membranes (Gurezka *et al.*, 1999;

Dennison *et al.*, 2002; Hofmann *et al.*, 2004; Ollesch *et al.*, 2007). TMDs within the bilayer increase the fusion rate probably due to a destabilisation of the bilayer structure that facilitates the restructuring of the membrane during the fusion process (Langosch *et al.*, 2001; Abdulreda *et al.*, 2008) (see section 1.2.4). Indeed, such large HDs were observed also in the absence of peptides in the GUV system validated by the distribution of N-NBD-PE. Supposably, HDs are formed here by the following reasons. First, the interaction of negatively charged phospholipids with divalent cations 'cross-links' GUVs leading to adhesion (Pantazatos and MacDonald, 1999; Nikolaus *et al.*, 2010b). Binding of Ca^{2+} and Mg^{2+} to the negatively charged PS, but also to the zwitterionic lipids PC and PE causes a shielding of the negative charge and the dehydration of head groups (Feigenson, 1986; Mattai *et al.*, 1989) and, hence, reduces repulsion between head groups. The TMD peptide is probably also facilitating HD formation and membrane fusion by a distortion of the lipid bilayer (Hofmann *et al.*, 2004; Ollesch *et al.*, 2007), although statistics on GUV size with and without peptides revealed no difference after incubation.

Second, monolayer studies revealed a 7.4 % decrease of the DOPS surface area upon addition of Ca^{2+} (Mattai *et al.*, 1989). A similar observation has been made for PC bilayers upon addition of Ca^{2+} although surface area reduction (5 %) was less pronounced in comparison to PS (Uhrikova *et al.*, 2008). Addition of Ca^{2+} to PS bilayers also leads to a phase change from the fluid to the crystalline state and condensation of the surface area (Papahadjopoulos *et al.*, 1977; Mattai *et al.*, 1989; Kozlov and Markin, 1984; Lei and MacDonald, 2003). Since divalent cations can only interact with the outer leaflet surface, but not with the luminal leaflet, surface area reduction is asymmetric (Chanturiya *et al.*, 2000) and the surface area difference between both leaflets has to be compensated in order to preserve stability of GUVs. Since lipid flip-flop rates, i.e. the transfer of lipids between the bilayer leaflets, are in the range of minutes in artificial systems (Svetina *et al.*, 1998), they exceed by far the timescale for HD formation in the model system used and are therefore not considered as possible compensation mechanism for the interleaflet area asymmetry. However, the necessary stability of the GUVs could be achieved by formation of an HD since merging of the outer leaflets would counteract the area reduction caused by cation addition, whereas the inner monolayer surface area is allowed to remain constant. Taking into account the molar fractions of phospholipids in GUVs (DOPC:DOPE:DOPS, 3:1:1, molar ratio) and the decrease of their molecular area in the presence of Ca^{2+} (Mattai *et al.*, 1989; Uhrikova *et al.*, 2008), the condensation of the outer monolayer should be about 5.5 % of total membrane surface. Since

no data on DOPE were available, the same reduction as for PC is assumed since PE and PC are both zwitterionic lipids. The dependence of the HD size upon cation condensation of lipids would predict that the HD size should increase with increasing surface area of GUVs which was indeed the case. That PS is not the sole contributor to surface condensation is sustained by the observation that reduction of the PS fraction by 10 mol% did not affect the area of the HD within the error of measurement (see Fig. 19).

Third, additionally to the cationic component, bilayer tension also drives hemifusion and fusion (Shillcock and Lipowsky, 2005). Analysis of 50 hemifused GUV pairs revealed that the relative surface area of HDs is about 8.7 % of the mean surface area of GUV pairs (Fig. 33 C). This is in good agreement with the predicted reduction of the outer leaflet by cation adsorption (5.5 %) plus a contribution of membrane tension driving HD growth, presumably in the range of the remainders (Jason M. Warner and Ben O'Shaughnessy, Columbia University, New York, personal communication, 2009). Additional bilayer tension in the performed experiments results from the addition of cations (Ohki, 1982; Sinn *et al.*, 2006), from the adhesion of vesicle bilayers that flatten against each other with their volume remaining constant (Kachar *et al.*, 1986) and from adhesion with the substrate (Radler *et al.*, 1995). Membrane tension may strongly affect the fusion pathway. Dissipative particle dynamics simulations for fusion events of a vesicle with a planar membrane by Grafmüller *et al.* (Grafmuller *et al.*, 2009) predict a variation of the adhesion time depending strongly on tension (large tension – fast fusion; small tension – large contact area and long adhesion times). Consistent with these findings either rapid full fusion (cf. Fig. 11) for high Ca^{2+} concentration or stable adhesion (cf. Fig. 14 A) and hemifusion (cf. Fig. 13 and Fig. 15) for low concentration of Mg^{2+} or Ca^{2+} was found for different cation concentrations causing a variation in membrane tension (Ohki, 1982). Interestingly, in an analytical model describing the formation of an HD in a vesicle system (see below) the bilayer tension in the HD was about twice the tension in the vesicle bilayer outside the HD. This elevated tension in the HD may facilitate the HD rupture as bilayer tension drives fusion pore formation.

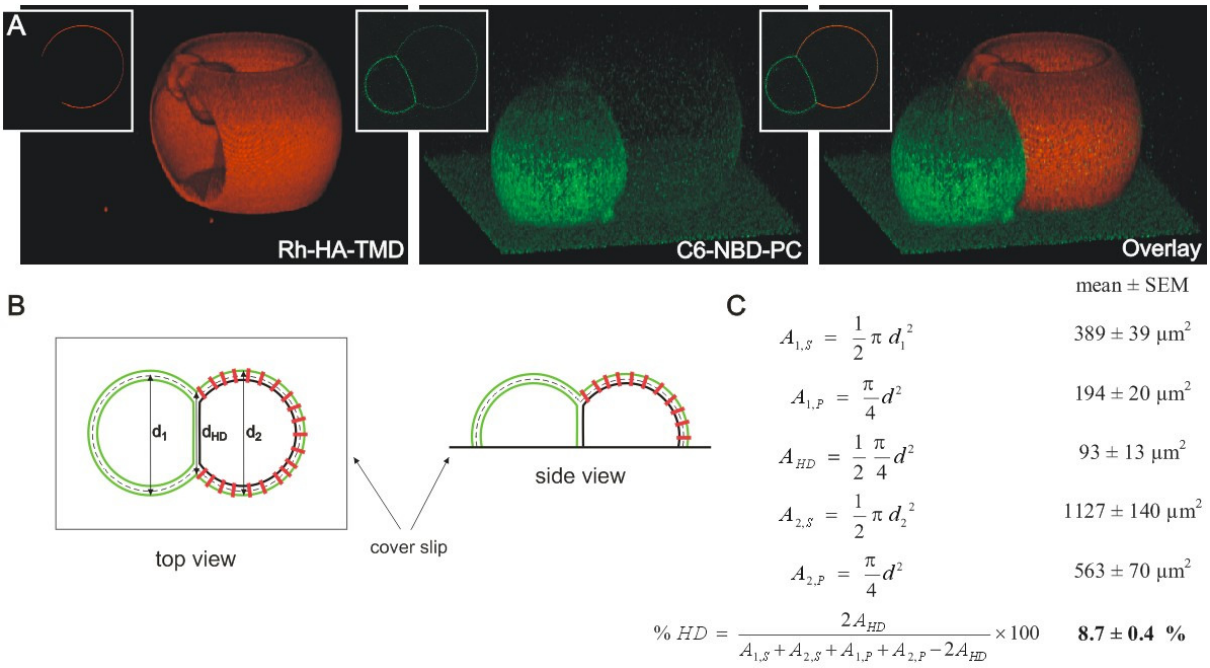

Fig. 33: Estimation of the relative surface area of hemifused GUVs. Due to a decrease of membrane tension upon hemifusion of GUVs, they flatten upon settling onto the cover slip (cf. Fig. 18). Based on the resulting geometry the relative surface area of the HD of the total surface of 50 attached GUV pairs with sequestered peptides was estimated. (**A**) Z-stack reconstruction of a GUV pair containing Rh-TMD peptide of HA and N-NBD-PE, respectively, after addition of 2 mM Ca^{2+}. Note that the upper part of the large GUVs was not imaged and therefore omitted. Inset: Confocal image of the equatorial plane of the GUV pair showing the HD with sequestered peptide. (**B**) Sketch of two hemifused GUVs settled on a cover slip. Top view shows the diameters of both GUVs (d_1, d_2) and of the HD (d_{HD}). GUVs are approximated by half spheres as the mean contact angle of hemifused GUVs with the cover slip was found to be close to 90°. (**C**) Calculation of the surface area (A) of GUV 1 and 2 approximated by half spheres (S) and the plane area in contact with the cover slip (P) and also of the HD area. The estimated relative surface area of the HD on the overall surface area of both GUVs is about 8.7 %.

5.1.4 Sequestering of transmembrane entities in model and biological membranes

The GUV model system allows studying µm-sized HDs, but these dimensions are not observed *in vivo*. Although microscopic HDs with sequestered full length HA protein reconstituted into GUVs were observed, the situation is different to viruses and cellular membranes. Membrane proteins in biological membranes are much more densely packed than in our model system with typically 1 mol% of TMD peptide. Merging of the contacting leaflets requires sequestering even of those proteins, which are not involved in fusion. Fig. 34

shows the densely packed membranes of an influenza A virus in a TEM image with the viral spike proteins and a molecular model of a synaptic vesicle constructed from quantitative data (Takamori *et al.*, 2006).

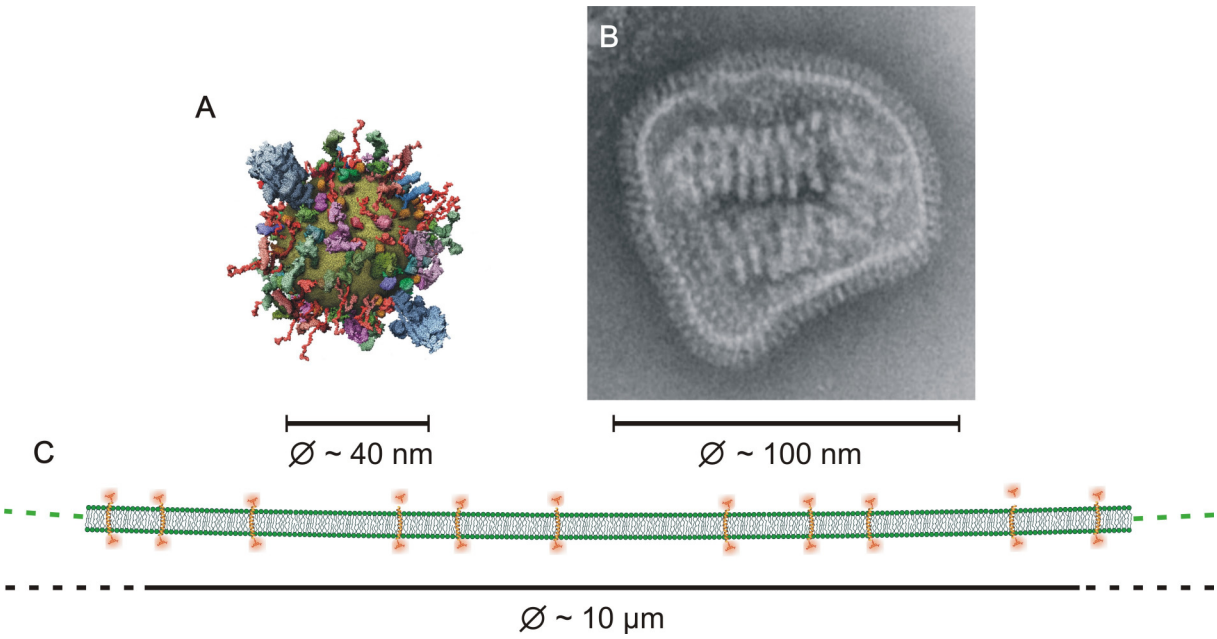

Fig. 34: Crowding of membrane proteins. Drawn to scale are a constructed synaptic vesicle based on quantitative data with a diameter of about 40 nm (Takamori *et al.*, 2006) (**A**), a TEM image of an influenza A virus with diameter of 80-120 nm (image by Cynthia Goldsmith) (**B**) and a GUV bilayer section with a diameter of about 10 µm including about 1 mol% of rhodamine-labelled transmembrane peptides. Obviously, the synaptic vesicle and the virus particle are densely packed with different membrane proteins and viral spike proteins HA and NA, respectively.

The required sequestering of so many membrane anchored proteins upon the merger of a synaptic vesicle or viral membrane with an also protein-loaded target membrane might be energetically unfavourable and interfere with expansion and even stability of an HD. Indeed, in the presence of peptides at higher concentration or in both attached GUVs a significantly reduced formation of HDs was found. Another factor could be the interaction of membrane proteins with the membrane cytoskeleton. Since in biological membranes some of the transmembrane embedded proteins are additionally linked to the membrane skeleton network on the cytoplasmic side, this probably would effectively render the sequestering of these proteins impossible and hence block the enlargement of a forming HD. This hindrance of free protein and also lipid diffusion is mainly discussed with the field of lateral membrane domains and rafts and is reviewed by Kusumi and Suzuki (2004, 2005) (Kusumi *et al.*, 2004; Kusumi and Suzuki, 2005). The addition of cations effectively reduces the outer membrane

leaflet and provides thus a major driving force for HD formation in the GUV model system, but whether similar mechanisms are available to cells is not known.

5.1.5 Simultaneous formation of several fusion stalks within one adhesion area

In the GUV model system rapid transition from a first transbilayer contact to full fusion occurred as can be concluded from Fig. 23. The formation of the small internal vesicles that harbour both rhodamine-labelled peptide and NBD lipid analogue from the formally separated GUV membranes indicates that several fusion stalks must have formed and proceeded to full fusion within the area of initial contact. In their coarse-grained molecular dynamics simulation Kasson *et al.* (2007) found a prevalence of a fusion pathway proceeding through a hemifusion intermediate, but also a direct transition from the fusion stalk to the opening of a fusion pore was observed. The latter pathway was found at a higher probability for lower amounts of PE within the simulated bilayers (Kasson and Pande, 2007). Whether a small HD was formed prior to full fusion in this experiment (Fig. 23 in section 4.1.8) remains elusive due to the very slow confocal imaging setup. As intuitively presumed, it was found in a simulation study that the formation of a fusion stalk gets more likely when the area of contact of the two vesicles gets larger, which increases the probability that lipid acyl chains protrude into the hydrophilic interface (Kasson *et al.*, 2010). Since the formation of internal vesicles was only observed rarely, the parallel formation of several fusion stalks within one adhesion area has to be considered unlikely.

5.1.6 Analytical model of the hemifusion pathway

As shown above, the addition of Ca^{2+} or Mg^{2+} to negatively charged membranes reduces the outer leaflet surface area of the GUVs and induces high membrane tensions. After fusion stalk formation, i.e. the nucleation point of an HD, the bilayer tension affecting the whole GUV membrane area wants to expand the HD, except for the tension within the HD membrane itself, which wants to reduce the HD area since bilayer tension wants to reduce membrane area. As two membranes fuse into one at the HD boundary, the reason for the growth of an HD becomes evident. Tension in two bilayers – both GUV membranes outside the HD – pull outwards and enlarge the HD, whereas only tension in one membrane – the HD membrane – resists this enlargement. Yet, another type of tension comes into play. Due to an area reduction

on the outer leaflet, caused by the growing HD and also by the influence of cation addition only affecting the outer leaflet, an interleaflet tension between inner and outer bilayer leaflet works against HD expansion. The greater this mismatch between the reduced outer and the inner leaflet the larger is the induced interleaflet tension. The description of the interleaflet tension was introduced by Jason M. Warner and Ben O'Shaughnessy (Columbia University, New York, personal communication). In equilibrium the bilayer and interleaflet tensions yield an equilibrium HD size. According to the model of Warner and O'Shaughnessy, the HD size in equilibrium is determined by the GUV areas and a force resulting from the outer leaflet reduction by cation addition and also from bilayer tension. In Fig. 19 the model prediction is plotted and agrees well with the measured data for hemifused GUVs with an area ratio <4.4. The analytical description of Warner and O'Shaughnessy was extended to also analyse the growth kinetics of the HD formation. Short time model prediction of the evolution of HD area in time agrees well with measured data presented in the fusion kinetics (Fig. 11 D). Whereas the analytical model predicts a linear short term growth rate of the HD of 24 $\mu m^2/s$, the experimentally obtained rates were found to be between 22 and 34 $\mu m^2/s$.

5.2 Bilayer properties and its influence on protein partition

5.2.1 Hemagglutinin partitions to raft domains in the plasma membrane

The formation of lateral lipid domains and the implications on cellular mechanisms have been studied and highly debated for more than two decades ever since the existence of microdomains enriched in sphingomyelin (SM) and cholesterol in the plasma membrane has been suggested by Simons and van Meer (Simons and van Meer, 1988). These domains, in cellular membranes also called rafts, are similar to the Lo domains observed in model membrane systems. Rafts are associated with important cellular functions such as membrane sorting and fusion, signal transduction and protein activation and partition (Poveda *et al.*, 2008).

The influenza virus hemagglutinin (HA) is considered to be a typical example for integral membrane proteins that partition to and strongly enrich in rafts. HA is sorted to the apical plasma membrane of polarized cells where the assembly and budding of progeny virus takes place. The apical membrane was shown to be enriched in sphingolipids and cholesterol. However, direct visualization of HA partition into such domains of mammalian cell plasma membranes expressing the virus protein has not been reported. The early studies used two criteria to analyse the partition of HA. First, as partition into rafts already in the trans-Golgi network was proposed to be necessary for the correct apical sorting of HA in polarized MDCK cells the location of HA in the apical or basolateral surface was investigated. Second, sorting of HA into detergent resistant membrane fractions (DRMs) as compared to the soluble membranes (DSMs) was used to judge raft partition. Indeed, wild type HA was found at the apical plasma membrane as well as in DRM fractions after treatment with cold detergent Triton X-100. Several mutations within the TMD of HA revealed the requirement for hydrophobic residues that are in contact with the exoplasmic leaflet of the membrane to fulfil the criteria mentioned above (Scheiffele *et al.*, 1997; Lin *et al.*, 1998; Barman *et al.*, 2001; Takeda *et al.*, 2003). The clustering of HA with a wild type TMD sequence at the plasma membrane of MDCK and fibroblast cells could be shown by gold particle labelled antibody staining and also in live FPALM experiments, respectively (Takeda *et al.*, 2003; Hess *et al.*, 2005; Leser and Lamb, 2005; Hess *et al.*, 2007). Here, again the mutation of hydrophobic residues residing in the outer membrane leaflet was found to disrupt clustering and render HA in a wide distribution across the plasma membrane (Takeda *et al.*, 2003). Recently, a clustering of HA and a HA derived construct (see Fig. 25 C and D) with plasma membrane

raft-markers was observed by FLIM-FRET in HA-transfected cells (Engel *et al.*, 2010; Scolari *et al.*, 2009).

In this study, model systems, which are known to form lipid domains in the microscopic range easily detectable by fluorescent lipid analogues with a preference for Ld domains were used. In one system, either the TMD peptide of HA and further model peptides or viral full length HA was reconstituted into GUVs prepared from a mixture of synthetic, well defined raft-lipids or from lipids extracted from the viral envelope. As another model system, GPMVs were obtained from cell plasma membranes, thus containing a large variety of lipids and, apart from the protein of interest – HA-Cer or TMD-HA-YFP – other membrane proteins. For all studied examples a strong preference for the Ld domain was observed. However, the preference of full length HA for the Ld domain was less pronounced in GPMVs, which mimic biological membranes much better than GUVs as it will be discuss below.

5.2.2 Hydrophobic mismatch of transmembrane entities in domain forming GUVs

Both HA-TMD peptides comprising the wild type sequence and the mutation GS520AA that was found to render the raft partition of full length HA to nonraft domains in the plasma membrane of the cells, respectively, as well as the full length HA were exclusively localized in the Ld domain in GUVs, either consisting of a well defined composition of synthetic lipids or viral lipid extracts. This extreme partition was observed not only at 25°C, but also at 10°C and 37°C. The enrichment of the HA TMD peptide, but also of the full length HA protein, membrane anchored by the TMD, in the Ld domain is unexpected when comparing the hydrophobic width of the bilayer with the hydrophobic stretch of the TMD. From electron density profiles obtained by Fourier analysis of X-ray diffraction pattern the thickness of the hydrophobic part of a DOPC:SSM:Chol (1:1:1) bilayer was calculated. The hydrophobic thickness is 36 Å in the Lo and 27 Å in the Ld phase (Fig. 35) (Gandhavadi *et al.*, 2002). A similar difference of about 10 Å of a membrane in Lo and Ld phase, respectively, was found in an ^{2}H NMR study (Vogel *et al.*, 2009). The HA TMD peptide is essentially of α-helical structure (Tatulian and Tamm, 2000). Considering 1.5 Å per amino acid in an α-helical conformation (Webb *et al.*, 1998), the hydrophobic stretch of the HA TMD peptide (25 aa) is 37.5 Å (Fig. 35). The same length was found for a KALP peptide comprising a 25 residue hydrophobic part (Kandasamy and Larson, 2006). Hence, one would expect partition of the TMD peptide in the Lo phase where it faces only a small positive mismatch of 1.5 Å.

Surprisingly, despite a positive mismatch of 10.5 Å, HA TMD peptides are incorporated into the Ld phase. However, this behaviour is consistent with recent studies on domain partition of various membrane proteins and peptides in model membranes (Fastenberg *et al.*, 2003; Bacia *et al.*, 2004; Vidal and McIntosh, 2005; Shogomori *et al.*, 2005; Almeida *et al.*, 2005; Hammond *et al.*, 2005; Kalvodova *et al.*, 2005). McIntosh and co-workers (McIntosh *et al.*, 2003; Vidal and McIntosh, 2005) studied lateral sorting of model transmembrane peptides of different hydrophobic length - 23 or 29 amino acids - between Lo and Ld domains by detergent extraction, but also by confocal fluorescence microscopy at 4°C and 37°C. These transmembrane domains match the hydrocarbon thickness of Ld and Lo domains, respectively. At both temperatures the peptides were primarily localized in the Ld domain independent of hydrophobic matching.

By reconstituting the LV model peptides into domain forming GUVs of synthetic lipids or viral lipid extracts allows for a similar comparison as in the work of McIntosh and co-workers (Vidal and McIntosh, 2005). The 17 hydrophobic residues of the Rh-LLV16-Rh have a length of 25.5 Å in an α-helical conformation (Fig. 35). This results in only a small negative mismatch of 1.5 Å compared to the Ld domain hydrocarbon thickness. For the Rh-LV16-G8P9-Rh with an 80 % β-sheet fraction the probable hydrophobic length would be about 28 Å considering 3.5 Å per residue and a turn in the centre at the Gly and Pro residues. The peptides also exhibit a small amount of a turn structure as determined by CD spectroscopy when flat lipid membranes were present (Ollesch *et al.*, 2007). Here, both peptides partition to the Ld domain in the GUVs. Interestingly also the relatively stiff molecular rod that comprises no voluminous side chains within the 3 nm long oligospiroketal backbone besides the two butyl groups also partitions to the Ld domain in phase separating GUVs (Fig. 35).

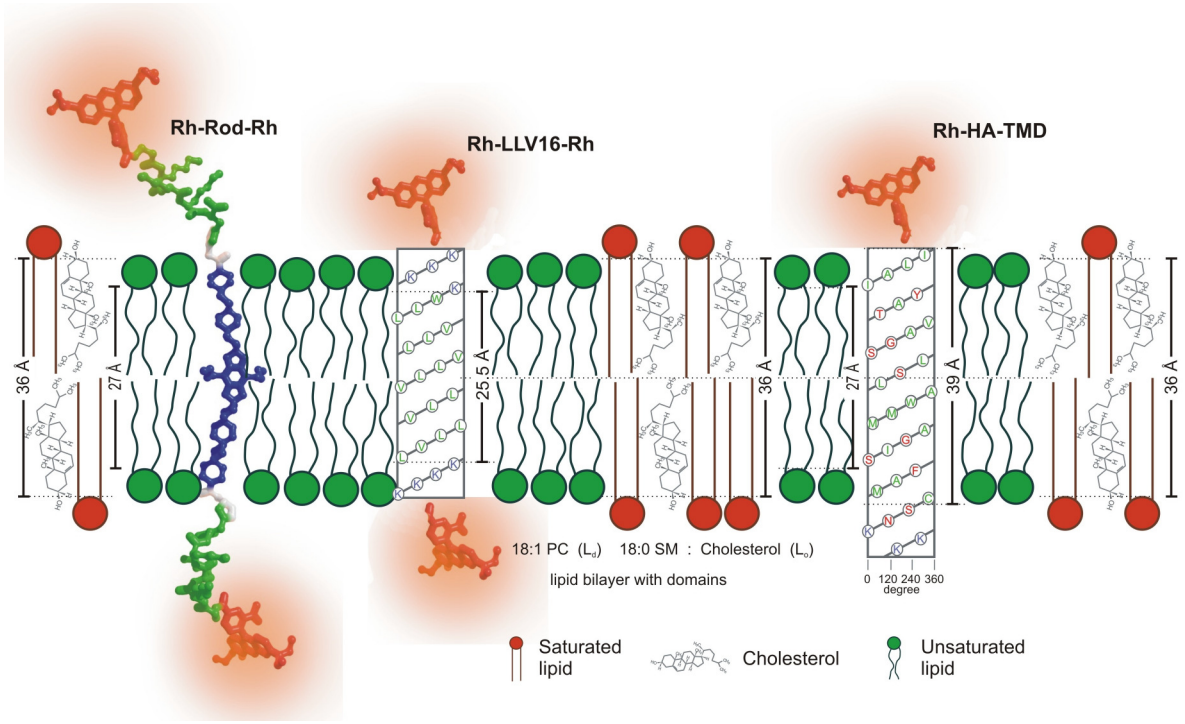

Fig. 35: Hydrophobic mismatch. Schematic drawing of a lateral lipid domain containing bilayer. Liquid disordered (Ld) domains are made up by unsaturated lipids (green) with a hydrophobic thickness of 27 Å whereas liquid ordered domains comprise a saturated lipid (red) and cholesterol with a hydrocarbon width of 36 Å. Note that the number of lipids per lateral domain is arbitrary and the exact lipid arrangement at the domain boundary as well as at the TMD-lipid surface is not known. Drawn to scale are the Rh-HA-TMD and the Rh-LLV16-Rh peptide as well as the Rh-Rod-Rh with the oligospiroketal backbone with a hydrophobic length of 39 Å, 25.5 Å and about 30 Å, respectively. Amino acid sequence is denoted within the peptides with hydrophobic, hydrophilic and basic residues in green, red and blue, respectively. Transmembrane entities are depicted in a rectangular orientation to the membrane normal and not tilted to better illustrate the hydrophobic matching situation.

5.2.3 Possible responds to mismatch by peptides and lipid bilayers

At present it is not known how the TMD peptides of HA respond to the positive hydrophobic mismatch that occurs in the Ld domain. Tilting of peptides might be one possibility to match the hydrophobic thickness of the bilayer avoiding exposure of hydrophobic side chains to polar environment, which is energetically unfavourable (Mouritsen and Bloom, 1984 and reviews Killian, 2003; Holt and Killian, 2010). In a MD simulation of KALP peptides of different length in lipid bilayers of various width Kandasamy and Larson (2006) could show that peptide tilting is an important factor compensating positive hydrophobic mismatch

(Kandasamy and Larson, 2006). Similar results were only recently obtained by Kim and Im (2010) investigating the mismatch response of WALP peptides (Kim and Im, 2010). For a peptide-lipid system with a positive mismatch of 12.7 Å, which is very close to the mismatch situation for the HA TMD peptide in the Ld domain in the present GUVs study, the authors find a tilt angle of up to 50° with respect to the membrane normal. In a NMR experiment on the transmembrane helix of Vpu, an accessory protein required for an efficient HIV-1 particle release (Neil *et al.*, 2008), in bilayers of different width a tilt of the TMD is found ranging from 27° to 51° for an increasing positive mismatch (S. H. Park and Opella, 2005). Here, the tilting alone is able to compensate for the mismatch. However, using polarized ATR-FTIR it could be shown that a TMD of HA in DMPC (di-C14:0PC) membranes having a hydrophobic thickness of about 21 Å is in an α-helical conformation and orientated almost parallel to the membrane normal (Tatulian and Tamm, 2000).

Besides tilting also side chain reorientation offers a possibility to reduce hydrophobic mismatch, even if only to a limited extent depending on the amino acid side chain (Killian, 2003). In addition to a response of the TMD peptide to the hydrophobic mismatch also the lipid bilayer is able to undergo changes to some degree. Lipids can adapt their effective length by increasing the acyl chain order. Although this adaptation was only found to be small it has been observed by ^{2}H NMR and EPR upon the reconstitution of KALP and WALP model peptides (P/L ratio 1:30) with a hydrophobic length exceeding the thickness of the bilayers (de Planque *et al.*, 1999). Here, the hydrophobic thickness of the membrane increased by 0.2 Å and 1.0 Å for KALP23 and WALP23 (both peptides comprising 23 hydrophobic amino acid) peptides in a DMPC (di-C14:0PC) bilayer, respectively. A similar and also small increase of the lipid acyl chains length was observed by ^{2}H NMR in short chain lipid bilayers upon addition of a double hexadecylated N-Ras heptapeptide (Vogel *et al.*, 2009). For DLPC (di-C12:0PC) and DMPC (di-C14:0PC) the chain extent of a single chain was stretched by 0.2 Å for both lipids upon the incorporation of the longer hexadecylated chains (C16:0) of the N-Ras peptide at a P/L ratio of 1:150. Interestingly also a strong adaptation of the lipid modification of N-Ras was found. These results are in line with own preliminary results on the lifetime $\tau_{2,Ld}$ of C6-NBD-PC in LUVs of DOPC (di-C18:1PC) comprising an unlabelled variant of the HA TMD peptide flanked by three lysine residues on both ends (thus comparable to KALP peptides) at a P/L ratio of 1:100. The lifetime $\tau_{2,Ld}$ was found to be $\tau_2 \sim 6.33 \pm 0.03$ ns and $\tau_2 \sim 6.45 \pm 0.03$ ns in LUVs without and with reconstituted TMD peptide, respectively. The slightly longer lifetime of the NBD lipid analogue reflects the

slightly higher degree of order introduced by the reconstitution of the TMD peptide. Increasing order of the lipids upon peptide incorporation was also found in further studies on the HA TMD peptide (Tatulian and Tamm, 2000; Tamm, 2003). But adaptation of lipid length was found to be small and by far not enough to compensate for the hydrophobic mismatch of the TMD peptides implying that there are significant energy cost for changing the lipid chain order by stretching (Killian, 2003; Vogel *et al.*, 2009).

Upon incorporation of the Rh-LLV16-Rh peptide in the Ld domains the peptide faces a negative mismatch of only 1.5 Å. It was found for transmembrane peptides comprising lysine residues at the peptide ends that the lysines can effectively increase the hydrophobic length in a situation of negative mismatch by snorkelling (Killian, 2003). Here the hydrophobic part of the lysine residue still resides in the hydrocarbon region and while the positively charged amino group stretches out and snorkels into the more polar interfacial region of the lipid bilayer.

5.2.4 Lipid-lipid interactions dominate bilayer properties in GUV

Taken together all transmembrane reconstituted entities partition to the Ld domain in the GUVs model system independent from their hydrophobic length, shape or lateral profile. This holds true for results of this study, but also for the various examples in the literature (see above). Distinct physical properties favour the incorporation of TMDs into the Ld phase. E.g., Lo domains have a higher bilayer compressibility, which for SM:cholesterol (1:1, molar ratio) is about 9 times that of a phosphatidylcholine bilayer (McIntosh *et al.*, 1992), and higher bending moduli compared to the non raft domains (Lundbaek *et al.*, 2003). That is, Lo domains are more tightly packed (Kaiser *et al.*, 2009), which leads to the significantly higher fluorescence lifetime of C6-NBD-PC in comparison to the Ld domain (Fig. 24 A and B) (Nikolaus *et al.*, 2010a; Stockl *et al.*, 2008). Hence, more energy is required to separate adjacent lipid molecules to enable incorporation of TMDs or molecular rods into the Lo compared to the Ld domains, which are of lower cohesive energies (Vidal and McIntosh, 2005). Thus, it is energetically favourable for TMDs to partition into the Ld domain (van Duyl *et al.*, 2002). In the Ld domain the probable disordering effect of the side chains of the α-helical TMD would be appreciated whereas in the tight packing of the Lo phase this would be energetically costly to accommodate (Simons and Vaz, 2004; Fastenberg *et al.*, 2003).

5.2.5 Influence of S acylation of HA cysteines in the GUV model system

These results of a partition of the peptides to the Ld domains confirm and extend previous studies showing that in lipid model systems the cohesive bilayer material properties determine the process of lateral sorting of transmembrane peptides (McIntosh *et al.*, 2003; Vidal and McIntosh, 2005) and even of full length integral membrane proteins. The strong enrichment of wild type HA in the Ld domain may be rather surprising, in particular, because reconstituted HA contains the typical raft targeting signals, such as palmitoylation and specific hydrophobic amino acids in its TMD. Thus, any partition signal that sorts HA into rafts of living cells (Lin *et al.*, 1998; Scheiffele *et al.*, 1997) and an unfavourable hydrophobic mismatch are not relevant for the partition of the TMD peptide of HA and wild type HA in GUVs.

Reconstituted viral full length HA protein was found to partition to the Ld domain in GUVs (Fig. 27 and Tab. 2). The palmitoylation of the three cysteines of the HA protein (see below) did not render the partition to the Lo domain in GUVs as compared to the non-palmitoylated HA TMD peptide. To get a complete data set the palmitoylation of the HA TMD peptide and of an extended HA peptide comprising transmembrane part plus the 11 residues long cytoplasmic tail (CT) was attempted. This was done together with Dr. Rudolf Volkmer, Ines Kretzschmar, Christiane Landgraf and Anja Krüger (Institute for Medical Immunology, Charité, Berlin). The sequence of the HA TMD and CT (strain A/FPV/Rostock/34 H7N1) comprises the following sequence of amino acids: TMD: KDVILWFSFGASCFLLLAIAMGLVFI**C**^{551}V plus CT: KNGNMR**C**^{559}TI**C**^{562}I. The last three C-terminal Cys at position 551, 559 and 562 are S acylated, hereby it was only recently shown that the Cys 551 at the boundary of TMD and CT is stearoylated (C18:0) and the two Cys in the CT are palmitoylated (C16:0) (Kordyukova *et al.*, 2008). This site-specific attachment of palmitate or stearate seems to be common along viral spike proteins as reported lately (Kordyukova *et al.*, 2010). To make a long story short, the attempts to yield an S palmitoylated TMD+CT construct failed (for details see 3.2.3) and it was thus not possible to study the influence of palmitoylation on the HA TMD peptide.

Using a different approach the group of Antoinette Killian (University Utrecht) yielded not S acylated, but N-terminally palmitoylated WALP peptides with one or two hexadecanyl chains linked by an amide or a structurally more flexible ester bond, respectively. They studied the partition behaviour of the palmitoylated peptides and of peptides with varying

length by detergent extraction and found that neither the palmitoylation nor the influence of hydrophobic mismatch renders the sorting of peptides out of the Ld domain, which is in line with above mentioned results (van Duyl *et al.*, 2002). The authors speculate that the palmitoylated peptides might be located at the interface of the Lo/Ld domain with the palmitate chains inserted into the Lo phase. Due to the constraints of the method this could not be verified. The partition of the N-Ras protein with a bulky branched farnesyl and a palmitoyl anchor to the Lo/Ld interface (see section 4.2.4.1) shows that introducing a palmitoyl anchors is able to sort lipidated proteins to the domain interface. A similar sorting mechanism was proposed for the TM influenza virus M2 protein (see below). Therefore it will be worth to check the partition of palmitoylated TM peptides by optical methods like fluorescence microscopy.

Besides the discussed influence of the acylation of HA on the protein sorting also another function might be taken into account. Acylation of TMDs might be responsible for a tilting of the respective TMD. In these cases it was speculated that tilting could alleviate a positive hydrophobic mismatch of the relatively long TMDs within the thinner ER and Golgi membranes (Abrami *et al.*, 2008; Hundt *et al.*, 2009; Conibear and Davis). An insertion of the HA TMD was found in a 35° to 55° angle relative to the membrane normal (see Introduction, section 1.2.4). Therefore, the tilt of the TM anchor of HA might be due to the stearoylated lipid modification (Kordyukova *et al.*, 2008) and support the lipid mixing activity of in membrane fusion (Bowen and Brunger, 2006).

5.2.6 Less pronounced partition of HA in GPMVs

Although a strong preference of full length HA-Cer and TMD-HA-YFP construct for the Ld domain in GPMVs derived from the plasma membrane of CHO-K1 cells was observed, their preference was less pronounced compared to full length HA and TMD peptide of HA in GUVs prepared from synthetic or virus lipids (Tab. 2). This is partially in line with latest results from the Baumgart lab (Johnson *et al.*, 2010) where a variable domain partitioning of the HA in GPMVs from HeLa cells was observed. The authors report of Ld, Lo and also non-preferential partition of HA and refer to a probable difference in the lipid composition of the single vesicles and underscore the possible importance of this composition for the sorting process of proteins. The results indicate that Lo domains of GPMVs may differ in their physical properties to that in GUVs. Indeed, lifetime of C6-NBD-PC shows that packing of

lipid domains in GPMVs is different from that of GUVs. In particular, the differences of lipid packing between Ld and Lo domains are much less pronounced for GPMVs (Fig. 24 C) in comparison to GUVs prepared from synthetic or virus lipids (Fig. 24 A and B). This is in agreement with the observations for GPMVs from HeLa cells (Stockl *et al.*, 2008) and data of (Kaiser *et al.*, 2009). The authors judged membrane order of the different systems by calculating the generalized polarization (GP) values of Laurdan giving a relative measure of the membrane order of GUVs, GPMVs and also for the recently described plasma membrane spheres (PMS) from the human epithelial carcinoma cell line A431 (Lingwood *et al.*, 2008). For the PMS where micrometer-scale phase separation is induced by cholera toxin-mediated cross-linking of the raft ganglioside GM1 the difference in membrane order between the GM1 and the remaining phases was even less pronounced as for the GPMV system and even at 10°C the bilayer lipids are by far not as densely packed as in the Lo domain of GUV (Kaiser *et al.*, 2009). Supposably due to the much higher membrane protein content of GPMVs and PMS, protein-lipid interactions may interfere with a very tight packing of Lo domain as found in GUVs (Jacobson *et al.*, 2007; Hancock, 2006; Kaiser *et al.*, 2009; Lingwood and Simons, 2010). This would reduce the energy barrier for intercalation of membrane proteins thus explaining the partial presence of HA in Lo domains of GPMVs. Interestingly the results on variable phase partition of HA in GPMV membranes obtained by Johnson *et al.* (Johnson *et al.*, 2010) from the Baumgart lab where obtained at 22°C whereas these experiments were performed at 10°C. Regarding this difference in temperature one can imagine that lipids in the Lo phase are packed less tight at higher temperatures thus allowing for a more easy incorporation of the protein. Furthermore, differences of partition between GPMVs and GUVs might also be due to lipid asymmetry in GPMVs affecting domain formation and properties. Although a partial loss of bilayer asymmetry upon formation of GPMVs compared to the cell membrane has been observed (Honerkamp-Smith *et al.*, 2009; Kaiser *et al.*, 2009), GUV do not show asymmetry at all. Finally, it was suggested that HA sorting to the Lo phases in GPMVs is also hampered by a possible effect of the reducing agent DTT used within the GPMV preparation buffer interfering with the thioester bond of the S acylation. Alterations of the palmitoylation might thus perturb the protein partition.

5.2.7 Possible protein partition and lipid sorting mechanisms prior to virus budding

A similar situation might be assumed for the organization of the virus envelope lipid phase. In the influenza virus envelope the cholesterol fraction is much higher than that of the host cell membranes (Scheiffele *et al.*, 1999; Zhang *et al.*, 2000). In the plasma membrane only about 30-40 mol% cholesterol and 10-15 mol% of sphingolipids are found whereas the remainders are phospholipids (Holthuis and Levine, 2005). Analysis of lipids from the influenza virus envelope shows that the fraction of phospholipids is decreased to about 30 mol% whereas cholesterol and sphingolipids are increased to 50 and 20 mol%, respectively (Michael Veit and Andreas Herrmann, 2009, unpublished results). Despite the high cholesterol content a recent NMR study on the plasma membrane – serving as a budding site for influenza viruses – and also on the viral envelope indicated that the physical state of those membranes at physiological temperature has Ld-like properties (Polozov *et al.*, 2008). Presumably, protein-lipid interactions interfere with the formation of tightly packed Lo domains. In the influenza virus envelope there are about 400 trimeric HA and 100 tetrameric NA proteins together with some copies of the M2 ion channel (Inglis *et al.*, 1976; Ruigrok *et al.*, 1984; Imai *et al.*, 2006; Harris *et al.*, 2006; K. K. Lee, 2010). As a single α-helical TMD occupies a surface area of about 1 nm^2 (Jacobson *et al.*, 2007) that leaves room for about 42 000 lipids in each virus membrane leaflets (Estimation for a virus of 100 nm in diameter and a lipid area of about 0.68 nm^2 (Jacobson *et al.*, 2007)). Thus each TMD is surrounded by about 30 lipids per protein in each bilayer leaflet. These numbers illustrate the high density of proteins within the viral membrane. In the plasma membrane the number of lipids per protein is about twice that of the viral envelope as the protein concentration is about 30 000 per μm^2 (Jacobson *et al.*, 2007).

These protein lipid interactions may not only prevent segregation of membrane proteins such as HA away from Lo domains, but may even facilitate partition in those lipid phases. However, it remains to identify the underlying mechanism of cholesterol enrichment in the virus envelope. Polozov *et al.* (2008) suggested the virus enriches itself in specific lipids such as cholesterol (see above). In particular, palmitoylation of HA may ensure a recruitment of saturated lipids and cholesterol. HAs with such a lipid environment could associate and form smaller clusters followed by the oligomerization of the virus matrix protein M1 and interaction of M1 with the CT of HA during virus assembly cross-linking HAs, which may lead to membrane patches enriched in cholesterol, which eventually form the virus budding

site. The oligomerization of proteins has already been considered by Simons and Vaz (Simons and Vaz, 2004) to be a driving force for raft partition of proteins since the partition coefficient of the protein oligomer is a product of its monomers. Is the partition to rafts only favoured weakly for the monomer this affinity is substantially increased for the oligomer. This in turn could be driving and stabilize aggregation of raft domains as it would be needed in the budding process of progeny viruses or in endocytosis (Hancock, 2006). Lateral cross-linking of membrane proteins and glycosphingolipids has been shown to trigger coalescence of nanoscale lipid heterogeneity into larger stabilized raft domains (R. Schroeder *et al.*, 1994; Kahya *et al.*, 2005), which play a functional role for uptake and endocytosis of proteins (Romer *et al.*, 2007), and viruses (Ewers *et al.*, 2010), and for cell signalling (Sohn *et al.*, 2008; Zech *et al.*, 2009).

These studies using model membranes clearly show that HA does not partition into tightly packed Lo domains of GUVs. To explain cholesterol dependent clustering of HA spikes at the plasma membrane visualized by immuno-EM (Hess *et al.*, 2005; Leser and Lamb, 2005) and FPALM (Hess *et al.*, 2007), and clustering of HA with "raft-markers" observed by FLIM-FRET (Engel *et al.*, 2010; Scolari *et al.*, 2009) in HA-transfected cells, it might be concluded that protein-lipid interactions reduce lipid packing of Lo domains in biological membranes enabling recruitment of proteins such as HA to those domains. This would be in line with the view that physical properties of lipid domains in biological membranes are tightly regulated by protein-lipid interactions (Ge *et al.*, 2003; Lingwood and Simons, 2010) and that protein-lipid interactions direct the formation of lipid domains around the integral membrane proteins (Poveda *et al.*, 2008). Besides differences in lipid packing, cellular and model membranes are also distinguished by the absence of cytoskeletal components in the latter. Recent reports indicated that microfilaments, especially cortical actin, might affect the formation, dynamics and maintenance of membrane-rafts in living cells (Suzuki *et al.*, 2007; Goswami *et al.*, 2008). Besides actin, also binding of other cytoskeletal proteins like spectrin to $PI(4,5)P_2$ in the plasma membrane might inhibit the formation of large-scale rafts (H. Keller *et al.*, 2009). However, other studies found submicroscopic membrane heterogeneity to be independent of actin (Lasserre *et al.*, 2008).

5.2.8 Small nanoclusters and signalling platforms in the plasma membrane

Finally, the question arises why macroscopic visible domains are not observed in the plasma membrane of living cells? As FLIM measurements revealed the lifetime of C6-NBD-PC in the plasma membrane of CHO-K1 cells displays only one rather long second lifetime with a broad maximum in the lifetime histogram. This lifetime is comparable to the lifetime $\tau_{2,Lo}$ in GPMVs (Fig. 24). Similar results were found for HepG2 and HeLa cells (Stockl *et al.*, 2008). But two long lifetimes, which is a strong indication for the formation of in this case nanoscopic domains, were determined for K562 cells (see section 4.2.1) and also further studies found evidence for small and transient lipid domains with nanometre dimensions at the plasma membrane of resting cells (Shaw *et al.*, 2006; Hancock, 2006; Jacobson *et al.*, 2007). Why are these small and transient domains not merging into larger and more stable, eventually macroscopic visible domains at the plasma membrane as they are found for the model systems derived from the plasma membrane? This coalescence of small diffusing domains would be stabilized by protein-protein interactions of proteins that reside in these lipid rafts (Hancock, 2006). Additionally the hydrophobic mismatch of raft and nonraft lipids at the domain boundary costs energy per length unit, also referred to as line tension (Garcia-Saez *et al.*, 2007). Domain merger and thus increasing raft diameter would reduce line tension due to a decrease of the total boundary length of growing domains. Proteins that reside at the Lo/Ld boundary, as found for the N-Ras protein (see Fig. 31 and (Vogel *et al.*, 2009)), would function as surfactant reducing the line tension thus stabilizing smaller raft domains (McConnell and Vrljic, 2003). Coalescence of rafts is also opposed by the electrostatic repulsion and entropy (Kuzmin *et al.*, 2005; Blanchette *et al.*, 2006; Veatch and Keller, 2005). Free diffusion and thus possible merger of nanoscopic rafts is hampered by the submicron-sized compartmentalization proposed by Kusumi et al. (2005) with compartment sizes between 32 and 68 nm for most mammalian cell lines studied. Besides the latter arguments also endocytosis might limit the domain size as found by a computational analysis. The selective and active removal of growing rafts by endocytosis and the disassembly of smaller rafts were described, thus keeping the domains at a nanoscopic size (Turner *et al.*, 2005).

Given the existence of multiple small and unstable rafts, what is their benefit? Here again the Ras protein family provides an example. Recently nanoclusters occupied by GTP loaded H-, N- or K-Ras were found to support Raf activation whereas GDP loaded Ras in different nanoclusters was not. These results clearly demonstrate that Ras in different nanoscale environments is able to configure the MAPK module in a way allowing the cell to generate

different output signals from one signalling cascade (Inder *et al.*, 2008; Inder and Hancock, 2008). One example for this specific sorting depending on GDP/GTP loading of the G-domain is the cholesterol-insensitive sorting of K-Ras4B to spatially distinct nanoclusters. Here a stronger membrane interaction of the inactive GDP loaded state was indicated in the FTIR spectra compared to the active GTP isoform (Weise *et al.*, 2010), which is in agreement with recent MD simulations (Abankwa *et al.*, 2010). Furthermore it could be shown that inhibition of Ras nanoclustering significantly affects Ras signalling (Hancock, 2006). The partition of a protein, e.g. N-Ras, to the interface of raft nanoclusters at the plasma membrane due to a favourable decrease in line tension might be imagined as an efficient strategy for possible protein interactions and a key parameter for the nanoclusters as a signalling platform. As FRET-based experiments of Sharma *et al.* (Sharma *et al.*, 2004) revealed, for GPI anchored GFP only four proteins at the most are present in small clusters of up to 10 nm in diameter. With this few molecules per nanocluster it seems beneficial to sort one component to the domain interface whereas another factor is within the raft. By this means an interaction is likely given the small domain length scale and the limited area within the nanoclusters is saved for the second component. In contrast to these small nanoclusters the much larger and more stable rafts formed by cross-linking and oligomerization of protein components might essentially play a roll in the formation of budding platforms accommodating viral components at the plasma membrane, in endocytosis and protein trafficking as well as for specialized functions like the T-cell synapse (Hancock, 2006).

5.2.9 K-Ras and N-Ras together yet separated at different spots in the Ld phase

Besides the incorporation of transmembrane proteins and their lipid raft dependent sorting also the partition of lipidated proteins from the Ras family was investigated within this study. The small GTPases K-Ras and N-Ras are found to be enriched in human tumours (Bos, 1989). Both Ras isoforms are found to partition to the Ld domain in the model systems of GUVs and GPMVs imaged by confocal fluorescence microscopy (Fig. 31 and Fig. 32) as well as in planar bilayers studied by AFM (Vogel *et al.*, 2009; Weise *et al.*, 2010) and also by ^{2}H-NMR comparing the order parameter and stretch of lipid and Ras acyl chains (Vogel *et al.*, 2009). In contrast to the exclusion of TMD peptides from the Lo domain in GUVs and GPMVs (see above) lipidated peptides are not prevented from partition to Lo phases per se as it could be shown for several proteins e.g. GPI anchored proteins (Johnson *et al.*, 2010; T. Y.

Wang *et al.*, 2000). Interestingly the palmitoylated and farnesylated N-Ras was found to diffuse to the Lo/Ld domain boundary in heterogeneous model membranes from synthetic lipids and viral lipid extracts (see section 4.2.4.1 and (Vogel *et al.*, 2009)). This partition in lateral domain forming model membranes is expected due to the rather bulky moiety of the farnesyl lipid anchor that would interfere with the tight lipid packing and the high degree of order in the Lo domain of the model system as described above. A similar exclusion from the Lo domain was found for a likewise branched tocopherol moiety by Bunge *et al.* (Kurz *et al.*, 2006; Bunge *et al.*, 2007). The enrichment of N-Ras at the domain interface might be explained by a preferential sorting of the palmitoyl anchor for the ordered phase. A somewhat similar mechanism was proposed for the transmembrane M2 ion channel of influenza virus with a rather short TMD helix residing in the Ld domain whereas the palmitate moiety might be extended into the Lo phase fixing the M2 at the raft interface (C. Schroeder *et al.*, 2005). Both active GTP- and inactive GDP-loaded K-Ras4B, membrane bound by a bulky and branched farnesyl anchor and a polybasic amino acid stretch, are located within the bulk Ld phase (see section 4.2.4.2 and (Weise *et al.*, 2010)). To give a more complete picture here it should also be mentioned that tapping mode AFM imaging showed the formation of new protein enriched domains within the Ld phase for a lipid mix of DOPC/DOPG/DPPC/DPPG/Chol (20:5:45:5:25, molar ratio) comprising anionic PG lipids as well as for neutral heterogeneous membranes of DOPC/DPPC/Chol (1:2:1, molar ratio) showing that electrostatic interactions of the polybasic stretch of K-Ras with the anionic and zwitterionic lipids would be able to locally attract acidic lipids (Weise *et al.*, 2010).

„The aim of an argument or discussion should not be victory, but progress."

Joseph Joubert (* 07.05.1754, † 04.05.1824)

6 Summary and perspectives

Hemifusion

Due their size, GUVs are an ideal tool to study the intermediates occurring in the process of bilayer fusion, which is an essential step in several cellular processes. Using confocal fluorescence microscopy, a direct experimental verification of the formation of the key fusion intermediate, the HD, was possible. In this hemifused state the outer membrane leaflets are fused, whereas the inner leaflets form the HD. GUVs containing negatively charged PS and fluorescent transmembrane peptides fused by means of addition of divalent cations. Time resolved imaging revealed that fusion was preceded by displacement of peptides and fluorescent lipid analogues from the GUV-GUV adhesion region. A detailed analysis of this area being several µm in size revealed that peptides were completely sequestered consistent with the formation of a HD. Lateral distribution of lipid analogues was consistent with formation of a HD, but not with the presence of two adherent bilayers. Based on results obtained in this study, formation and size of the HD were dependent on lipid composition and peptide concentration. An analytical model of hemifusion equilibrium and kinetics was verified by Jason M. Warner and Ben O'Shaughnessy (Columbia University, New York) identifying membrane tension as driving force for HD formation and interleaflet tension as its

opponent. Using the GUV model, one could corroborate the predicted equilibrium HD size and initial growth kinetics.

These findings and the combination of experiments and theoretical interpretation will help to better understand the pathway of bilayer fusion of biological membranes in cells. Better understanding of the mechanism how proteins like SNAREs or viral fusion proteins guide the way to HD formation, growth and the final opening of the HD will hopefully help to develop new applications for an enhanced drug delivery and the inhibition of viral infections.

Therefore, it would be interesting to study the influence of shorter TM peptides or molecular rods on the formation and also on the rupture of the HD. Thus one could elucidate the importance of the TM anchor of fusion proteins. Likewise, it might be of interest to attach hydrophilic polymers like complementary DNA or PNA oligomers to the membrane anchoring peptides or rods and thus simulate a minimal fusion machinery and study their influence on the HD.

Lipid domain formation and protein partition

In the plasma membrane of cells nanoscopic raft domains enriched in sphingolipids, cholesterol and specific proteins are found. Ternary model membranes separating into Lo and Ld domains resemble this lateral heterogeneity and have been studied intensely. However, a much tighter lipid packing in the Lo domain of GUVs was found compared to the ordered phase in GPMVs by comparing the fluorescence lifetime of C6-NBD-PC. As an almost exclusive domain specific partition of transmembrane peptides and proteins as well as a new molecular rod to the Ld domain reveals that the tight lipid packing in GUVs interferes with an efficient partition of all these transmembrane entities to the Lo domain of GUVs, although the hydrophobic matching, protein acylation and amino acid sequence would argue in favour of such a partition for some of these molecules. Sorting of transmembrane anchored HA protein in GPMVs is found to be less strict due to less tight lipid packing in the ordered domain. These findings are in line with latest results on the membrane order in GUVs, GPMVs and also in PMS as judged by the GP value of Laurdan (Kaiser *et al.*, 2009). All these results suggest that in GUVs lipid-lipid interactions govern the partition of transmembrane proteins, whereas in GPMVs and especially in the plasma membrane lipid-protein interactions

overcome this lipid dominated regime due to the much higher protein content and also due to a variety of different lipids, which decrease the differences between the domains. Besides the partition of transmembrane proteins, also lipid anchored proteins from the Ras family, namely N- and K-Ras were investigated. Whereas N-Ras was found to sort to the Ld phase and subsequently enrich in the Lo/Ld boundary, K-Ras partitions to the bulk of the Ld domain.

Further studies could shed light on lipid interactions in membrane systems comprising lipids with different acyl chain length in Ld and Lo domains and various amounts of cholesterol. This would affect membrane width and thus line tension at the domains interface. In this respect, also the sorting behaviour and the influence of TMD peptides on the membrane order might be investigated further. Very promising first results were achieved with a new class of fluorescent dyes having a large Stokes shift and long fluorescence lifetimes being able to report on the surrounding water content. Therefore, studies on the membrane order seem promising since the penetration of water into the bilayer depends on the lipid packing.

Addendum

"...science is, above all, communication."

Josiah Willard Gibbs (* 11.02.1839; † 28.04.1903)

Bibliography

Abankwa, D., Gorfe, A. A., Inder, K., & Hancock, J. F. (2010). Ras membrane orientation and nanodomain localization generate isoform diversity. *Proc Natl Acad Sci U S A, 107*(3), 1130-1135.

Abdulreda, M. H., Bhalla, A., Chapman, E. R., & Moy, V. T. (2008). Atomic force microscope spectroscopy reveals a hemifusion intermediate during soluble N-ethylmaleimide-sensitive factor-attachment protein receptors-mediated membrane fusion. *Biophys J, 94*(2), 648-655.

Abrami, L., Kunz, B., Iacovache, I., & van der Goot, F. G. (2008). Palmitoylation and ubiquitination regulate exit of the Wnt signaling protein LRP6 from the endoplasmic reticulum. *Proc Natl Acad Sci U S A, 105*(14), 5384-5389.

Almeida, P. F., Pokorny, A., & Hinderliter, A. (2005). Thermodynamics of membrane domains. *Biochim Biophys Acta, 1720*(1-2), 1-13.

Alvarez de Toledo, G., Fernandez-Chacon, R., & Fernandez, J. M. (1993). Release of secretory products during transient vesicle fusion. *Nature, 363*(6429), 554-558.

Amatore, C., Arbault, S., Bouret, Y., Guille, M., Lemaitre, F., & Verchier, Y. (2006). Regulation of exocytosis in chromaffin cells by trans-insertion of lysophosphatidylcholine and arachidonic acid into the outer leaflet of the cell membrane. *Chembiochem, 7*(12), 1998-2003.

Angelova, M., Soléau, S., Méléard, P., Faucon, J. F., & Bothorel, P. (1992). Preparation of giant vesicles by external AC electric fields: kinetics and application. *Prog. Colloid Polym. Sci. , 89*, 127-131.

Angelova, M. I., & Dimitrov, D. S. (1986). Liposome electroformation. *Faraday Discuss. Chem. Soc. , 81*, 303-311.

Apel, C. L., Deamer, D. W., & Mautner, M. N. (2002). Self-assembled vesicles of monocarboxylic acids and alcohols: conditions for stability and for the encapsulation of biopolymers. *Biochim Biophys Acta, 1559*(1), 1-9.

Armstrong, R. T., Kushnir, A. S., & White, J. M. (2000). The transmembrane domain of influenza hemagglutinin exhibits a stringent length requirement to support the hemifusion to fusion transition. *J Cell Biol, 151*(2), 425-437.

Axelrod, D., Koppel, D. E., Schlessinger, J., Elson, E., & Webb, W. W. (1976). Mobility measurement by analysis of fluorescence photobleaching recovery kinetics. *Biophys J, 16*(9), 1055-1069.

Ayuyan, A. G., & Cohen, F. S. (2006). Lipid peroxides promote large rafts: effects of excitation of probes in fluorescence microscopy and electrochemical reactions during vesicle formation. *Biophys J, 91*(6), 2172-2183.

Bacia, K., Schuette, C. G., Kahya, N., Jahn, R., & Schwille, P. (2004). SNAREs prefer liquid-disordered over "raft" (liquid-ordered) domains when reconstituted into giant unilamellar vesicles. *J Biol Chem, 279*(36), 37951-37955.

Bacia, K., Schwille, P., & Kurzchalia, T. (2005). Sterol structure determines the separation of phases and the curvature of the liquid-ordered phase in model membranes. *Proc Natl Acad Sci U S A, 102*(9), 3272-3277.

Bader, B., Kuhn, K., Owen, D. J., Waldmann, H., Wittinghofer, A., & Kuhlmann, J. (2000). Bioorganic synthesis of lipid-modified proteins for the study of signal transduction. *Nature, 403*(6766), 223-226.

Bagatolli, L. A. (2006). To see or not to see: lateral organization of biological membranes and fluorescence microscopy. *Biochim Biophys Acta, 1758*(10), 1541-1556.

Baker, K. A., Dutch, R. E., Lamb, R. A., & Jardetzky, T. S. (1999). Structural basis for paramyxovirus-mediated membrane fusion. *Mol Cell, 3*(3), 309-319.

Barman, S., Ali, A., Hui, E. K., Adhikary, L., & Nayak, D. P. (2001). Transport of viral proteins to the apical membranes and interaction of matrix protein with glycoproteins in the assembly of influenza viruses. *Virus Res, 77*(1), 61-69.

Barman, S., & Nayak, D. P. (2000). Analysis of the transmembrane domain of influenza virus neuraminidase, a type II transmembrane glycoprotein, for apical sorting and raft association. *J Virol, 74*(14), 6538-6545.

Baumgart, T., Hammond, A. T., Sengupta, P., Hess, S. T., Holowka, D. A., Baird, B. A., et al. (2007a). Large-scale fluid/fluid phase separation of proteins and lipids in giant plasma membrane vesicles. *Proc Natl Acad Sci U S A, 104*(9), 3165-3170.

Baumgart, T., Hess, S. T., & Webb, W. W. (2003). Imaging coexisting fluid domains in biomembrane models coupling curvature and line tension. *Nature, 425*(6960), 821-824.

Baumgart, T., Hunt, G., Farkas, E. R., Webb, W. W., & Feigenson, G. W. (2007b). Fluorescence probe partitioning between Lo/Ld phases in lipid membranes. *Biochim Biophys Acta, 1768*(9), 2182-2194.

Bavari, S., Bosio, C. M., Wiegand, E., Ruthel, G., Will, A. B., Geisbert, T. W., et al. (2002). Lipid raft microdomains: a gateway for compartmentalized trafficking of Ebola and Marburg viruses. *J Exp Med, 195*(5), 593-602.

Bittman, R., Kasireddy, C. R., Mattjus, P., & Slotte, J. P. (1994). Interaction of cholesterol with sphingomyelin in monolayers and vesicles. *Biochemistry, 33*(39), 11776-11781.

Blanchette, C. D., Lin, W. C., Ratto, T. V., & Longo, M. L. (2006). Galactosylceramide domain microstructure: impact of cholesterol and nucleation/growth conditions. *Biophys J, 90*(12), 4466-4478.

Bligh, E. G., & Dyer, W. J. (1959). A rapid method of total lipid extraction and purification. *Can J Biochem Physiol, 37*(8), 911-917.

Borrego-Diaz, E., Peeples, M. E., Markosyan, R. M., Melikyan, G. B., & Cohen, F. S. (2003). Completion of trimeric hairpin formation of influenza virus hemagglutinin promotes fusion pore opening and enlargement. *Virology, 316*(2), 234-244.

Bos, J. L. (1989). ras oncogenes in human cancer: a review. *Cancer Res, 49*(17), 4682-4689.

Bottcher, C., Ludwig, K., Herrmann, A., van Heel, M., & Stark, H. (1999). Structure of influenza haemagglutinin at neutral and at fusogenic pH by electron cryo-microscopy. *FEBS Lett, 463*(3), 255-259.

Bowen, M., & Brunger, A. T. (2006). Conformation of the synaptobrevin transmembrane domain. *Proc Natl Acad Sci U S A, 103*(22), 8378-8383.

Bretscher, M. S., & Munro, S. (1993). Cholesterol and the Golgi apparatus. *Science, 261*(5126), 1280-1281.

Brown, D. A. (2006). Lipid rafts, detergent-resistant membranes, and raft targeting signals. *Physiology (Bethesda), 21*, 430-439.

Brown, D. A., & London, E. (2000). Structure and function of sphingolipid- and cholesterol-rich membrane rafts. *J Biol Chem, 275*(23), 17221-17224.

Brown, D. A., & Rose, J. K. (1992). Sorting of GPI-anchored proteins to glycolipid-enriched membrane subdomains during transport to the apical cell surface. *Cell, 68*(3), 533-544.

Bullough, P. A., Hughson, F. M., Skehel, J. J., & Wiley, D. C. (1994). Structure of influenza haemagglutinin at the pH of membrane fusion. *Nature, 371*(6492), 37-43.

Bunge, A., Kurz, A., Windeck, A. K., Korte, T., Flasche, W., Liebscher, J., et al. (2007). Lipophilic oligonucleotides spontaneously insert into lipid membranes, bind complementary DNA strands, and sequester into lipid-disordered domains. *Langmuir, 23*(8), 4455-4464.

Bunge, A., Muller, P., Stockl, M., Herrmann, A., & Huster, D. (2008). Characterization of the ternary mixture of sphingomyelin, POPC, and cholesterol: support for an inhomogeneous lipid distribution at high temperatures. *Biophys J, 94*(7), 2680-2690.

Caffrey, M., Cai, M., Kaufman, J., Stahl, S. J., Wingfield, P. T., Covell, D. G., et al. (1998). Three-dimensional solution structure of the 44 kDa ectodomain of SIV gp41. *Embo J, 17*(16), 4572-4584.

Campbell, S. M., Crowe, S. M., & Mak, J. (2001). Lipid rafts and HIV-1: from viral entry to assembly of progeny virions. *J Clin Virol, 22*(3), 217-227.

Carr, C. M., & Kim, P. S. (1993). A spring-loaded mechanism for the conformational change of influenza hemagglutinin. *Cell, 73*(4), 823-832.

Chakrabandhu, K., Herincs, Z., Huault, S., Dost, B., Peng, L., Conchonaud, F., et al. (2007). Palmitoylation is required for efficient Fas cell death signaling. *Embo J, 26*(1), 209-220.

Chan, D. C., Fass, D., Berger, J. M., & Kim, P. S. (1997). Core structure of gp41 from the HIV envelope glycoprotein. *Cell, 89*(2), 263-273.

Chanturiya, A., Chernomordik, L. V., & Zimmerberg, J. (1997). Flickering fusion pores comparable with initial exocytotic pores occur in protein-free phospholipid bilayers. *Proc Natl Acad Sci U S A, 94*(26), 14423-14428.

Chanturiya, A., Scaria, P., & Woodle, M. C. (2000). The role of membrane lateral tension in calcium-induced membrane fusion. *J Membr Biol, 176*(1), 67-75.

Chattopadhyay, A., & Mukherjee, S. (1993). Fluorophore environments in membrane-bound probes: a red edge excitation shift study. *Biochemistry, 32*(14), 3804-3811.

Chen, B. J., Takeda, M., & Lamb, R. A. (2005). Influenza virus hemagglutinin (H3 subtype) requires palmitoylation of its cytoplasmic tail for assembly: M1 proteins of two subtypes differ in their ability to support assembly. *J Virol, 79*(21), 13673-13684.

Chen, E. H., & Olson, E. N. (2005). Unveiling the mechanisms of cell-cell fusion. *Science, 308*(5720), 369-373.

Chen, J., Skehel, J. J., & Wiley, D. C. (1999). N- and C-terminal residues combine in the fusion-pH influenza hemagglutinin HA(2) subunit to form an N cap that terminates the triple-stranded coiled coil. *Proc Natl Acad Sci U S A, 96*(16), 8967-8972.

Chen, Y. A., & Scheller, R. H. (2001). SNARE-mediated membrane fusion. *Nat Rev Mol Cell Biol, 2*(2), 98-106.

Chen, Y. X., Koch, S., Uhlenbrock, K., Weise, K., Das, D., Gremer, L., et al. (2010). Synthesis of the Rheb and K-Ras4B GTPases. *Angew Chem Int Ed Engl, 49*(35), 6090-6095.

Cheng, H. T., Megha, & London, E. (2009). Preparation and properties of asymmetric vesicles that mimic cell membranes: effect upon lipid raft formation and transmembrane helix orientation. *J Biol Chem, 284*(10), 6079-6092.

Chernomordik, L. (1996). Non-bilayer lipids and biological fusion intermediates. *Chem Phys Lipids, 81*(2), 203-213.

Chernomordik, L., Chanturiya, A., Green, J., & Zimmerberg, J. (1995). The hemifusion intermediate and its conversion to complete fusion: regulation by membrane composition. *Biophys J, 69*(3), 922-929.

Chernomordik, L. V., Frolov, V. A., Leikina, E., Bronk, P., & Zimmerberg, J. (1998). The pathway of membrane fusion catalyzed by influenza hemagglutinin: restriction of lipids, hemifusion, and lipidic fusion pore formation. *J Cell Biol, 140*(6), 1369-1382.

Chernomordik, L. V., & Kozlov, M. M. (2003). Protein-lipid interplay in fusion and fission of biological membranes. *Annu Rev Biochem, 72*, 175-207.

Chernomordik, L. V., & Kozlov, M. M. (2005). Membrane hemifusion: crossing a chasm in two leaps. *Cell, 123*(3), 375-382.

Chernomordik, L. V., & Kozlov, M. M. (2008). Mechanics of membrane fusion. *Nat Struct Mol Biol, 15*(7), 675-683.

Chernomordik, L. V., Leikina, E., Frolov, V., Bronk, P., & Zimmerberg, J. (1997). An early stage of membrane fusion mediated by the low pH conformation of influenza hemagglutinin depends upon membrane lipids. *J Cell Biol, 136*(1), 81-93.

Chernomordik, L. V., Melikyan, G. B., & Chizmadzhev, Y. A. (1987). Biomembrane fusion: a new concept derived from model studies using two interacting planar lipid bilayers. *Biochim Biophys Acta, 906*(3), 309-352.

Chernomordik, L. V., Vogel, S. S., Sokoloff, A., Onaran, H. O., Leikina, E. A., & Zimmerberg, J. (1993). Lysolipids reversibly inhibit Ca(2+)-, GTP- and pH-dependent fusion of biological membranes. *FEBS Lett, 318*(1), 71-76.

Chernomordik, L. V., Zimmerberg, J., & Kozlov, M. M. (2006). Membranes of the world unite! *J Cell Biol, 175*(2), 201-207.

Cleverley, D. Z., Geller, H. M., & Lenard, J. (1997). Characterization of cholesterol-free insect cells infectible by baculoviruses: effects of cholesterol on VSV fusion and infectivity and on cytotoxicity induced by influenza M2 protein. *Exp Cell Res, 233*(2), 288-296.

Cleverley, D. Z., & Lenard, J. (1998). The transmembrane domain in viral fusion: essential role for a conserved glycine residue in vesicular stomatitis virus G protein. *Proc Natl Acad Sci U S A, 95*(7), 3425-3430.

Cohen, F. S., Zimmerberg, J., & Finkelstein, A. (1980). Fusion of phospholipid vesicles with planar phospholipid bilayer membranes. II. Incorporation of a vesicular membrane marker into the planar membrane. *J Gen Physiol, 75*(3), 251-270.

Collins, M. D., & Keller, S. L. (2008). Tuning lipid mixtures to induce or suppress domain formation across leaflets of unsupported asymmetric bilayers. *Proc Natl Acad Sci U S A*.

Conibear, E., & Davis, N. G. (2010). Palmitoylation and depalmitoylation dynamics at a glance. *J Cell Sci, 123*(Pt 23), 4007-4010.

Copeland, C. S., Doms, R. W., Bolzau, E. M., Webster, R. G., & Helenius, A. (1986). Assembly of influenza hemagglutinin trimers and its role in intracellular transport. *J Cell Biol, 103*(4), 1179-1191.

Das, S., & Rand, R. P. (1984). Diacylglycerol causes major structural transitions in phospholipid bilayer membranes. *Biochem Biophys Res Commun, 124*(2), 491-496.

de Almeida, R. F., Borst, J., Fedorov, A., Prieto, M., & Visser, A. J. (2007). Complexity of lipid domains and rafts in giant unilamellar vesicles revealed by combining imaging, microscopic and macroscopic time-resolved fluorescence. *Biophys J*.

de Almeida, R. F., Fedorov, A., & Prieto, M. (2003). Sphingomyelin/phosphatidylcholine/cholesterol phase diagram: boundaries and composition of lipid rafts. *Biophys J, 85*(4), 2406-2416.

de Almeida, R. F., Loura, L. M., Fedorov, A., & Prieto, M. (2005). Lipid rafts have different sizes depending on membrane composition: a time-resolved fluorescence resonance energy transfer study. *J Mol Biol, 346*(4), 1109-1120.

de Planque, M. R., Kruijtzer, J. A., Liskamp, R. M., Marsh, D., Greathouse, D. V., Koeppe, R. E., 2nd, et al. (1999). Different membrane anchoring positions of tryptophan and lysine in synthetic transmembrane alpha-helical peptides. *J Biol Chem, 274*(30), 20839-20846.

Deamer, D. W. (2008). Origins of life: How leaky were primitive cells? *Nature, 454*(7200), 37-38.

Dennison, S. M., Greenfield, N., Lenard, J., & Lentz, B. R. (2002). VSV transmembrane domain (TMD) peptide promotes PEG-mediated fusion of liposomes in a conformationally sensitive fashion. *Biochemistry, 41*(50), 14925-14934.

Devaux, P. F., & Morris, R. (2004). Transmembrane asymmetry and lateral domains in biological membranes. *Traffic, 5*(4), 241-246.

Diao, J., Su, Z., Ishitsuka, Y., Lu, B., Lee, K. S., Lai, Y., et al. (2010). A single-vesicle content mixing assay for SNARE-mediated membrane fusion. *Nat Commun, 1*(5), 1-6.

Dietrich, C., Bagatolli, L. A., Volovyk, Z. N., Thompson, N. L., Levi, M., Jacobson, K., et al. (2001). Lipid rafts reconstituted in model membranes. *Biophys J, 80*(3), 1417-1428.

Dietrich, C., Yang, B., Fujiwara, T., Kusumi, A., & Jacobson, K. (2002). Relationship of lipid rafts to transient confinement zones detected by single particle tracking. *Biophys J, 82*(1 Pt 1), 274-284.

Dimitrov, D. S., & Angelova, M. I. (1987). Lipid swelling and liposome formation on solid surfaces in external electric fields. *Prog. Colloid Polym. Sci. , 73*.

Divito, C. B., & Amara, S. G. (2009). Close encounters of the oily kind: regulation of transporters by lipids. *Mol Interv, 9*(5), 252-262.

Dodge, J. T., Mitchell, C., & Hanahan, D. J. (1963). The preparation and chemical characteristics of hemoglobin-free ghosts of human erythrocytes. *Arch Biochem Biophys, 100*, 119-130.

Doeven, M. K., Folgering, J. H., Krasnikov, V., Geertsma, E. R., van den Bogaart, G., & Poolman, B. (2005). Distribution, lateral mobility and function of membrane proteins incorporated into giant unilamellar vesicles. *Biophys J, 88*(2), 1134-1142.

Domanska, M. K., Kiessling, V., & Tamm, L. K. (2010). Docking and fast fusion of synaptobrevin vesicles depends on the lipid compositions of the vesicle and the acceptor SNARE complex-containing target membrane. *Biophys J, 99*(9), 2936-2946.

Douglass, A. D., & Vale, R. D. (2005). Single-molecule microscopy reveals plasma membrane microdomains created by protein-protein networks that exclude or trap signaling molecules in T cells. *Cell, 121*(6), 937-950.

Dykstra, M., Cherukuri, A., Sohn, H. W., Tzeng, S. J., & Pierce, S. K. (2003). Location is everything: lipid rafts and immune cell signaling. *Annu Rev Immunol, 21*, 457-481.

Earp, L. J., Delos, S. E., Park, H. E., & White, J. M. (2005). The many mechanisms of viral membrane fusion proteins. *Curr Top Microbiol Immunol, 285*, 25-66.

Eckert, D. M., & Kim, P. S. (2001). Mechanisms of viral membrane fusion and its inhibition. *Annu Rev Biochem, 70*, 777-810.

Efrat, A., Chernomordik, L. V., & Kozlov, M. M. (2007). Point-like protrusion as a prestalk intermediate in membrane fusion pathway. *Biophys J, 92*(8), L61-63.

Eggeling, C., Ringemann, C., Medda, R., Schwarzmann, G., Sandhoff, K., Polyakova, S., et al. (2009). Direct observation of the nanoscale dynamics of membrane lipids in a living cell. *Nature, 457*(7233), 1159-1162.

Egner, A., & Hell, S. W. (2005). Fluorescence microscopy with super-resolved optical sections. *Trends Cell Biol, 15*(4), 207-215.

Eisenblatter, J., & Winter, R. (2006). Pressure effects on the structure and phase behavior of DMPC-gramicidin lipid bilayers: a synchrotron SAXS and 2H-NMR spectroscopy study. *Biophys J, 90*(3), 956-966.

Engel, S., Scolari, S., Thaa, B., Krebs, N., Korte, T., Herrmann, A., et al. (2010). FLIM-FRET and FRAP reveal association of influenza virus haemagglutinin with membrane rafts. *Biochem J, 425*(3), 567-573.

Epand, R. M. (2008). Proteins and cholesterol-rich domains. *Biochim Biophys Acta, 1778*(7-8), 1576-1582.

Ewers, H., Romer, W., Smith, A. E., Bacia, K., Dmitrieff, S., Chai, W., et al. (2010). GM1 structure determines SV40-induced membrane invagination and infection. *Nat Cell Biol, 12*(1), 11-18; sup pp 11-12.

Fastenberg, M. E., Shogomori, H., Xu, X., Brown, D. A., & London, E. (2003). Exclusion of a transmembrane-type peptide from ordered-lipid domains (rafts) detected by fluorescence quenching: extension of quenching analysis to account for the effects of domain size and domain boundaries. *Biochemistry, 42*(42), 12376-12390.

Feigenson, G. W. (1986). On the nature of calcium ion binding between phosphatidylserine lamellae. *Biochemistry, 25*(19), 5819-5825.

Floyd, D. L., Ragains, J. R., Skehel, J. J., Harrison, S. C., & van Oijen, A. M. (2008). Single-particle kinetics of influenza virus membrane fusion. *Proc Natl Acad Sci U S A, 105*(40), 15382-15387.

Frolov, V. A., Cho, M. S., Bronk, P., Reese, T. S., & Zimmerberg, J. (2000). Multiple local contact sites are induced by GPI-linked influenza hemagglutinin during hemifusion and flickering pore formation. *Traffic, 1*(8), 622-630.

Gandhavadi, M., Allende, D., Vidal, A., Simon, S. A., & McIntosh, T. J. (2002). Structure, composition, and peptide binding properties of detergent soluble bilayers and detergent resistant rafts. *Biophys J, 82*(3), 1469-1482.

Garcia-Saez, A. J., Chiantia, S., & Schwille, P. (2007). Effect of line tension on the lateral organization of lipid membranes. *J Biol Chem, 282*(46), 33537-33544.

Gaudin, Y. (2000). Rabies virus-induced membrane fusion pathway. *J Cell Biol, 150*(3), 601-612.

Ge, M., Gidwani, A., Brown, H. A., Holowka, D., Baird, B., & Freed, J. H. (2003). Ordered and disordered phases coexist in plasma membrane vesicles of RBL-2H3 mast cells. An ESR study. *Biophys J, 85*(2), 1278-1288.

Gennis, R. B. (1989). *Biomembranes - molecular structure and function*. New York.

Gibbons, D. L., Vaney, M. C., Roussel, A., Vigouroux, A., Reilly, B., Lepault, J., et al. (2004). Conformational change and protein-protein interactions of the fusion protein of Semliki Forest virus. *Nature, 427*(6972), 320-325.

Girard, P., Pecreaux, J., Lenoir, G., Falson, P., Rigaud, J. L., & Bassereau, P. (2004). A new method for the reconstitution of membrane proteins into giant unilamellar vesicles. *Biophys J, 87*(1), 419-429.

Giraudo, C. G., Hu, C., You, D., Slovic, A. M., Mosharov, E. V., Sulzer, D., et al. (2005). SNAREs can promote complete fusion and hemifusion as alternative outcomes. *J Cell Biol, 170*(2), 249-260.

Goswami, D., Gowrishankar, K., Bilgrami, S., Ghosh, S., Raghupathy, R., Chadda, R., et al. (2008). Nanoclusters of GPI-anchored proteins are formed by cortical actin-driven activity. *Cell, 135*(6), 1085-1097.

Grafmuller, A., Shillcock, J., & Lipowsky, R. (2007). Pathway of membrane fusion with two tension-dependent energy barriers. *Phys Rev Lett, 98*(21), 218101.

Grafmuller, A., Shillcock, J., & Lipowsky, R. (2009). The fusion of membranes and vesicles: pathway and energy barriers from dissipative particle dynamics. *Biophys J, 96*(7), 2658-2675.

Graham, T. R., & Kozlov, M. M. (2010). Interplay of proteins and lipids in generating membrane curvature. *Curr Opin Cell Biol, 22*(4), 430-436.

Greaves, J., & Chamberlain, L. H. (2007). Palmitoylation-dependent protein sorting. *J Cell Biol, 176*(3), 249-254.

Greaves, J., Prescott, G. R., Gorleku, O. A., & Chamberlain, L. H. (2009). The fat controller: roles of palmitoylation in intracellular protein trafficking and targeting to membrane microdomains (Review). *Mol Membr Biol, 26*(1), 67-79.

Gri, G., Molon, B., Manes, S., Pozzan, T., & Viola, A. (2004). The inner side of T cell lipid rafts. *Immunol Lett, 94*(3), 247-252.

Grote, E., Baba, M., Ohsumi, Y., & Novick, P. J. (2000). Geranylgeranylated SNAREs are dominant inhibitors of membrane fusion. *J Cell Biol, 151*(2), 453-466.

Gurezka, R., Laage, R., Brosig, B., & Langosch, D. (1999). A heptad motif of leucine residues found in membrane proteins can drive self-assembly of artificial transmembrane segments. *J Biol Chem, 274*(14), 9265-9270.

Haluska, C. K., Riske, K. A., Marchi-Artzner, V., Lehn, J. M., Lipowsky, R., & Dimova, R. (2006). Time scales of membrane fusion revealed by direct imaging of vesicle fusion with high temporal resolution. *Proc Natl Acad Sci U S A, 103*(43), 15841-15846.

Hammond, A. T., Heberle, F. A., Baumgart, T., Holowka, D., Baird, B., & Feigenson, G. W. (2005). Crosslinking a lipid raft component triggers liquid ordered-liquid disordered phase separation in model plasma membranes. *Proc Natl Acad Sci U S A, 102*(18), 6320-6325.

Han, X., Bushweller, J. H., Cafiso, D. S., & Tamm, L. K. (2001). Membrane structure and fusion-triggering conformational change of the fusion domain from influenza hemagglutinin. *Nat Struct Biol, 8*(8), 715-720.

Han, X., Steinhauer, D. A., Wharton, S. A., & Tamm, L. K. (1999). Interaction of mutant influenza virus hemagglutinin fusion peptides with lipid bilayers: probing the role of hydrophobic residue size in the central region of the fusion peptide. *Biochemistry, 38*(45), 15052-15059.

Hancock, J. F. (2006). Lipid rafts: contentious only from simplistic standpoints. *Nat Rev Mol Cell Biol, 7*(6), 456-462.

Hansen, G. H., Niels-Christiansen, L. L., Thorsen, E., Immerdal, L., & Danielsen, E. M. (2000). Cholesterol depletion of enterocytes. Effect on the Golgi complex and apical membrane trafficking. *J Biol Chem, 275*(7), 5136-5142.

Harder, T., Scheiffele, P., Verkade, P., & Simons, K. (1998). Lipid domain structure of the plasma membrane revealed by patching of membrane components. *J Cell Biol, 141*(4), 929-942.

Harder, T., & Simons, K. (1999). Clusters of glycolipid and glycosylphosphatidylinositol-anchored proteins in lymphoid cells: accumulation of actin regulated by local tyrosine phosphorylation. *Eur J Immunol, 29*(2), 556-562.

Harris, A., Cardone, G., Winkler, D. C., Heymann, J. B., Brecher, M., White, J. M., et al. (2006). Influenza virus pleiomorphy characterized by cryoelectron tomography. *Proc Natl Acad Sci U S A, 103*(50), 19123-19127.

Harrison, S. C. (2008). Viral membrane fusion. *Nat Struct Mol Biol, 15*(7), 690-698.

Heberle, F. A., Buboltz, J. T., Stringer, D., & Feigenson, G. W. (2005). Fluorescence methods to detect phase boundaries in lipid bilayer mixtures. *Biochim Biophys Acta, 1746*(3), 186-192.

Heerklotz, H. (2002). Triton promotes domain formation in lipid raft mixtures. *Biophys J, 83*(5), 2693-2701.

Heldwein, E. E., Lou, H., Bender, F. C., Cohen, G. H., Eisenberg, R. J., & Harrison, S. C. (2006). Crystal structure of glycoprotein B from herpes simplex virus 1. *Science, 313*(5784), 217-220.

Helfrich, W. (1973). Elastic properties of lipid bilayers: theory and possible experiments. *Z Naturforsch C, 28*(11), 693-703.

Hess, S. T., Gould, T. J., Gudheti, M. V., Maas, S. A., Mills, K. D., & Zimmerberg, J. (2007). Dynamic clustered distribution of hemagglutinin resolved at 40 nm in living cell membranes discriminates between raft theories. *Proc Natl Acad Sci U S A, 104*(44), 17370-17375.

Hess, S. T., Kumar, M., Verma, A., Farrington, J., Kenworthy, A., & Zimmerberg, J. (2005). Quantitative electron microscopy and fluorescence spectroscopy of the membrane distribution of influenza hemagglutinin. *J Cell Biol, 169*(6), 965-976.

Hesselink, R. W., Koehorst, R. B., Nazarov, P. V., & Hemminga, M. A. (2005). Membrane-bound peptides mimicking transmembrane Vph1p helix 7 of yeast V-ATPase: a spectroscopic and polarity mismatch study. *Biochim Biophys Acta, 1716*(2), 137-145.

Heuvingh, J., Pincet, F., & Cribier, S. (2004). Hemifusion and fusion of giant vesicles induced by reduction of inter-membrane distance. *Eur Phys J E Soft Matter, 14*(3), 269-276.

Hofmann, M. W., Peplowska, K., Rohde, J., Poschner, B. C., Ungermann, C., & Langosch, D. (2006). Self-interaction of a SNARE transmembrane domain promotes the hemifusion-to-fusion transition. *J Mol Biol, 364*(5), 1048-1060.

Hofmann, M. W., Weise, K., Ollesch, J., Agrawal, P., Stalz, H., Stelzer, W., et al. (2004). De novo design of conformationally flexible transmembrane peptides driving membrane fusion. *Proc Natl Acad Sci U S A, 101*(41), 14776-14781.

Holowka, D., & Baird, B. (1983). Structural studies on the membrane-bound immunoglobulin E-receptor complex. 1. Characterization of large plasma membrane vesicles from rat basophilic leukemia cells and insertion of amphipathic fluorescent probes. *Biochemistry, 22*(14), 3466-3474.

Holowka, D., Gosse, J. A., Hammond, A. T., Han, X., Sengupta, P., Smith, N. L., et al. (2005). Lipid segregation and IgE receptor signaling: a decade of progress. *Biochim Biophys Acta, 1746*(3), 252-259.

Holowka, D., Sheets, E. D., & Baird, B. (2000). Interactions between Fc(epsilon)RI and lipid raft components are regulated by the actin cytoskeleton. *J Cell Sci, 113 (Pt 6)*, 1009-1019.

Holt, A., & Killian, J. A. (2010). Orientation and dynamics of transmembrane peptides: the power of simple models. *Eur Biophys J, 39*(4), 609-621.

Holthuis, J. C., & Levine, T. P. (2005). Lipid traffic: floppy drives and a superhighway. *Nat Rev Mol Cell Biol, 6*(3), 209-220.

Holthuis, J. C., van Meer, G., & Huitema, K. (2003). Lipid microdomains, lipid translocation and the organization of intracellular membrane transport (Review). *Mol Membr Biol, 20*(3), 231-241.

Honerkamp-Smith, A. R., Veatch, S. L., & Keller, S. L. (2009). An introduction to critical points for biophysicists; observations of compositional heterogeneity in lipid membranes. *Biochim Biophys Acta, 1788*(1), 53-63.

Huang, J., & Feigenson, G. W. (1999). A microscopic interaction model of maximum solubility of cholesterol in lipid bilayers. *Biophys J, 76*(4), 2142-2157.

Huang, Q., Chen, C. L., & Herrmann, A. (2004). Bilayer conformation of fusion peptide of influenza virus hemagglutinin: a molecular dynamics simulation study. *Biophys J, 87*(1), 14-22.

Huang, Q., Korte, T., Rachakonda, P. S., Knapp, E. W., & Herrmann, A. (2009). Energetics of the loop-to-helix transition leading to the coiled-coil structure of influenza virus hemagglutinin HA2 subunits. *Proteins, 74*(2), 291-303.

Hundt, M., Harada, Y., De Giorgio, L., Tanimura, N., Zhang, W., & Altman, A. (2009). Palmitoylation-dependent plasma membrane transport but lipid raft-independent signaling by linker for activation of T cells. *J Immunol, 183*(3), 1685-1694.

Imai, M., Mizuno, T., & Kawasaki, K. (2006). Membrane fusion by single influenza hemagglutinin trimers. Kinetic evidence from image analysis of hemagglutinin-reconstituted vesicles. *J Biol Chem, 281*(18), 12729-12735.

Inder, K., & Hancock, J. F. (2008). System output of the MAPK module is spatially regulated. *Commun Integr Biol, 1*(2), 178-179.

Inder, K., Harding, A., Plowman, S. J., Philips, M. R., Parton, R. G., & Hancock, J. F. (2008). Activation of the MAPK module from different spatial locations generates distinct system outputs. *Mol Biol Cell, 19*(11), 4776-4784.

Inglis, S. C., Carroll, A. R., Lamb, R. A., & Mahy, B. W. (1976). Polypeptides specified by the influenza virus genome I. Evidence for eight distinct gene products specified by fowl plague virus. *Virology, 74*(2), 489-503.

Ishiguro, R., Matsumoto, M., & Takahashi, S. (1996). Interaction of fusogenic synthetic peptide with phospholipid bilayers: orientation of the peptide alpha-helix and binding isotherm. *Biochemistry, 35*(15), 4976-4983.

Jackson, M. B., & Chapman, E. R. (2006). Fusion pores and fusion machines in Ca2+-triggered exocytosis. *Annu Rev Biophys Biomol Struct, 35*, 135-160.

Jacobson, K., Mouritsen, O. G., & Anderson, R. G. (2007). Lipid rafts: at a crossroad between cell biology and physics. *Nat Cell Biol, 9*(1), 7-14.

Jahn, R., Lang, T., & Sudhof, T. C. (2003). Membrane fusion. *Cell, 112*(4), 519-533.

Jahn, R., & Scheller, R. H. (2006). SNAREs--engines for membrane fusion. *Nat Rev Mol Cell Biol, 7*(9), 631-643.

Janes, P. W., Ley, S. C., & Magee, A. I. (1999). Aggregation of lipid rafts accompanies signaling via the T cell antigen receptor. *J Cell Biol, 147*(2), 447-461.

Johnson, S. A., Stinson, B. M., Go, M., Carmona, L. M., Reminick, J. I., Fang, X., et al. (2010). Temperature dependent phase behavior and protein partitioning in giant plasma membrane vesicles. *Biochim Biophys Acta*.

Joo, K. I., Tai, A., Lee, C. L., Wong, C., & Wang, P. (2010). Imaging multiple intermediates of single-virus membrane fusion mediated by distinct fusion proteins. *Microsc Res Tech, 73*(9), 886-900.

Joseph, M., & Nagaraj, R. (1995). Interaction of peptides corresponding to fatty acylation sites in proteins with model membranes. *J Biol Chem, 270*(28), 16749-16755.

Jun, Y., & Wickner, W. (2007). Assays of vacuole fusion resolve the stages of docking, lipid mixing, and content mixing. *Proc Natl Acad Sci U S A, 104*(32), 13010-13015.

Kachar, B., Fuller, N., & Rand, R. P. (1986). Morphological responses to calcium-induced interaction of phosphatidylserine-containing vesicles. *Biophys J, 50*(5), 779-788.

Kahya, N., Brown, D. A., & Schwille, P. (2005). Raft partitioning and dynamic behavior of human placental alkaline phosphatase in giant unilamellar vesicles. *Biochemistry, 44*(20), 7479-7489.

Kahya, N., Scherfeld, D., Bacia, K., & Schwille, P. (2004). Lipid domain formation and dynamics in giant unilamellar vesicles explored by fluorescence correlation spectroscopy. *J Struct Biol, 147*(1), 77-89.

Kaiser, H. J., Lingwood, D., Levental, I., Sampaio, J. L., Kalvodova, L., Rajendran, L., et al. (2009). Order of lipid phases in model and plasma membranes. *Proc Natl Acad Sci U S A, 106*(39), 16645-16650.

Kalvodova, L., Kahya, N., Schwille, P., Ehehalt, R., Verkade, P., Drechsel, D., et al. (2005). Lipids as modulators of proteolytic activity of BACE: involvement of cholesterol, glycosphingolipids, and anionic phospholipids in vitro. *J Biol Chem, 280*(44), 36815-36823.

Kandasamy, S. K., & Larson, R. G. (2006). Molecular dynamics simulations of model trans-membrane peptides in lipid bilayers: a systematic investigation of hydrophobic mismatch. *Biophys J, 90*(7), 2326-2343.

Kasson, P. M., Kelley, N. W., Singhal, N., Vrljic, M., Brunger, A. T., & Pande, V. S. (2006). Ensemble molecular dynamics yields submillisecond kinetics and intermediates of membrane fusion. *Proc Natl Acad Sci U S A, 103*(32), 11916-11921.

Kasson, P. M., Lindahl, E., & Pande, V. S. (2010). Atomic-resolution simulations predict a transition state for vesicle fusion defined by contact of a few lipid tails. *PLoS Comput Biol, 6*(6), e1000829.

Kasson, P. M., & Pande, V. S. (2007). Control of membrane fusion mechanism by lipid composition: predictions from ensemble molecular dynamics. *PLoS Comput Biol, 3*(11), e220.

Kasson, P. M., Zomorodian, A., Park, S., Singhal, N., Guibas, L. J., & Pande, V. S. (2007). Persistent voids: a new structural metric for membrane fusion. *Bioinformatics, 23*(14), 1753-1759.

Katsov, K., Muller, M., & Schick, M. (2004). Field theoretic study of bilayer membrane fusion. I. Hemifusion mechanism. *Biophys J, 87*(5), 3277-3290.

Katsov, K., Muller, M., & Schick, M. (2006). Field theoretic study of bilayer membrane fusion: II. Mechanism of a stalk-hole complex. *Biophys J, 90*(3), 915-926.

Keller, H., Lorizate, M., & Schwille, P. (2009). PI(4,5)P2 degradation promotes the formation of cytoskeleton-free model membrane systems. *Chemphyschem, 10*(16), 2805-2812.

Keller, P., & Simons, K. (1998). Cholesterol is required for surface transport of influenza virus hemagglutinin. *J Cell Biol, 140*(6), 1357-1367.

Keller, P., Toomre, D., Diaz, E., White, J., & Simons, K. (2001). Multicolour imaging of post-Golgi sorting and trafficking in live cells. *Nat Cell Biol, 3*(2), 140-149.

Kemble, G. W., Danieli, T., & White, J. M. (1994). Lipid-anchored influenza hemagglutinin promotes hemifusion, not complete fusion. *Cell, 76*(2), 383-391.

Kenworthy, A. K., & Edidin, M. (1998). Distribution of a glycosylphosphatidylinositol-anchored protein at the apical surface of MDCK cells examined at a resolution of <100 A using imaging fluorescence resonance energy transfer. *J Cell Biol, 142*(1), 69-84.

Kesavan, J., Borisovska, M., & Bruns, D. (2007). v-SNARE actions during Ca(2+)-triggered exocytosis. *Cell, 131*(2), 351-363.

Kielian, M., & Rey, F. A. (2006). Virus membrane-fusion proteins: more than one way to make a hairpin. *Nat Rev Microbiol, 4*(1), 67-76.

Kiessling, V., Crane, J. M., & Tamm, L. K. (2006). Transbilayer effects of raft-like lipid domains in asymmetric planar bilayers measured by single molecule tracking. *Biophys J, 91*(9), 3313-3326.

Kiessling, V., Wan, C., & Tamm, L. K. (2009). Domain coupling in asymmetric lipid bilayers. *Biochim Biophys Acta, 1788*(1), 64-71.

Killian, J. A. (2003). Synthetic peptides as models for intrinsic membrane proteins. *FEBS Lett, 555*(1), 134-138.

Kim, T., & Im, W. (2010). Revisiting hydrophobic mismatch with free energy simulation studies of transmembrane helix tilt and rotation. *Biophys J, 99*(1), 175-183.

Kinnunen, P. K. (1992). Fusion of lipid bilayers: a model involving mechanistic connection to HII phase forming lipids. *Chem Phys Lipids, 63*(3), 251-258.

Kinnunen, P. K., & Holopainen, J. M. (2000). Mechanisms of initiation of membrane fusion: role of lipids. *Biosci Rep, 20*(6), 465-482.

Klyachko, V. A., & Jackson, M. B. (2002). Capacitance steps and fusion pores of small and large-dense-core vesicles in nerve terminals. *Nature, 418*(6893), 89-92.

Knecht, V., & Grubmuller, H. (2003). Mechanical coupling via the membrane fusion SNARE protein syntaxin 1A: a molecular dynamics study. *Biophys J, 84*(3), 1527-1547.

Knecht, V., Mark, A. E., & Marrink, S. J. (2006). Phase behavior of a phospholipid/fatty acid/water mixture studied in atomic detail. *J Am Chem Soc, 128*(6), 2030-2034.

Knecht, V., & Marrink, S. J. (2007). Molecular dynamics simulations of lipid vesicle fusion in atomic detail. *Biophys J, 92*(12), 4254-4261.

Kobe, B., Center, R. J., Kemp, B. E., & Poumbourios, P. (1999). Crystal structure of human T cell leukemia virus type 1 gp21 ectodomain crystallized as a maltose-binding protein chimera reveals structural evolution of retroviral transmembrane proteins. *Proc Natl Acad Sci U S A, 96*(8), 4319-4324.

Kordyukova, L. V., Serebryakova, M. V., Baratova, L. A., & Veit, M. (2008). S acylation of the hemagglutinin of influenza viruses: mass spectrometry reveals site-specific attachment of stearic acid to a transmembrane cysteine. *J Virol, 82*(18), 9288-9292.

Kordyukova, L. V., Serebryakova, M. V., Baratova, L. A., & Veit, M. (2010). Site-specific attachment of palmitate or stearate to cytoplasmic versus transmembrane cysteines is a common feature of viral spike proteins. *Virology, 398*(1), 49-56.

Korlach, J., Baumgart, T., Webb, W. W., & Feigenson, G. W. (2005). Detection of motional heterogeneities in lipid bilayer membranes by dual probe fluorescence correlation spectroscopy. *Biochim Biophys Acta, 1668*(2), 158-163.

Korlach, J., Schwille, P., Webb, W. W., & Feigenson, G. W. (1999). Characterization of lipid bilayer phases by confocal microscopy and fluorescence correlation spectroscopy. *Proc Natl Acad Sci U S A, 96*(15), 8461-8466.

Kozerski, C., Ponimaskin, E., Schroth-Diez, B., Schmidt, M. F., & Herrmann, A. (2000). Modification of the cytoplasmic domain of influenza virus hemagglutinin affects enlargement of the fusion pore. *J Virol, 74*(16), 7529-7537.

Kozlov, M. M., & Chernomordik, L. V. (1998). A mechanism of protein-mediated fusion: coupling between refolding of the influenza hemagglutinin and lipid rearrangements. *Biophys J, 75*(3), 1384-1396.

Kozlov, M. M., & Markin, V. S. (1983). [Possible mechanism of membrane fusion]. *Biofizika, 28*(2), 242-247.

Kozlov, M. M., & Markin, V. S. (1984). On the theory of membrane fusion. The adhesion-condensation mechanism. *Gen Physiol Biophys, 3*(5), 379-402.

Kozlov, M. M., McMahon, H. T., & Chernomordik, L. V. (2010). Protein-driven membrane stresses in fusion and fission. *Trends Biochem Sci*.

Kozlovsky, Y., Chernomordik, L. V., & Kozlov, M. M. (2002). Lipid intermediates in membrane fusion: formation, structure, and decay of hemifusion diaphragm. *Biophys J, 83*(5), 2634-2651.

Kozlovsky, Y., Efrat, A., Siegel, D. P., & Kozlov, M. M. (2004). Stalk phase formation: effects of dehydration and saddle splay modulus. *Biophys J, 87*(4), 2508-2521.

Kozlovsky, Y., & Kozlov, M. M. (2002). Stalk model of membrane fusion: solution of energy crisis. *Biophys J, 82*(2), 882-895.

Krumbiegel, M., Herrmann, A., & Blumenthal, R. (1994). Kinetics of the low pH-induced conformational changes and fusogenic activity of influenza hemagglutinin. *Biophys J, 67*(6), 2355-2360.

Kuhl, T., Guo, Y., Alderfer, J. L., Berman, A. D., Leckband, D., Israelachvili, J., et al. (1996). Direct Measurement of Polyethylene Glycol Induced Depletion Attraction between Lipid Bilayers. *Langmuir, 12*, 3003-3014.

Kundu, A., Avalos, R. T., Sanderson, C. M., & Nayak, D. P. (1996). Transmembrane domain of influenza virus neuraminidase, a type II protein, possesses an apical sorting signal in polarized MDCK cells. *J Virol, 70*(9), 6508-6515.

Kurad, D., Jeschke, G., & Marsh, D. (2004). Lateral ordering of lipid chains in cholesterol-containing membranes: high-field spin-label EPR. *Biophys J, 86*(1 Pt 1), 264-271.

Kurz, A., Bunge, A., Windeck, A. K., Rost, M., Flasche, W., Arbuzova, A., et al. (2006). Lipid-anchored oligonucleotides for stable double-helix formation in distinct membrane domains. *Angew Chem Int Ed Engl, 45*(27), 4440-4444.

Kusumi, A., Koyama-Honda, I., & Suzuki, K. (2004). Molecular dynamics and interactions for creation of stimulation-induced stabilized rafts from small unstable steady-state rafts. *Traffic, 5*(4), 213-230.

Kusumi, A., & Suzuki, K. (2005). Toward understanding the dynamics of membrane-raft-based molecular interactions. *Biochim Biophys Acta, 1746*(3), 234-251.

Kuzmin, P. I., Akimov, S. A., Chizmadzhev, Y. A., Zimmerberg, J., & Cohen, F. S. (2005). Line tension and interaction energies of membrane rafts calculated from lipid splay and tilt. *Biophys J, 88*(2), 1120-1133.

Kuzmin, P. I., Zimmerberg, J., Chizmadzhev, Y. A., & Cohen, F. S. (2001). A quantitative model for membrane fusion based on low-energy intermediates. *Proc Natl Acad Sci U S A, 98*(13), 7235-7240.

Kwon, G., Axelrod, D., & Neubig, R. R. (1994). Lateral mobility of tetramethylrhodamine (TMR) labelled G protein alpha and beta gamma subunits in NG 108-15 cells. *Cell Signal, 6*(6), 663-679.

Lague, P., Roux, B., & Pastor, R. W. (2005). Molecular dynamics simulations of the influenza hemagglutinin fusion peptide in micelles and bilayers: conformational analysis of peptide and lipids. *J Mol Biol, 354*(5), 1129-1141.

Langosch, D., Crane, J. M., Brosig, B., Hellwig, A., Tamm, L. K., & Reed, J. (2001). Peptide mimics of SNARE transmembrane segments drive membrane fusion depending on their conformational plasticity. *J Mol Biol, 311*(4), 709-721.

Larson, D. R., Gosse, J. A., Holowka, D. A., Baird, B. A., & Webb, W. W. (2005). Temporally resolved interactions between antigen-stimulated IgE receptors and Lyn kinase on living cells. *J Cell Biol, 171*(3), 527-536.

Lasserre, R., Guo, X. J., Conchonaud, F., Hamon, Y., Hawchar, O., Bernard, A. M., et al. (2008). Raft nanodomains contribute to Akt/PKB plasma membrane recruitment and activation. *Nat Chem Biol, 4*(9), 538-547.

Lee, J., & Lentz, B. R. (1997). Evolution of lipidic structures during model membrane fusion and the relation of this process to cell membrane fusion. *Biochemistry, 36*(21), 6251-6259.

Lee, J. Y., & Schick, M. (2007). Field Theoretic Study of Bilayer Membrane Fusion III: Membranes with Leaves of Different Composition. *Biophys J, 92*(11), 3938-3948.

Lee, K. K. (2010). Architecture of a nascent viral fusion pore. *Embo J, 29*(7), 1299-1311.

Lei, G., & MacDonald, R. C. (2003). Lipid bilayer vesicle fusion: intermediates captured by high-speed microfluorescence spectroscopy. *Biophys J, 85*(3), 1585-1599.

Lei, G., & MacDonald, R. C. (2008). Effects on interactions of oppositely charged phospholipid vesicles of covalent attachment of polyethylene glycol oligomers to their surfaces: adhesion, hemifusion, full fusion and "endocytosis". *J Membr Biol, 221*(2), 97-106.

Leikin, S. L., Kozlov, M. M., Chernomordik, L. V., Markin, V. S., & Chizmadzhev, Y. A. (1987). Membrane fusion: overcoming of the hydration barrier and local restructuring. *J Theor Biol, 129*(4), 411-425.

Lenne, P. F., Wawrezinieck, L., Conchonaud, F., Wurtz, O., Boned, A., Guo, X. J., et al. (2006). Dynamic molecular confinement in the plasma membrane by microdomains and the cytoskeleton meshwork. *Embo J, 25*(14), 3245-3256.

Lentz, B. R. (2007). PEG as a tool to gain insight into membrane fusion. *Eur Biophys J, 36*(4-5), 315-326.

Lentz, B. R., Malinin, V., Haque, M. E., & Evans, K. (2000). Protein machines and lipid assemblies: current views of cell membrane fusion. *Curr Opin Struct Biol, 10*(5), 607-615.

Leser, G. P., & Lamb, R. A. (2005). Influenza virus assembly and budding in raft-derived microdomains: a quantitative analysis of the surface distribution of HA, NA and M2 proteins. *Virology, 342*(2), 215-227.

Levental, I., Grzybek, M., & Simons, K. (2010). Greasing their way: lipid modifications determine protein association with membrane rafts. *Biochemistry, 49*(30), 6305-6316.

Li, D. W., & Liu, X. Y. (2005). Examination of membrane fusion by dissipative particle dynamics simulation and comparison with continuum elastic models. *J Chem Phys, 122*(17), 174909.

Li, F., Pincet, F., Perez, E., Eng, W. S., Melia, T. J., Rothman, J. E., et al. (2007). Energetics and dynamics of SNAREpin folding across lipid bilayers. *Nat Struct Mol Biol, 14*(10), 890-896.

Li, Y., Han, X., Lai, A. L., Bushweller, J. H., Cafiso, D. S., & Tamm, L. K. (2005). Membrane structures of the hemifusion-inducing fusion peptide mutant G1S and the fusion-blocking mutant G1V of influenza virus hemagglutinin suggest a mechanism for pore opening in membrane fusion. *J Virol, 79*(18), 12065-12076.

Lichtenberg, D., Goni, F. M., & Heerklotz, H. (2005). Detergent-resistant membranes should not be identified with membrane rafts. *Trends Biochem Sci, 30*(8), 430-436.

Lin, S., Naim, H. Y., Rodriguez, A. C., & Roth, M. G. (1998). Mutations in the middle of the transmembrane domain reverse the polarity of transport of the influenza virus hemagglutinin in MDCK epithelial cells. *J Cell Biol, 142*(1), 51-57.

Lindau, M., & Almers, W. (1995). Structure and function of fusion pores in exocytosis and ectoplasmic membrane fusion. *Curr Opin Cell Biol, 7*(4), 509-517.

Lingwood, D., Ries, J., Schwille, P., & Simons, K. (2008). Plasma membranes are poised for activation of raft phase coalescence at physiological temperature. *Proc Natl Acad Sci U S A*.

Lingwood, D., & Simons, K. (2010). Lipid Rafts As a Membrane-Organizing Principle. *Science, 327*(5961), 46-50.

Lipowsky, R. (1993). Domain-induced budding of fluid membranes. *Biophys J, 64*(4), 1133-1138.

Lisanti, M. P., Caras, I. W., Davitz, M. A., & Rodriguez-Boulan, E. (1989). A glycophospholipid membrane anchor acts as an apical targeting signal in polarized epithelial cells. *J Cell Biol, 109*(5), 2145-2156.

Liu, T., Wang, T., Chapman, E. R., & Weisshaar, J. C. (2008). Productive hemifusion intermediates in fast vesicle fusion driven by neuronal SNAREs. *Biophys J, 94*(4), 1303-1314.

London, E., & Brown, D. A. (2000). Insolubility of lipids in triton X-100: physical origin and relationship to sphingolipid/cholesterol membrane domains (rafts). *Biochim Biophys Acta, 1508*(1-2), 182-195.

Lu, X., Zhang, F., McNew, J. A., & Shin, Y. K. (2005). Membrane fusion induced by neuronal SNAREs transits through hemifusion. *J Biol Chem, 280*(34), 30538-30541.

Luan, P., Yang, L., & Glaser, M. (1995). Formation of membrane domains created during the budding of vesicular stomatitis virus. A model for selective lipid and protein sorting in biological membranes. *Biochemistry, 34*(31), 9874-9883.

Ludolph, B., Eisele, F., & Waldmann, H. (2002). Solid-phase synthesis of lipidated peptides. *J Am Chem Soc, 124*(21), 5954-5955.

Lundbaek, J. A., Andersen, O. S., Werge, T., & Nielsen, C. (2003). Cholesterol-induced protein sorting: an analysis of energetic feasibility. *Biophys J, 84*(3), 2080-2089.

Macosko, J. C., Kim, C. H., & Shin, Y. K. (1997). The membrane topology of the fusion peptide region of influenza hemagglutinin determined by spin-labeling EPR. *J Mol Biol, 267*(5), 1139-1148.

Malashkevich, V. N., Chan, D. C., Chutkowski, C. T., & Kim, P. S. (1998). Crystal structure of the simian immunodeficiency virus (SIV) gp41 core: conserved helical interactions underlie the broad inhibitory activity of gp41 peptides. *Proc Natl Acad Sci U S A, 95*(16), 9134-9139.

Malashkevich, V. N., Schneider, B. J., McNally, M. L., Milhollen, M. A., Pang, J. X., & Kim, P. S. (1999). Core structure of the envelope glycoprotein GP2 from Ebola virus at 1.9-A resolution. *Proc Natl Acad Sci U S A, 96*(6), 2662-2667.

Mansy, S. S., Schrum, J. P., Krishnamurthy, M., Tobe, S., Treco, D. A., & Szostak, J. W. (2008). Template-directed synthesis of a genetic polymer in a model protocell. *Nature, 454*(7200), 122-125.

Margineanu, A., Hotta, J., Van der Auweraer, M., Ameloot, M., Stefan, A., Beljonne, D., et al. (2007). Visualization of membrane rafts using a perylene monoimide derivative and fluorescence lifetime imaging. *Biophys J, 93*(8), 2877-2891.

Markosyan, R. M., Cohen, F. S., & Melikyan, G. B. (2000). The lipid-anchored ectodomain of influenza virus hemagglutinin (GPI-HA) is capable of inducing nonenlarging fusion pores. *Mol Biol Cell, 11*(4), 1143-1152.

Markvoort, A. J., Pfleger, N., Staffhorst, R., Hilbers, P. A., van Santen, R. A., Killian, J. A., et al. (2010). Self-reproduction of Fatty Acid vesicles: a combined experimental and simulation study. *Biophys J, 99*(5), 1520-1528.

Marrink, S. J., & Mark, A. E. (2003). The mechanism of vesicle fusion as revealed by molecular dynamics simulations. *J Am Chem Soc, 125*(37), 11144-11145.

Marrink, S. J., & Tieleman, D. P. (2002). Molecular dynamics simulation of spontaneous membrane fusion during a cubic-hexagonal phase transition. *Biophys J, 83*(5), 2386-2392.

Marsh, M., & Helenius, A. (2006). Virus entry: open sesame. *Cell, 124*(4), 729-740.

Mathivet, L., Cribier, S., & Devaux, P. F. (1996). Shape change and physical properties of giant phospholipid vesicles prepared in the presence of an AC electric field. *Biophys J, 70*(3), 1112-1121.

Mattai, J., Hauser, H., Demel, R. A., & Shipley, G. G. (1989). Interactions of metal ions with phosphatidylserine bilayer membranes: effect of hydrocarbon chain unsaturation. *Biochemistry, 28*(5), 2322-2330.

May, S. (2002). Structure and energy of fusion stalks: the role of membrane edges. *Biophys J, 83*(6), 2969-2980.

Mayor, S., & Riezman, H. (2004). Sorting GPI-anchored proteins. *Nat Rev Mol Cell Biol, 5*(2), 110-120.

Mays, R. W., Siemers, K. A., Fritz, B. A., Lowe, A. W., van Meer, G., & Nelson, W. J. (1995). Hierarchy of mechanisms involved in generating Na/K-ATPase polarity in MDCK epithelial cells. *J Cell Biol, 130*(5), 1105-1115.

McConnell, H. M., & Radhakrishnan, A. (2003). Condensed complexes of cholesterol and phospholipids. *Biochim Biophys Acta, 1610*(2), 159-173.

McConnell, H. M., & Vrljic, M. (2003). Liquid-liquid immiscibility in membranes. *Annu Rev Biophys Biomol Struct, 32*, 469-492.

McIntosh, T. J., Simon, S. A., Needham, D., & Huang, C. H. (1992). Structure and cohesive properties of sphingomyelin/cholesterol bilayers. *Biochemistry, 31*(7), 2012-2020.

McIntosh, T. J., Vidal, A., & Simon, S. A. (2003). Sorting of lipids and transmembrane peptides between detergent-soluble bilayers and detergent-resistant rafts. *Biophys J, 85*(3), 1656-1666.

McNew, J. A., Weber, T., Engelman, D. M., Sollner, T. H., & Rothman, J. E. (1999). The length of the flexible SNAREpin juxtamembrane region is a critical determinant of SNARE-dependent fusion. *Mol Cell, 4*(3), 415-421.

McNew, J. A., Weber, T., Parlati, F., Johnston, R. J., Melia, T. J., Sollner, T. H., et al. (2000). Close is not enough: SNARE-dependent membrane fusion requires an active mechanism that transduces force to membrane anchors. *J Cell Biol, 150*(1), 105-117.

Melikyan, G. B., Barnard, R. J., Abrahamyan, L. G., Mothes, W., & Young, J. A. (2005). Imaging individual retroviral fusion events: from hemifusion to pore formation and growth. *Proc Natl Acad Sci U S A, 102*(24), 8728-8733.

Melikyan, G. B., Brener, S. A., Ok, D. C., & Cohen, F. S. (1997). Inner but not outer membrane leaflets control the transition from glycosylphosphatidylinositol-anchored influenza hemagglutinin-induced hemifusion to full fusion. *J Cell Biol, 136*(5), 995-1005.

Melikyan, G. B., Lin, S., Roth, M. G., & Cohen, F. S. (1999). Amino acid sequence requirements of the transmembrane and cytoplasmic domains of influenza virus hemagglutinin for viable membrane fusion. *Mol Biol Cell, 10*(6), 1821-1836.

Melikyan, G. B., Markosyan, R. M., Hemmati, H., Delmedico, M. K., Lambert, D. M., & Cohen, F. S. (2000). Evidence that the transition of HIV-1 gp41 into a six-helix bundle, not the bundle configuration, induces membrane fusion. *J Cell Biol, 151*(2), 413-423.

Melikyan, G. B., Niles, W. D., & Cohen, F. S. (1993). Influenza virus hemagglutinin-induced cell-planar bilayer fusion: quantitative dissection of fusion pore kinetics into stages. *J Gen Physiol, 102*(6), 1151-1170.

Melikyan, G. B., White, J. M., & Cohen, F. S. (1995). GPI-anchored influenza hemagglutinin induces hemifusion to both red blood cell and planar bilayer membranes. *J Cell Biol, 131*(3), 679-691.

Meyer, B. H., Segura, J. M., Martinez, K. L., Hovius, R., George, N., Johnsson, K., et al. (2006). FRET imaging reveals that functional neurokinin-1 receptors are monomeric and reside in membrane microdomains of live cells. *Proc Natl Acad Sci U S A, 103*(7), 2138-2143.

Mima, J., Hickey, C. M., Xu, H., Jun, Y., & Wickner, W. (2008). Reconstituted membrane fusion requires regulatory lipids, SNAREs and synergistic SNARE chaperones. *Embo J, 27*(15), 2031-2042.

Mitra, K., Ubarretxena-Belandia, I., Taguchi, T., Warren, G., & Engelman, D. M. (2004). Modulation of the bilayer thickness of exocytic pathway membranes by membrane proteins rather than cholesterol. *Proc Natl Acad Sci U S A, 101*(12), 4083-4088.

Mohler, W. A., Shemer, G., del Campo, J. J., Valansi, C., Opoku-Serebuoh, E., Scranton, V., et al. (2002). The type I membrane protein EFF-1 is essential for developmental cell fusion. *Dev Cell, 2*(3), 355-362.

Moscho, A., Orwar, O., Chiu, D. T., Modi, B. P., & Zare, R. N. (1996). Rapid preparation of giant unilamellar vesicles. *Proc Natl Acad Sci U S A, 93*(21), 11443-11447.

Mouritsen, O. G., & Bloom, M. (1984). Mattress model of lipid-protein interactions in membranes. *Biophys J, 46*(2), 141-153.

Mouritsen, O. G., & Zuckermann, M. J. (2004). What's so special about cholesterol? *Lipids, 39*(11), 1101-1113.

Muller, P., Nikolaus, J., Schiller, S., Herrmann, A., Mollnitz, K., Czapla, S., et al. (2009). Molecular rods with oligospiroketal backbones as anchors in biological membranes. *Angew Chem Int Ed Engl, 48*(24), 4433-4435.

Munro, S. (2003). Lipid rafts: elusive or illusive? *Cell, 115*(4), 377-388.

Neher, E., & Marty, A. (1982). Discrete changes of cell membrane capacitance observed under conditions of enhanced secretion in bovine adrenal chromaffin cells. *Proc Natl Acad Sci U S A, 79*(21), 6712-6716.

Neil, S. J., Zang, T., & Bieniasz, P. D. (2008). Tetherin inhibits retrovirus release and is antagonized by HIV-1 Vpu. *Nature, 451*(7177), 425-430.

Nezil, F. A., & Bloom, M. (1992). Combined influence of cholesterol and synthetic amphiphillic peptides upon bilayer thickness in model membranes. *Biophys J, 61*(5), 1176-1183.

Nikolaus, J., Scolari, S., Bayraktarov, E., Jungnick, N., Engel, S., Plazzo, A. P., et al. (2010a). Hemagglutinin of influenza virus partitions into the nonraft domain of model membranes. *Biophys J, 99*(2), 489-498.

Nikolaus, J., Stockl, M., Langosch, D., Volkmer, R., & Herrmann, A. (2010b). Direct visualization of large and protein-free hemifusion diaphragms. *Biophys J, 98*(7), 1192-1199.

Noguchi, H., & Takasu, M. (2001). Self-assembly of amphiphiles into vesicles: a Brownian dynamics simulation. *Phys Rev E Stat Nonlin Soft Matter Phys, 64*(4 Pt 1), 041913.

Nussler, F., Clague, M. J., & Herrmann, A. (1997). Meta-stability of the hemifusion intermediate induced by glycosylphosphatidylinositol-anchored influenza hemagglutinin. *Biophys J, 73*(5), 2280-2291.

Ohki, S. (1982). A mechanism of divalent ion-induced phosphatidylserine membrane fusion. *Biochim Biophys Acta, 689*(1), 1-11.

Ohta-Iino, S., Pasenkiewicz-Gierula, M., Takaoka, Y., Miyagawa, H., Kitamura, K., & Kusumi, A. (2001). Fast lipid disorientation at the onset of membrane fusion revealed by molecular dynamics simulations. *Biophys J, 81*(1), 217-224.

Ollesch, J., Poschner, B. C., Nikolaus, J., Hofmann, M. W., Herrmann, A., Gerwert, K., et al. (2007). Secondary structure and distribution of fusogenic LV-peptides in lipid membranes. *Eur Biophys J*.

Oren-Suissa, M., & Podbilewicz, B. (2007). Cell fusion during development. *Trends Cell Biol, 17*(11), 537-546.

Owen, D. M., Lanigan, P. M., Dunsby, C., Munro, I., Grant, D., Neil, M. A., et al. (2006). Fluorescence lifetime imaging provides enhanced contrast when imaging the phase-sensitive dye di-4-ANEPPDHQ in model membranes and live cells. *Biophys J, 90*(11), L80-82.

Pantazatos, D. P., & MacDonald, R. C. (1999). Directly observed membrane fusion between oppositely charged phospholipid bilayers. *J Membr Biol, 170*(1), 27-38.

Papadopulos, A., Vehring, S., Lopez-Montero, I., Kutschenko, L., Stockl, M., Devaux, P. F., et al. (2007). Flippase activity detected with unlabeled lipids by shape changes of giant unilamellar vesicles. *J Biol Chem, 282*(21), 15559-15568.

Papahadjopoulos, D., Nir, S., & Duzgunes, N. (1990). Molecular mechanisms of calcium-induced membrane fusion. *J Bioenerg Biomembr, 22*(2), 157-179.

Papahadjopoulos, D., Vail, W. J., Newton, C., Nir, S., Jacobson, K., Poste, G., et al. (1977). Studies on membrane fusion. III. The role of calcium-induced phase changes. *Biochim Biophys Acta, 465*(3), 579-598.

Park, H. E., Gruenke, J. A., & White, J. M. (2003). Leash in the groove mechanism of membrane fusion. *Nat Struct Biol, 10*(12), 1048-1053.

Park, S. H., & Opella, S. J. (2005). Tilt angle of a trans-membrane helix is determined by hydrophobic mismatch. *J Mol Biol, 350*(2), 310-318.

Petit, V. A., & Edidin, M. (1974). Lateral phase separation of lipids in plasma membranes: effect of temperature on the mobility of membrane antigens. *Science, 184*(142), 1183-1185.

Pike, L. J. (2006). Rafts defined: a report on the Keystone Symposium on Lipid Rafts and Cell Function. *J Lipid Res, 47*(7), 1597-1598.

Plowman, S. J., Ariotti, N., Goodall, A., Parton, R. G., & Hancock, J. F. (2008). Electrostatic interactions positively regulate K-Ras nanocluster formation and function. *Mol Cell Biol, 28*(13), 4377-4385.

Plowman, S. J., Muncke, C., Parton, R. G., & Hancock, J. F. (2005). H-ras, K-ras, and inner plasma membrane raft proteins operate in nanoclusters with differential dependence on the actin cytoskeleton. *Proc Natl Acad Sci U S A, 102*(43), 15500-15505.

Podbilewicz, B., Leikina, E., Sapir, A., Valansi, C., Suissa, M., Shemer, G., et al. (2006). The C. elegans developmental fusogen EFF-1 mediates homotypic fusion in heterologous cells and in vivo. *Dev Cell, 11*(4), 471-481.

Polozov, I. V., Bezrukov, L., Gawrisch, K., & Zimmerberg, J. (2008). Progressive ordering with decreasing temperature of the phospholipids of influenza virus. *Nat Chem Biol, 4*(4), 248-255.

Pomorski, T., Hrafnsdottir, S., Devaux, P. F., & van Meer, G. (2001). Lipid distribution and transport across cellular membranes. *Semin Cell Dev Biol, 12*(2), 139-148.

Poveda, J. A., Fernandez, A. M., Encinar, J. A., & Gonzalez-Ros, J. M. (2008). Protein-promoted membrane domains. *Biochim Biophys Acta, 1778*(7-8), 1583-1590.

Pralle, A., Keller, P., Florin, E. L., Simons, K., & Horber, J. K. (2000). Sphingolipid-cholesterol rafts diffuse as small entities in the plasma membrane of mammalian cells. *J Cell Biol, 148*(5), 997-1008.

Prior, I. A., Harding, A., Yan, J., Sluimer, J., Parton, R. G., & Hancock, J. F. (2001). GTP-dependent segregation of H-ras from lipid rafts is required for biological activity. *Nat Cell Biol, 3*(4), 368-375.

Prior, I. A., Muncke, C., Parton, R. G., & Hancock, J. F. (2003). Direct visualization of Ras proteins in spatially distinct cell surface microdomains. *J Cell Biol, 160*(2), 165-170.

Qiao, H., Armstrong, R. T., Melikyan, G. B., Cohen, F. S., & White, J. M. (1999). A specific point mutant at position 1 of the influenza hemagglutinin fusion peptide displays a hemifusion phenotype. *Mol Biol Cell, 10*(8), 2759-2769.

Quint, S., Widmaier, S., Minde, D., Hornburg, D., Langosch, D., & Scharnagl, C. (2010). Residue-specific side-chain packing determines the backbone dynamics of transmembrane model helices. *Biophys J, 99*(8), 2541-2549.

Radler, J. O., Feder, T. J., Strey, H. H., & Sackmann, E. (1995). Fluctuation analysis of tension-controlled undulation forces between giant vesicles and solid substrates. *Phys Rev E Stat Phys Plasmas Fluids Relat Interdiscip Topics, 51*(5), 4526-4536.

Rajendran, L., & Simons, K. (2005). Lipid rafts and membrane dynamics. *J Cell Sci, 118*(Pt 6), 1099-1102.

Rand, R. P., & Parsegian, V. A. (1984). Physical force considerations in model and biological membranes. *Can J Biochem Cell Biol, 62*(8), 752-759.

Rand, R. P., & Parsegian, V. A. (1989). Hydration forces between phospholipid bilayers. *Biochim Biophys Acta, 988*(3), 351-376.

Razinkov, V. I., Melikyan, G. B., Epand, R. M., Epand, R. F., & Cohen, F. S. (1998). Effects of spontaneous bilayer curvature on influenza virus-mediated fusion pores. *J Gen Physiol, 112*(4), 409-422.

Reese, C., Heise, F., & Mayer, A. (2005). Trans-SNARE pairing can precede a hemifusion intermediate in intracellular membrane fusion. *Nature, 436*(7049), 410-414.

Rizo, J. (2006). Illuminating membrane fusion. *Proc Natl Acad Sci U S A, 103*(52), 19611-19612.

Rizo, J., & Dai, H. (2007). How much can SNAREs flex their muscles? *Nat Struct Mol Biol, 14*(10), 880-882.

Rizzo, M. A., Springer, G. H., Granada, B., & Piston, D. W. (2004). An improved cyan fluorescent protein variant useful for FRET. *Nat Biotechnol, 22*(4), 445-449.

Robson Marsden, H., Elbers, N. A., Bomans, P. H., Sommerdijk, N. A., & Kros, A. (2009). A reduced SNARE model for membrane fusion. *Angew Chem Int Ed Engl, 48*(13), 2330-2333.

Roche, S., Bressanelli, S., Rey, F. A., & Gaudin, Y. (2006). Crystal structure of the low-pH form of the vesicular stomatitis virus glycoprotein G. *Science, 313*(5784), 187-191.

Rodriguez, N., Pincet, F., & Cribier, S. (2005). Giant vesicles formed by gentle hydration and electroformation: a comparison by fluorescence microscopy. *Colloids Surf B Biointerfaces, 42*(2), 125-130.

Rogasevskaia, T., & Coorssen, J. R. (2006). Sphingomyelin-enriched microdomains define the efficiency of native Ca(2+)-triggered membrane fusion. *J Cell Sci, 119*(Pt 13), 2688-2694.

Romer, W., Berland, L., Chambon, V., Gaus, K., Windschiegl, B., Tenza, D., et al. (2007). Shiga toxin induces tubular membrane invaginations for its uptake into cells. *Nature, 450*(7170), 670-675.

Rothman, J. E., & Lenard, J. (1977). Membrane asymmetry. *Science, 195*(4280), 743-753.

Ruigrok, R. W., Andree, P. J., Hooft van Huysduynen, R. A., & Mellema, J. E. (1984). Characterization of three highly purified influenza virus strains by electron microscopy. *J Gen Virol, 65 (Pt 4)*, 799-802.

Russell, C. J., Jardetzky, T. S., & Lamb, R. A. (2001). Membrane fusion machines of paramyxoviruses: capture of intermediates of fusion. *Embo J, 20*(15), 4024-4034.

Salaun, C., James, D. J., & Chamberlain, L. H. (2004). Lipid rafts and the regulation of exocytosis. *Traffic, 5*(4), 255-264.

Salzwedel, K., Johnston, P. B., Roberts, S. J., Dubay, J. W., & Hunter, E. (1993). Expression and characterization of glycophospholipid-anchored human immunodeficiency virus type 1 envelope glycoproteins. *J Virol, 67*(9), 5279-5288.

Sapir, A., Avinoam, O., Podbilewicz, B., & Chernomordik, L. V. (2008). Viral and developmental cell fusion mechanisms: conservation and divergence. *Dev Cell, 14*(1), 11-21.

Sapir, A., Choi, J., Leikina, E., Avinoam, O., Valansi, C., Chernomordik, L. V., et al. (2007). AFF-1, a FOS-1-regulated fusogen, mediates fusion of the anchor cell in C. elegans. *Dev Cell, 12*(5), 683-698.

Scheiffele, P., Rietveld, A., Wilk, T., & Simons, K. (1999). Influenza viruses select ordered lipid domains during budding from the plasma membrane. *J Biol Chem, 274*(4), 2038-2044.

Scheiffele, P., Roth, M. G., & Simons, K. (1997). Interaction of influenza virus haemagglutinin with sphingolipid-cholesterol membrane domains via its transmembrane domain. *Embo J, 16*(18), 5501-5508.

Schroeder, C., Heider, H., Moncke-Buchner, E., & Lin, T. I. (2005). The influenza virus ion channel and maturation cofactor M2 is a cholesterol-binding protein. *Eur Biophys J, 34*(1), 52-66.

Schroeder, R., London, E., & Brown, D. (1994). Interactions between saturated acyl chains confer detergent resistance on lipids and glycosylphosphatidylinositol (GPI)-anchored proteins: GPI-anchored proteins in liposomes and cells show similar behavior. *Proc Natl Acad Sci U S A, 91*(25), 12130-12134.

Schroth-Diez, B., Ludwig, K., Baljinnyam, B., Kozerski, C., Huang, Q., & Herrmann, A. (2000). The role of the transmembrane and of the intraviral domain of glycoproteins in membrane fusion of enveloped viruses. *Biosci Rep, 20*(6), 571-595.

Schroth-Diez, B., Ponimaskin, E., Reverey, H., Schmidt, M. F., & Herrmann, A. (1998). Fusion activity of transmembrane and cytoplasmic domain chimeras of the influenza virus glycoprotein hemagglutinin. *J Virol, 72*(1), 133-141.

Schuck, S., & Simons, K. (2004). Polarized sorting in epithelial cells: raft clustering and the biogenesis of the apical membrane. *J Cell Sci, 117*(Pt 25), 5955-5964.

Scolari, S., Engel, S., Krebs, N., Plazzo, A. P., De Almeida, R. F., Prieto, M., et al. (2009). Lateral distribution of the transmembrane domain of influenza virus hemagglutinin revealed by time-resolved fluorescence imaging. *J Biol Chem, 284*(23), 15708-15716.

Scott, R. E. (1976). Plasma membrane vesiculation: a new technique for isolation of plasma membranes. *Science, 194*(4266), 743-745.

Scott, R. E., & Maercklein, P. B. (1979). Plasma membrane vesiculation in 3T3 and SV3T3 cells. II. Factors affecting the process of vesiculation. *J Cell Sci, 35*, 245-252.

Sengupta, P., Hammond, A., Holowka, D., & Baird, B. (2008). Structural determinants for partitioning of lipids and proteins between coexisting fluid phases in giant plasma membrane vesicles. *Biochim Biophys Acta*(1778), 20-32.

Sengupta, P., Holowka, D., & Baird, B. (2007). Fluorescence Resonance Energy Transfer between Lipid Probes Detects Nanoscopic Heterogeneity in the Plasma Membrane of Live Cells. *Biophys J, 92*(10), 3564-3574.

Shahinian, S., & Silvius, J. R. (1995). Doubly-lipid-modified protein sequence motifs exhibit long-lived anchorage to lipid bilayer membranes. *Biochemistry, 34*(11), 3813-3822.

Sharma, P., Varma, R., Sarasij, R. C., Ira, Gousset, K., Krishnamoorthy, G., et al. (2004). Nanoscale organization of multiple GPI-anchored proteins in living cell membranes. *Cell, 116*(4), 577-589.

Shaw, J. E., Epand, R. F., Epand, R. M., Li, Z., Bittman, R., & Yip, C. M. (2006). Correlated fluorescence-atomic force microscopy of membrane domains: structure of fluorescence probes determines lipid localization. *Biophys J, 90*(6), 2170-2178.

Shemer, G., & Podbilewicz, B. (2003). The story of cell fusion: big lessons from little worms. *Bioessays, 25*(7), 672-682.

Shillcock, J. C., & Lipowsky, R. (2005). Tension-induced fusion of bilayer membranes and vesicles. *Nat Mater, 4*(3), 225-228.

Shogomori, H., Hammond, A. T., Ostermeyer-Fay, A. G., Barr, D. J., Feigenson, G. W., London, E., et al. (2005). Palmitoylation and intracellular domain interactions both contribute to raft targeting of linker for activation of T cells. *J Biol Chem, 280*(19), 18931-18942.

Siddiqui, T. J., Vites, O., Stein, A., Heintzmann, R., Jahn, R., & Fasshauer, D. (2007). Determinants of synaptobrevin regulation in membranes. *Mol Biol Cell, 18*(6), 2037-2046.

Siegel, D. P., Banschbach, J., Alford, D., Ellens, H., Lis, L. J., Quinn, P. J., et al. (1989). Physiological levels of diacylglycerols in phospholipid membranes induce membrane fusion and stabilize inverted phases. *Biochemistry, 28*(9), 3703-3709.

Siegel, D. P., Cherezov, V., Greathouse, D. V., Koeppe, R. E., 2nd, Killian, J. A., & Caffrey, M. (2006). Transmembrane peptides stabilize inverted cubic phases in a biphasic length-dependent manner: implications for protein-induced membrane fusion. *Biophys J, 90*(1), 200-211.

Silvius, J. R. (2003). Fluorescence energy transfer reveals microdomain formation at physiological temperatures in lipid mixtures modeling the outer leaflet of the plasma membrane. *Biophys J, 85*(2), 1034-1045.

Silvius, J. R., & Nabi, I. R. (2006). Fluorescence-quenching and resonance energy transfer studies of lipid microdomains in model and biological membranes. *Mol Membr Biol, 23*(1), 5-16.

Simons, K., & Ikonen, E. (1997). Functional rafts in cell membranes. *Nature, 387*(6633), 569-572.

Simons, K., & van Meer, G. (1988). Lipid sorting in epithelial cells. *Biochemistry, 27*(17), 6197-6202.

Simons, K., & Vaz, W. L. (2004). Model systems, lipid rafts, and cell membranes. *Annu Rev Biophys Biomol Struct, 33*, 269-295.

Singer, S. J., & Nicolson, G. L. (1972). The fluid mosaic model of the structure of cell membranes. *Science, 175*(23), 720-731.

Sinn, C. G., Antonietti, M., & Dimova, R. (2006). Binding of calcium to phosphatidylcholine-phosphatidylserine membranes. *Colloids and Surfaces A, 282-283*, 410-419.

Skehel, J. J., & Wiley, D. C. (1998). Coiled coils in both intracellular vesicle and viral membrane fusion. *Cell, 95*(7), 871-874.

Skehel, J. J., & Wiley, D. C. (2000). Receptor binding and membrane fusion in virus entry: the influenza hemagglutinin. *Annu Rev Biochem, 69*, 531-569.

Smeijers, A. F., Markvoort, A. J., Pieterse, K., & Hilbers, P. A. (2006). A detailed look at vesicle fusion. *J Phys Chem B, 110*(26), 13212-13219.

Smotrys, J. E., & Linder, M. E. (2004). Palmitoylation of intracellular signaling proteins: regulation and function. *Annu Rev Biochem, 73*, 559-587.

Sohn, H. W., Tolar, P., & Pierce, S. K. (2008). Membrane heterogeneities in the formation of B cell receptor-Lyn kinase microclusters and the immune synapse. *J Cell Biol, 182*(2), 367-379.

Stegmann, T., Hoekstra, D., Scherphof, G., & Wilschut, J. (1985). Kinetics of pH-dependent fusion between influenza virus and liposomes. *Biochemistry, 24*(13), 3107-3113.

Stevens, M. J., Hoh, J. H., & Woolf, T. B. (2003). Insights into the molecular mechanism of membrane fusion from simulation: evidence for the association of splayed tails. *Phys Rev Lett, 91*(18), 188102.

Stockl, M., & Herrmann, A. (2010). Detection of lipid domains in model and cell membranes by fluorescence lifetime imaging microscopy. *Biochim Biophys Acta, 1798*(7), 1444-1456.

Stockl, M., Plazzo, A. P., Korte, T., & Herrmann, A. (2008). Detection of lipid domains in model and cell membranes by fluorescence lifetime imaging microscopy of fluorescent lipid analogues. *J Biol Chem, 283*(45), 30828-30837.

Struck, D. K., Hoekstra, D., & Pagano, R. E. (1981). Use of resonance energy transfer to monitor membrane fusion. *Biochemistry, 20*(14), 4093-4099.

Sudhof, T. C., & Rothman, J. E. (2009). Membrane fusion: grappling with SNARE and SM proteins. *Science, 323*(5913), 474-477.

Sutton, R. B., Fasshauer, D., Jahn, R., & Brunger, A. T. (1998). Crystal structure of a SNARE complex involved in synaptic exocytosis at 2.4 A resolution. *Nature, 395*(6700), 347-353.

Suzuki, K. G., Fujiwara, T. K., Sanematsu, F., Iino, R., Edidin, M., & Kusumi, A. (2007). GPI-anchored receptor clusters transiently recruit Lyn and G alpha for temporary cluster immobilization and Lyn activation: single-molecule tracking study 1. *J Cell Biol, 177*(4), 717-730.

Svetina, S., Zeks, B., Waugh, R. E., & Raphael, R. M. (1998). Theoretical analysis of the effect of the transbilayer movement of phospholipid molecules on the dynamic behavior of a microtube pulled out of an aspirated vesicle. *Eur Biophys J, 27*(3), 197-209.

Takamori, S., Holt, M., Stenius, K., Lemke, E. A., Gronborg, M., Riedel, D., et al. (2006). Molecular anatomy of a trafficking organelle. *Cell, 127*(4), 831-846.

Takeda, M., Leser, G. P., Russell, C. J., & Lamb, R. A. (2003). Influenza virus hemagglutinin concentrates in lipid raft microdomains for efficient viral fusion. *Proc Natl Acad Sci U S A, 100*(25), 14610-14617.

Tamm, L. K. (2003). Hypothesis: spring-loaded boomerang mechanism of influenza hemagglutinin-mediated membrane fusion. *Biochim Biophys Acta, 1614*(1), 14-23.

Tan, K., Liu, J., Wang, J., Shen, S., & Lu, M. (1997). Atomic structure of a thermostable subdomain of HIV-1 gp41. *Proc Natl Acad Sci U S A, 94*(23), 12303-12308.

Tanford, C. (1980). *The Hydrophobic Effect. Formation of micelles and biological membranes.* New York: Wiley.

Tatulian, S. A., & Tamm, L. K. (2000). Secondary structure, orientation, oligomerization, and lipid interactions of the transmembrane domain of influenza hemagglutinin. *Biochemistry, 39*(3), 496-507.

Thomas, A., & Brasseur, R. (2006). Tilted peptides: the history. *Curr Protein Pept Sci, 7*(6), 523-527.

Tillack, T. W., Allietta, M., Moran, R. E., & Young, W. W., Jr. (1983). Localization of globoside and Forssman glycolipids on erythrocyte membranes. *Biochim Biophys Acta, 733*(1), 15-24.

Tong, S., & Compans, R. W. (2000). Oligomerization, secretion, and biological function of an anchor-free parainfluenza virus type 2 (PI2) fusion protein. *Virology, 270*(2), 368-376.

Trabelsi, S., Zhang, S., Lee, T. R., & Schwartz, D. K. (2008). Linactants: surfactant analogues in two dimensions. *Phys Rev Lett, 100*(3), 037802.

Tse, F. W., Iwata, A., & Almers, W. (1993). Membrane flux through the pore formed by a fusogenic viral envelope protein during cell fusion. *J Cell Biol, 121*(3), 543-552.

Turner, M. S., Sens, P., & Socci, N. D. (2005). Nonequilibrium raftlike membrane domains under continuous recycling. *Phys Rev Lett, 95*(16), 168301.

Uhrikova, D., Kucerka, N., Teixeira, J., Gordeliy, V., & Balgavy, P. (2008). Structural changes in dipalmitoylphosphatidylcholine bilayer promoted by Ca2+ ions: a small-angle neutron scattering study. *Chem Phys Lipids, 155*(2), 80-89.

Ungermann, C., & Langosch, D. (2005). Functions of SNAREs in intracellular membrane fusion and lipid bilayer mixing. *J Cell Sci, 118*(Pt 17), 3819-3828.

Vaidya, N. K., Huang, H., & Takagi, S. (2010). Coarse Grained Molecular Dynamics Simulation of Interaction between Hemagglutinin Fusion Peptides and Lipid Bilayer Membranes. *Adv. Appl. Math. Mech., 2*(4), 430-450.

van Duyl, B. Y., Rijkers, D. T., de Kruijff, B., & Killian, J. A. (2002). Influence of hydrophobic mismatch and palmitoylation on the association of transmembrane alpha-helical peptides with detergent-resistant membranes. *FEBS Lett, 523*(1-3), 79-84.

van Meer, G., Stelzer, E. H., Wijnaendts-van-Resandt, R. W., & Simons, K. (1987). Sorting of sphingolipids in epithelial (Madin-Darby canine kidney) cells. *J Cell Biol, 105*(4), 1623-1635.

Varma, R., & Mayor, S. (1998). GPI-anchored proteins are organized in submicron domains at the cell surface. *Nature, 394*(6695), 798-801.

Veatch, S. L., & Keller, S. L. (2002). Organization in lipid membranes containing cholesterol. *Phys Rev Lett, 89*(26), 268101.

Veatch, S. L., & Keller, S. L. (2003). Separation of liquid phases in giant vesicles of ternary mixtures of phospholipids and cholesterol. *Biophys J, 85*(5), 3074-3083.

Veatch, S. L., & Keller, S. L. (2005). Seeing spots: complex phase behavior in simple membranes. *Biochim Biophys Acta, 1746*(3), 172-185.

Veit, M., Kretzschmar, E., Kuroda, K., Garten, W., Schmidt, M. F., Klenk, H. D., et al. (1991). Site-specific mutagenesis identifies three cysteine residues in the cytoplasmic tail as acylation sites of influenza virus hemagglutinin. *J Virol, 65*(5), 2491-2500.

Vicogne, J., Vollenweider, D., Smith, J. R., Huang, P., Frohman, M. A., & Pessin, J. E. (2006). Asymmetric phospholipid distribution drives in vitro reconstituted SNARE-dependent membrane fusion. *Proc Natl Acad Sci U S A, 103*(40), 14761-14766.

Vidal, A., & McIntosh, T. J. (2005). Transbilayer peptide sorting between raft and nonraft bilayers: comparisons of detergent extraction and confocal microscopy. *Biophys J, 89*(2), 1102-1108.

Vogel, A., Reuther, G., Weise, K., Triola, G., Nikolaus, J., Tan, K. T., et al. (2009). The lipid modifications of Ras that sense membrane environments and induce local enrichment. *Angew Chem Int Ed Engl, 48*(46), 8784-8787.

Walde, P., Cosentino, K., Engel, H., & Stano, P. (2010). Giant vesicles: preparations and applications. *Chembiochem, 11*(7), 848-865.

Wang, C. T., Lu, J. C., Bai, J., Chang, P. Y., Martin, T. F., Chapman, E. R., et al. (2003). Different domains of synaptotagmin control the choice between kiss-and-run and full fusion. *Nature, 424*(6951), 943-947.

Wang, T., Smith, E. A., Chapman, E. R., & Weisshaar, J. C. (2009). Lipid mixing and content release in single-vesicle, SNARE-driven fusion assay with 1-5 ms resolution. *Biophys J, 96*(10), 4122-4131.

Wang, T. Y., Leventis, R., & Silvius, J. R. (2000). Fluorescence-based evaluation of the partitioning of lipids and lipidated peptides into liquid-ordered lipid microdomains: a model for molecular partitioning into "lipid rafts". *Biophys J, 79*(2), 919-933.

Wang, Y., Dulubova, I., Rizo, J., & Sudhof, T. C. (2001). Functional analysis of conserved structural elements in yeast syntaxin Vam3p. *J Biol Chem, 276*(30), 28598-28605.

Wawrezinieck, L., Rigneault, H., Marguet, D., & Lenne, P. F. (2005). Fluorescence correlation spectroscopy diffusion laws to probe the submicron cell membrane organization. *Biophys J, 89*(6), 4029-4042.

Webb, R. J., East, J. M., Sharma, R. P., & Lee, A. G. (1998). Hydrophobic mismatch and the incorporation of peptides into lipid bilayers: a possible mechanism for retention in the Golgi. *Biochemistry, 37*(2), 673-679.

Weber, M. E., Schlesinger, P. H., & Gokel, G. W. (2005). Dynamic assessment of bilayer thickness by varying phospholipid and hydraphile synthetic channel chain lengths. *J Am Chem Soc, 127*(2), 636-642.

Weis, W., Brown, J. H., Cusack, S., Paulson, J. C., Skehel, J. J., & Wiley, D. C. (1988). Structure of the influenza virus haemagglutinin complexed with its receptor, sialic acid. *Nature, 333*(6172), 426-431.

Weise, K., Kapoor, S., Denter, C., Nikolaus, J., Opitz, N., Koch, S., et al. (2010). Membrane-mediated Induction and Sorting of K-Ras Microdomain Signaling Platforms. *J Am Chem Soc*.

Weise, K., Triola, G., Brunsveld, L., Waldmann, H., & Winter, R. (2009a). Influence of the lipidation motif on the partitioning and association of N-Ras in model membrane subdomains. *J Am Chem Soc, 131*(4), 1557-1564.

Weise, K., Triola, G., Janosch, S., Waldmann, H., & Winter, R. (2009b). Visualizing association of lipidated signaling proteins in heterogeneous membranes-Partitioning into subdomains, lipid sorting, interfacial adsorption, and protein association. *Biochim Biophys Acta*.

Weiss, C. D., & White, J. M. (1993). Characterization of stable Chinese hamster ovary cells expressing wild-type, secreted, and glycosylphosphatidylinositol-anchored human immunodeficiency virus type 1 envelope glycoprotein. *J Virol, 67*(12), 7060-7066.

Weissenhorn, W., Carfi, A., Lee, K. H., Skehel, J. J., & Wiley, D. C. (1998). Crystal structure of the Ebola virus membrane fusion subunit, GP2, from the envelope glycoprotein ectodomain. *Mol Cell, 2*(5), 605-616.

Weissenhorn, W., Dessen, A., Harrison, S. C., Skehel, J. J., & Wiley, D. C. (1997). Atomic structure of the ectodomain from HIV-1 gp41. *Nature, 387*(6631), 426-430.

Weissenhorn, W., Hinz, A., & Gaudin, Y. (2007). Virus membrane fusion. *FEBS Lett*.

Wharton, S. A., Calder, L. J., Ruigrok, R. W., Skehel, J. J., Steinhauer, D. A., & Wiley, D. C. (1995). Electron microscopy of antibody complexes of influenza virus haemagglutinin in the fusion pH conformation. *Embo J, 14*(2), 240-246.

White, J. M. (1995). Membrane fusion: the influenza paradigm. *Cold Spring Harb Symp Quant Biol, 60*, 581-588.

Wilschut, J., Duzgunes, N., Fraley, R., & Papahadjopoulos, D. (1980). Studies on the mechanism of membrane fusion: kinetics of calcium ion induced fusion of phosphatidylserine vesicles followed by a new assay for mixing of aqueous vesicle contents. *Biochemistry, 19*(26), 6011-6021.

Wilson, I. A., Skehel, J. J., & Wiley, D. C. (1981). Structure of the haemagglutinin membrane glycoprotein of influenza virus at 3 A resolution. *Nature, 289*(5796), 366-373.

Xu, Y., Zhang, F., Su, Z., McNew, J. A., & Shin, Y. K. (2005). Hemifusion in SNARE-mediated membrane fusion. *Nat Struct Mol Biol, 12*(5), 417-422.

Yang, L., & Huang, H. W. (2002). Observation of a membrane fusion intermediate structure. *Science, 297*(5588), 1877-1879.

Yang, L., & Huang, H. W. (2003). A rhombohedral phase of lipid containing a membrane fusion intermediate structure. *Biophys J, 84*(3), 1808-1817.

Yeagle, P. L., Smith, F. T., Young, J. E., & Flanagan, T. D. (1994). Inhibition of membrane fusion by lysophosphatidylcholine. *Biochemistry, 33*(7), 1820-1827.

Yethiraj, A., & Weisshaar, J. C. (2007). Why are lipid rafts not observed in vivo? *Biophys J, 93*(9), 3113-3119.

Yguerabide, J., Schmidt, J. A., & Yguerabide, E. E. (1982). Lateral mobility in membranes as detected by fluorescence recovery after photobleaching. *Biophys J, 40*(1), 69-75.

Yoon, T. Y., Okumus, B., Zhang, F., Shin, Y. K., & Ha, T. (2006). Multiple intermediates in SNARE-induced membrane fusion. *Proc Natl Acad Sci U S A, 103*(52), 19731-19736.

Yousefi-Salakdeh, E., Johansson, J., & Stromberg, R. (1999). A method for S- and O-palmitoylation of peptides: synthesis of pulmonary surfactant protein-C models. *Biochem J, 343 Pt 3*, 557-562.

Zacharias, D. A., Violin, J. D., Newton, A. C., & Tsien, R. Y. (2002). Partitioning of lipid-modified monomeric GFPs into membrane microdomains of live cells. *Science, 296*(5569), 913-916.

Zampighi, G. A., Zampighi, L. M., Fain, N., Lanzavecchia, S., Simon, S. A., & Wright, E. M. (2006). Conical Electron Tomography of a Chemical Synapse: Vesicles Docked to the Active Zone are Hemi-Fused. *Biophys J, 91*(8), 2910-2918.

Zech, T., Ejsing, C. S., Gaus, K., de Wet, B., Shevchenko, A., Simons, K., et al. (2009). Accumulation of raft lipids in T-cell plasma membrane domains engaged in TCR signalling. *Embo J, 28*(5), 466-476.

Zhang, J., Pekosz, A., & Lamb, R. A. (2000). Influenza virus assembly and lipid raft microdomains: a role for the cytoplasmic tails of the spike glycoproteins. *J Virol, 74*(10), 4634-4644.

Zhao, X., Singh, M., Malashkevich, V. N., & Kim, P. S. (2000). Structural characterization of the human respiratory syncytial virus fusion protein core. *Proc Natl Acad Sci U S A, 97*(26), 14172-14177.

Zhu, T. F., & Szostak, J. W. (2009). Coupled growth and division of model protocell membranes. *J Am Chem Soc, 131*(15), 5705-5713.

Zimmerberg, J., & Chernomordik, L. V. (1999). Membrane fusion. *Adv Drug Deliv Rev, 38*(3), 197-205.

Zimmerberg, J., Cohen, F. S., & Finkelstein, A. (1980). Fusion of phospholipid vesicles with planar phospholipid bilayer membranes. I. Discharge of vesicular contents across the planar membrane. *J Gen Physiol, 75*(3), 241-250.

Zimmerberg, J., & Kozlov, M. M. (2006). How proteins produce cellular membrane curvature. *Nat Rev Mol Cell Biol, 7*(1), 9-19.

Acknowledgements

First and foremost I want to thank Prof. Andreas Herrmann for letting me be a part of his lab. Aside from his time, knowledge and ideas he is a truly valuable mentor, always willing to discuss results and ideas with a special enthusiasm. The immense effort he puts in the different projects is a constant inspiration to me.

I'm indebted to Prof. Sandro Keller who gladly took the poorly paid job as my second supervisor. Thanks also belong to Prof. Bernd Reif for the organization of the LGS.

I am very grateful to Dr. Thomas Korte and Dr. Peter Müller helping me with all the upcoming questions of microscopy and influenza as well as fluorescence and lipids but also for the discussions about special solvents and all kinds of electronic equipment.

I am especially thankful to my lab mate Dr. Martin Stöckl for his incredible patience and optimism. Also for the time and effort he put into reviewing the almost endless lines above.

Thanks belong to Prof. Michael Kozlov and Prof. Dieter Langosch for ongoing help discussing the arising questions within this work.

I want to thank Jason Warner and Prof. Ben O'Shaughnessy for backing up our results on hemifusion with some excellent theory.

I'm indebted to our collaborators within the different projects I could be part of, namely, Dr. Katrin Weise and Prof. Roland Winter, Prof. Daniel Huster and Dr. Alexander Vogel, Prof. Pablo Wessig, Dr. Sylvia Czapla, Kristian Möllnitz and Robert Wawrzinek for the possibility to join this exciting work.

I want to thank Dr. Rudolf Volkmer, Ines Kretzschmar, Christiane Landgraf and Anja Krüger for the help in our adventure of peptide synthesis and palmitoylation efforts.

Special thanks also belong to our permanent lab team Sabine Schiller and Gudrun Habermann for all the help in the everyday lab life making experiments so much easier.

In the end I want to thank again all people in our lab and the biophysics building and also everyone from the Veit lab for their help during this time. Thanks goes to all the people who helped to create the friendly and productive atmosphere that made life in the lab so easygoing.

Finally, but not least, I want the thank Chris Höfer and Stefan Baumgartner for careful proofreading parts of the manuscript. I'm deeply grateful for their support that goes far beyond correcting comma placement.

Thanks also belong to the Leibniz Graduate School for Molecular Biophysics and the DAAD for funding work and travel within this PhD time.

Publications

Talks

Joint Meeting of the Danish and German Biophysical Society, Hünfeld. 22.05.2009. 'Direct visualization of large and protein-free hemifusion diaphragms'

54th Annual Meeting of the Biophysical Society, San Francisco, CA, USA. 22.02.2010. `Lipid phase specific organisation of the transmembrane anchor of influenza hemagglutinin ´

1st Leibniz Graduate School Spring Meeting 2010, Hinterzarten, 17.03.2010 `Lipid phase specific organisation of the transmembrane anchor of influenza hemagglutinin ´

Posters

52nd Annual Meeting of the Biophysical Society, Long Beach, CA, USA. 06.02.2008. `Transmembrane Peptides Sequestered from the Hemifusion Site in Giant Unilamellar Vesicles´

German Biophysical Society Meeting, Berlin. 29.09.2008. `Direct Visualization of Large and Protein-free Hemifusion diaphragms´

53rd Annual Meeting of the Biophysical Society, Boston, MA, USA. 02.03.2009. `Direct Visualization of Large and Protein-free Hemifusion diaphragms´

International Symposium – Membranes and Modules, SFB 449 & 740, Berlin, 10-13.12.2009. `Lipid phase specific organisation of the transmembrane anchor of influenza hemagglutinin ´

Awards

Student Research Achievement Award (SRAA) –
Poster Competition at the 53rd Annual Meeting of the Biophysical Society, 2009

Publications

Ollesch J., Poschner B., **Nikolaus J**., Hofmann M., Herrmann A., Gerwert K., Langosch D. (2008) Secondary structure and distribution of fusogenic LV-peptides in lipid membranes. *Europ Biophys J* **37**:435-445

Müller P., **Nikolaus J**., Schiller S., Herrmann A., Möllnitz K., Czapla S., Wessig P. (2009) Molecular rods with oligospiroketal backbone as anchors in biological membranes. *Angew Chem Int Ed* **48**:4433-4435 doi:10.1002/anie.200901133

Vogel, A., Reuther, G., Weise, K., Triola, G., **Nikolaus, J**., Tan, K.-T., Nowak, C., Herrmann, A., Waldmann, H., Winter, R., Huster, D. (2009) Lipid Modifications of Ras Sense the Membrane Environment and Induce Local Enrichment. *Angew Chem Int Ed* 48 (46), 8784-8787

Stöckl M., **Nikolaus J**., Herrmann A. (2010). Visualization of lipid domain specific protein sorting in giant unilamellar vesicles. *Liposomes: Methods and protocols: Vol. 2: Biological Membrane Models.* (Ed. V. Weissig) Humana Press, Springer N.Y. Dordrecht, Heidelberg, London. ISBN:978-1-60761-446-3. pp.115-126.

Nikolaus J., Stöckl M., Langosch D., Volkmer R., Herrmann, A. (2010) Direct visualization of large and protein-free hemifusion diaphragms. *Biophys J* 98:1192-1199

Nikolaus, J., Scolari, S., Bayraktarov, E., Jungnick, N., Engel, S., Plazzo, A.P., Stöckl, M., Volkmer, R., Veit, M., Herrmann, A. (2010) Hemagglutinin of influenza virus partitions into the nonraft domain of model membranes. *Biophys J* 99:489-498.

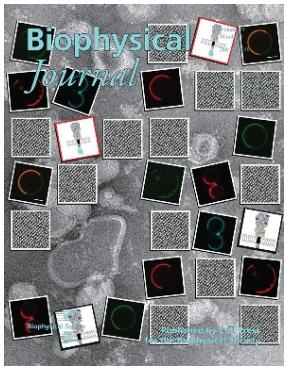

Corresponding Biophysical Journal cover illustration:

Weise, K., Kapoor, S., Denter, C., **Nikolaus, J**., Opitz, N., Koch, S., Triola, G., Herrmann, A., Waldmann, H., Winter, R. (2010) Membrane-mediated Induction and Sorting of K-Ras Microdomain Signaling Platforms. *JACS.* Accepted

Courses

24.-27.05.2007	Transbilayer lipid dynamics and membrane elasticity, EU Marie Curie Research Training Network: Flippases, Utrecht University, Netherlands
23.-27.07.2007	Membrane biophysics, LGS course with PD Dr. Ulrike Alexiev, FU, Berlin
03.-07.09.2007	Approaches to Membrane Proteins, LGS course with Dr. Sandro Keller, FMP, Berlin
24.-29.09.2007	Analysing Membrane Proteoms: Methods and Approaches, CMP Summer School, Center for Membrane Proteomics, Frankfurt/Main

Conferences

12.-13.04. 2007	1st Max Planck Symposium `Virology´, Berlin
02.07.2007	2nd Mini-Symposium: `Light Optical Analysis of Functional Modules´ SFB 740, Berlin
16.-17.11.2007	Folding and Stability of beta-sheets, FOR 475, University Potsdam, Golm
02.-06.02.2008	52nd Annual Biophysical Society Meeting, Long Beach, CA, USA
28.09.-1.10.2008	German Biophysical Society Meeting, Berlin
28.02.-4.03.2009	53rd Annual Biophysical Society Meeting, Boston, MA, USA
21.-24.05.2009	Joint Meeting of Danish and German Biophysical Society, Hünfeld
10.-13.12.2009	International Symposium – Membranes and Modules, Berlin
20.-24.02.2010	54th Annual Biophysical Society Meeting, San Francisco, CA, USA
10.-11.06.2010	EC Marie Curie Network, Virus Entry, Berlin

Collaborations

Partner	Project
Prof. Dr. Dieter Langosch	Microscopy of GUVs comprising different LV peptides
Prof. Dr. Pablo Wessig Dr. Sylvia Czapla Kristian Möllnitz	Microscopy of GUVs and RBC comprising molecular rods
Prof. Dr. Pablo Wessig Robert Wawrzinek	FLIM measurements of a new fluorescent dye
Prof. Dr. Daniel Huster Dr. Alexander Vogel	Microscopy of N-Ras protein with GUVs and GPMVs
Prof. Dr. Roland Winter Dr. Katrin Weise	Microscopy of K-Ras proteins with GUVs
Prof. Dr. Ben O'Shaughnessy Jason Mark Warner	Extensive data analysis on hemifusion and further experiments to determine membrane tension
PD Dr. Christina Kühn	Formation and microscopy/FLIM of GUVs from plant plasma membrane lipids and protoplasts
Prof. Dr. Rudolf Tauber Dr. Jens Dernedde Sebastian Riese	Microscopy and FLIM measurements on K562 cell
Dr. Michael Kolbe Michele Lunelli	Experiments on binding of SipD protein to GUVs
Prof. Dr. Michael Linscheid Frederic Müller	Formation and microscopy/FLIM of GUVs from lipid extracts of B. stolpii

Eidesstattliche Erklärung

Hiermit erkläre ich, die vorliegende Arbeit selbständig und nur unter Verwendung der angegebenen Hilfsmittel angefertigt habe. Alle Stellen, die dem Wortlaut oder dem Sinn nach anderen Werken entnommen sind, sind nach bestem Wissen und Gewissen durch Angabe der Quellen als Entlehnung kenntlich gemacht worden.

Ein Teil der beschriebenen Ergebnisse wurde in Zusammenarbeit mit anderen Mitarbeitern der Arbeitsgruppe Molekulare Biophysik erzielt und sind entsprechend gekennzeichnet.

Ich besitze keinen entsprechenden Doktorgrad und habe mich anderwärts nicht um einen Doktorgrad beworben.

Die dem Promotionsverfahren zugrunde liegende Promotionsordnung ist mir bekannt.

Jörg Nikolaus

Berlin, 16 Dezember 2010